UNICA

UNIVERSITÀ
DEGLI STUDI
DI CAGLIARI

Ph.D. DEGREE IN

Neuroscience

Cycle XXXVII

TITLE OF THE Ph.D. THESIS

POST-MORTEM INTERVAL ESTIMATION THROUGH METABOLOMICS OF PINEAL GLAND

Scientific Disciplinary Sector(s)

MED/43

Ph.D. Student: Radhika Kesharwani

Supervisor: Prof. Roberto Demontis

Final exam. Academic Year 2023/2024
Thesis defence session: April 2025

ACKNOWLEDGMENTS

This thesis is the culmination of my Ph.D. journey, and I would like to acknowledge everyone who have supported me academically and personally along the way. I extend my sincere gratitude to my Ph.D. supervisors, Prof. Roberto Demontis and Prof. Emanuela Locci. Your invaluable guidance, support, and openness to my ideas provided an ideal environment in which I could grow as a researcher. Prof. Locci, your mentorship, has profoundly influenced my development, and I am truly thankful for the privilege of learning under your supervision.

I am grateful to Prof. Christian D'ovidio and Prof. Tiziana Pietrangelo for their time, thoughtful and constructive feedback while reviewing my thesis.

My sincere appreciation goes to Prof. Ernesto D'Aloja, Dr. Alberto Chighine, Dr. Daniela Casu, and Dr. Matteo Nioi, for generously providing the post-mortem pineal glands that made this study possible. I am equally indebted to Dr. Giulio Ferino, for his hands-on support, valuable suggestions, and scientific dialogue. I extend my thanks to Prof. Luigi Atzori for his helpful insights regarding my thesis, as well as to Dr. Vera Leoni and Dr. Christina Perra, whose thoughtful suggestions helped refine both the content and clarity of my thesis.

I also wish to acknowledge Prof. Stefano Pluchino and Prof. Luca Peruzzotti-Jametti at the University of Cambridge, UK, for welcoming me into their group, guiding me, and assisting in the characterization of cellular phenotypes within white matter lesions from post-mortem brain specimens of patients with progressive multiple sclerosis.

A big thank you to my love, Pathik, for being there every minute of this amazing journey. Your support and love kept me strong during the darkest times and I am so grateful that you had there got me. You have made the happy moments even more beautiful and the difficult times more bearable. Finally, I express my deepest appreciation to my family, whose unconditional love and support laid the foundation for all my endeavors. To my parents, thank you so much for your patience, for granting me the freedom to choose my own path, and for instilling in me the resilience and determination needed to reach this milestone.

बहुत-बहुत धन्यवाद**! Thank you very much! Grazie Mille!**

<u>This thesis is dedicated to all of you!!!</u>

CONTENTS

PREFACE

Embarking on the study of post-mortem interval (PMI) has been both a challenging and fascinating journey. The complexities of determining the time since death, a concept known as chronothanatognosis, extend far beyond academic interest. Accurate PMI estimation is critical to forensic science, with profound implications for criminal investigations, legal proceedings, and historical inquiries. As such, it forms a cornerstone of forensic practice, shaping the timeline of events and often guiding the direction of investigations.

My interest in this subject was sparked by the sheer complexity and the importance of accurately determining PMI. Traditional methods to detect early post-mortem changes, such as algor mortis, rigor mortis, and livor mortis, while foundational, often lack the accuracy needed in modern forensic investigations. This led me to explore the field of metabolomics, which promises a more detailed and reliable approach to PMI estimation. Metabolomics is a study of small molecules/metabolites within biological systems, which provides a window into the biochemical changes that occur after death, promising a more precise timeline to estimate PMI.

Throughout this thesis, I investigate the biochemical changes that occur after death, with a particular focus on the pineal gland. This small, but functionally significant endocrine organ, located deep within the brain, has intrigued me due to its unique biochemical properties and relative protection from external environmental influences. The pineal gland's role in melatonin secretion and regulation of circadian rhythms may provide a stable metabolic profile. These further assist in the evaluation of whether the death of an individual might have occurred at night-time or day-time, rendering the pineal gland an ideal candidate for forensic investigation.

In Chapter 1, I provide a comprehensive introduction to the concept of PMI and its significance. Chapter 2 explores the traditional methods used for PMI estimation based on the stages of post-mortem changes and their limitations. Chapter 3 presents advancements in PMI estimation techniques, particularly metabolomics. Chapter 4 entails a detailed description of the pineal gland, including its relevance in PMI estimation. This thesis is the culmination of years of research, curiosity, and a drive to contribute something meaningful to the field of forensic science. I hope that the findings presented here not only advance our understanding of PMI estimation but also inspire further research into the applications of metabolomics in forensic investigations.

INTRODUCTION

1. Post-mortem interval (PMI): An overview

The post-mortem interval (PMI) refers to the time elapsed between physiological death and the examination of the deceased (Haas et al., 2021). Accurate estimation of PMI is a cornerstone of forensic investigations due to its significant impact on both criminal and civil cases. In criminal investigations, establishing the precise time of death is crucial for verifying witness statements, narrowing down the pool of suspects, and corroborating alibis. By determining the time frame in which death occurred, investigators can better focus their efforts, directing attention towards suspects who may have been present at the time of death. For example, if a suspect claims to have been elsewhere, an accurate PMI can either confirm or refute their alibi, refining the scope of the investigation and potentially identifying the correct individuals involved. In civil cases, PMI estimation can be equally significant, for determining the order of deaths in incidents involving multiple victims. Furthermore, accurate PMI estimation is invaluable in understanding the circumstances surrounding a death, particularly in cases of suspicious, homicide, or unexplained fatalities. It allows forensic pathologists and investigators to reconstruct the timeline of events leading up to the death, providing critical insights into the cause and manner of death.

However, accurately determining the PMI is brimming with challenges, particularly in instances where bodies are severely decomposed or exposed to fluctuating environmental conditions. Traditional methods of PMI estimation, while foundational, often lack the precision required for more complex cases. These methods are typically influenced by various environmental and biological factors, including temperature, humidity, and the physical condition of the body, leading to potentially inaccurate or ambiguous results. To address these limitations, the forensic field has increasingly turned to advanced techniques that provide more reliable PMI estimates. Approaches such as biochemical analysis, molecular biology, and various “omics” technologies, including lipidomics, proteomics, and metabolomics, have shown significant potential. These methods offer a deeper insight into the biochemical and molecular changes that occur after death, enabling forensic investigators to estimate PMI with greater accuracy. By leveraging these cutting-edge technologies, forensic science can support criminal and civil legal processes with a higher degree of precision, ultimately contributing to more reliable justice outcomes.

2. Estimating post-mortem interval (PMI): Traditional methods and their constraints

Estimating the PMI relies on understanding the physiological changes that occur after death. These changes are a result of a series of chemical and physical processes, broadly divided into three stages: immediate, early, and late post-mortem changes, based on their order of appearance (Tsokos M & Byard RW, 2016) **(Table 1)**.

2.1. Immediate post-mortem changes

Immediate changes refer to the rapid biochemical and physiological alterations that occur immediately after death, often called “signs of death”. These include the permanent cessation of the respiratory, circulatory, and nervous systems (Almulhim & Menezes, 2023). This phase is primarily characterized by several detectable changes, in the eyes and skin, providing valuable clues for estimating PMI. One of the earliest signs is 'trucking' or segmentation of retinal blood vessels, which appears as breaks in the blood column within the retinal vessels (Jaafar & Nokes, 1994). This phenomenon typically manifests within 30 minutes to 2 hours post-mortem (Jaafar & Nokes, 1994). Additionally, intraocular pressure decreases sharply, often reaching 4 mmHg or less within 6 hours (Van Den Oever, 1976), while corneal clouding begins within 2 hours, progressively obscuring intraocular examinations (Wróblewski & Ellis, 1970).

On the skin, a loss of elasticity and luster occurs within a few hours after death, causing a pale appearance, although histological changes (Bardale et al., 2012) and cellular and biochemical alterations (Babapulle & Jayasundera, 1993) are typically absent during the initial 3 to 6 hours post-mortem. Gastric emptying can also provide clues for estimating PMI: small, light meals are typically emptied from the stomach within 1 to 3 hours, allowing forensic pathologists to estimate PMI based on the time of the last meal and stomach contents (Madea, 2016). This immediate post-mortem phase, encompassing the first 2 to 3 hours after death, is marked by these subtle yet informative changes, crucial for early PMI estimation and forming the basis for further forensic analysis.

2.2. Early post-mortem changes

The early post-mortem phase, spanning from 3 to 72 hours after death, is a critical period for PMI estimation, frequently examined in most of the medico-legal cases. During this time frame, forensic investigators rely on a classical triad of observable post-mortem changes: livor mortis, rigor mortis, and algor mortis (Almulhim & Menezes, 2023). These changes, which develop in predictable patterns, can provide clues about the time of death and the conditions in which it occurred.

Livor mortis: Livor mortis (also known as livores, post-mortem lividity, or hypostasis), manifests as a purplish-blue discoloration of the skin on the dependent parts of the body (Meurs, 2023). This discoloration is caused by the gravitational pooling of blood into the capillaries within the dermis after the cessation of cardiovascular function (Marks & Tersigni, 2005). Livor mortis typically begins within an hour after death, becomes noticeable between 2 to 4 hours, and is fully fixed in place by 6 to 8 hours (Goff, 2009). The dermal capillaries, specifically in the papillary and reticular layers, become engorged with blood, resulting in the characteristic purplish discoloration (Tsokos, 2005). The distribution of livor mortis can reveal valuable information about the position of the body at the time of death. For example, lividity on the anterior parts of the body indicates that the deceased was lying face down (prone position), while lividity on the posterior suggests a supine position (Prahlow & Byard, 2012). The presence of livor mortis may also provide information if the body was moved after death, making it a crucial observation in forensic investigations (Meurs, 2023).

Rigor mortis: Rigor mortis (also known as post-mortem rigidity), is the stiffening of both voluntary and involuntary muscles following death due to chemical changes within muscle tissues. The depletion of adenosine triphosphate (ATP) and accumulation of lactate in muscle fibres prevent the release of the actin-myosin bonds, leading to muscle contraction and stiffening (Goff, 2009). Rigor mortis begins in the smaller muscles, such as those in the jaw and eyelids, within 1 to 4 hours post-mortem, due to faster ATP depletion, and then gradually spreads to larger muscle groups. By 6 hours, most muscles will show signs of rigor, with full body stiffness occurring by 12 hours. The rigidity lasts for approximately 12 more hours before muscles begin to relax again due to the enzymatic breakdown of muscle tissue as decomposition sets in (Kori, 2018). This process

of stiffness and relaxation can be influenced by external factors, such as ambient (environmental) temperature, where high temperatures accelerate the onset and progression of rigor mortis, while lower temperatures delay it (Almulhim & Menezes, 2023).

Algor mortis: Algor mortis (also known as post-mortem cooling) refers to the second stage of death, which is characterized by the normal cooling of the body until it reaches equilibrium with the ambient temperature (Eden & Thomas, 2023). During life, the average rectal temperature is approximately 36.9°C (ranging from 34.2°C to 37.6°C) (Sund-Levander et al., 2002). However, assuming that the deceased had a ‘‘normal’’ body (rectal) temperature at the time of death can be misleading, as many factors, such as illness, activity level before death, or external conditions, can influence body temperature at the time of death. The primary mechanisms of heat exchange between the body and the surroundings are primarily mediated by conduction and convection, while evaporation becomes significant if the body or clothing is wet (De Saram et al., 1956). The rate of post-mortem cooling depends on various factors, including body mass, the temperature gradient between the deceased and the ambient environment, gender, clothing, and body posture at the time of death (Almulhim & Menezes, 2023; Goff, 2009; Teo Chee Hau et al., 2014). Initially, after death, the body temperature remains relatively stable for 1 to 3 hours, this phase is referred to as the ‘‘post-mortem temperature plateau.’’ After this plateau, body temperature begins to decline at a rate of 0.5°C and 1.5°C per hour, depending on the surrounding conditions. This linear cooling continues for approximately 10 to 16 hours (Byard, 2020). Once the body temperature approaches equilibrium with the ambient temperature, the cooling rate slows considerably (Byard, 2020). Estimating PMI based solely on body temperature can be inaccurate due to the variability of the temperature plateau duration and the numerous factors affecting heat loss. Moreover, once the body has reached equilibrium with the environment, temperature-based methods become ineffective for estimating PMI (Byard, 2020).

2.3. Late post-mortem changes

The late post-mortem phase involves autolysis (tissue decay by enzymatic degradation process) and putrefaction (tissue decay by bacterial activity), leading to the complete decomposition of the body (Cockle & Bell, 2017).

Autolysis: It refers to the self-digestion of cells and tissues caused by the action of intracellular enzymes, beginning approximately 4 minutes after death. This process occurs due to the leakages of hydrolytic enzymes from lysosomes after death, leading to the breakdown of cell membranes and organelles. Autolysis is a sterile process that happens without microbial involvement, and its effects are primarily microscopic rather than macroscopic (Shirley et al., 2011). Organs with high enzymatic activity, such as the liver, are particularly susceptible to rapid autolysis (Pasca & Ulasan, 2014). Temperature plays a significant role in the rate of autolysis, with higher temperatures accelerating enzymatic degradation and lower temperatures slowing it down.

Putrefaction: Following autolysis, the body undergoes putrefaction, a process in which tissue decay is driven by microbial activity. Microorganisms, such as bacteria, fungi, and protozoa, normally present in the body's microbiota, proliferate in the nutrient-rich environment created by cellular breakdown, further decomposing tissues (Clark et al., 1997; Paczkowski & Schütz, 2011; Zhou & Byard, 2011). Putrefaction is characterized by visible changes at the macroscopic level, including a greenish discoloration of the abdomen, bloating of the face, abdomen, breast, and scrotum, and the release of foul-smelling gases (Almulhim & Menezes, 2023). The production of putrefactive gases, such as methane, carbon dioxide, and hydrogen sulfide, causes the body to swell as these gases accumulate within the tissues (Almulhim & Menezes, 2023). The rate of putrefaction varies widely and is influenced by external factors such as temperature, humidity, and microbial presence, with warmer, more humid environments accelerating decomposition.

Adipocere: Adipocere (also known as grave wax or corpse wax) involves the transformation of adipose tissues into a wax-like substance through a process of hydrolysis and hydrogenation (Ubelaker & Zarenko, 2011). This yellowish-greasy material is primarily composed of fatty acids, such as palmitic, oleic, and stearic acids, along with some glycerol (Fiedler & Graw, 2003). Adipocere typically forms in fatty areas such as the cheeks, chin, abdomen, and buttocks (Fiedler & Graw, 2003). Initially soft and yellow, adipocere becomes white, brittle, and hard, as fatty acids crystallize, preserving the shape of the body and even injuries. This process occurs alongside other forms of putrefaction in different body regions (Shedge et al., 2023).

Mummification: It is characterized by the desiccation, the drying-up process of soft tissues, resulting in dry, brown, hard, and brittle skin stretched over bones. Mummification may affect

the entire body or only specific parts that have been exposed to the environment, and it typically occurs in arid, hot, or extremely cold environments. Unlike putrefaction, mummification, typically preserves facial features and external injuries, although the body undergoes shrinkage (Houlton & Wilkinson, 2018). Mummification processes are mainly of two types: primary and secondary. Primary mummification is generally not accompanied by significant putrefaction processes. It predominantly occurs in environments that facilitate rapid desiccation of soft tissues, such as dry and hot climates, where the lack of moisture prevents bacterial putrefaction. In contrast, secondary mummification happens after substantial putrefaction has already occurred, often in open spaces where environmental conditions lead to partial drying of the body. In some cases, a single body may exhibit both mummified and putrefied tissues, with different regions of the body undergoing different decomposition processes (Leccia et al., 2018).

Understanding the different phases of post-mortem and their progression is essential for forensic pathologists and investigators. Recognizing these specific physical and chemical changes allows for more accurate PMI estimation, which is critical in reconstructing the sequence of events leading to death and providing crucial information for both criminal and civil investigations.

Sr. No.	**Stages of Post-Mortem Changes**	**Characteristics**	**Time Since Death (Approximate)**	**Limitations for PMI Estimation**
1.	Immediate Phase	Cessation of heartbeat, respiration, and brain function; oxygen depletion begins.	Occurs immediately, within seconds to minutes after death.	Extremely brief time window; requires real-time monitoring to identify the exact time of death, not practical for most forensic cases.
2.	Early Phase			
	A. Livor mortis (Lividity, post-mortem hypostasis)	Pooling of blood due to gravity, causing purplish discoloration of the skin	Begins 20 minutes to 4 hours after death; becomes fixed after 6-8 hours.	Limited by factors such as body position, external pressure, and ambient temperature. Inconsistent timing makes it difficult to estimate PMI precisely.

	B. Rigor mortis (Stiffening of muscles)	Stiffening of muscles starting from smaller muscles (jaw, face) to larger ones	1-2 hours onset, fully developed at 12 hours after the death and dissipates after 12 hours.	Duration varies widely based on environmental factors, the physical condition of the deceased, and the cause of death.
	C. Algor mortis (Cooling of the body)	Body temperature decreases to match ambient temperature.	1-16 hours after death	Highly dependent on environmental conditions (e.g., temperature, humidity, clothing), making it unreliable without proper controls. Works only for shorter PMI.
3.	Late Phase			
	A. Autolysis (Cellular self-digestion)	Breakdown of cells due to enzyme activity, most noticeable in softer and high enzymatic activity tissues (e.g., pancreas, liver)	Within hours after the death.	Highly dependent on environmental factors and body temperature. Difficult to assess without histological or biochemical analysis.
	B. Putrefaction (Decomposition by bacteria)	Greenish discoloration of the skin, bloating of face, breasts, and scrotum, gas formation, and foul smell. Tissue decay by bacterial activity.	Starts within an hour after death, and peak activity of microbes occurs around 24 hours.	Rates of putrefaction vary widely based on external factors (temperature, moisture, burial conditions), leading to inaccuracies in PMI estimation.
	C. Adipocere	Formation of "grave wax" (adipocere) from fat tissues due to anaerobic bacterial activity; tissues become	Can begin as early as 3 weeks, but usually, it takes 3 months to form.	Occurs in cool, moist, anaerobic environments); slows down decomposition significantly, making PMI estimation more

		white, waxy, and firm. Typically forms in fatty areas such as cheeks, chin, abdomen, and buttocks.		difficult and requiring specialized methods (e.g., chemical analysis of adipocere).
	D. Mummification	Drying and preservation of the body tissues in dry, arid, or cold conditions; tissues become leathery and shrunken.	N/A	Mummified bodies undergo very slow decomposition, making it difficult to estimate PMI without knowing environmental conditions; requires specific forensic techniques (e.g., DNA testing, radiocarbon dating) for PMI determination.

Table 1: Different stages of post-mortem changes, their key characteristics, estimated time since death, and limitations for PMI estimation. The table categorizes each stage of decomposition from immediate post-mortem changes to advanced decomposition processes, such as adipocere formation and mummification. Abbreviations: PMI, post-mortem interval; DNA, deoxyribonucleic acid; TCA cycle, tricarboxylic acid cycle; N/A, Not available.

2.4. Limitations of traditional methods of post-mortem interval (PMI) estimation

The complex interplay of intrinsic and extrinsic variables in the decomposition process makes the development of accurate PMI estimation models challenging. Traditional methods, such as estimating PMI based on body and ambient temperature (which rely on the predictability of algor mortis), or visually assessing gross morphological changes to the body, offer broad PMI ranges and are subject to significant limitations.

For instance, algor mortis-based models work only within short PMIs and become unreliable once the body reaches ambient temperature. Similarly, visual assessments of decomposition stages, while useful, suffer from poor accuracy and precision due to the variable rate of decomposition. This can be influenced by environmental factors like temperature, humidity, and the presence of scavengers. Additionally, these methods are subject to interobserver variability, where different investigators may score decomposition stages differently, further reducing reliability. Moreover, as decomposition progresses, the accuracy of traditional methods diminishes, particularly when the bodies are severely decomposed or skeletonized (Henssge and Madea, 2007; Madea, 2016). These limitations underscore the urgent need for advanced PMI estimation methods that can offer greater accuracy, even in cases where the body is in an advanced state of decomposition. In the following section, we will explore advanced forensic techniques, including biochemical and molecular approaches, that promise to revolutionize PMI estimation by addressing the shortcomings of traditional methods.

3. Advancements in post-mortem interval (PMI) estimation techniques: Integrating molecular, biochemical, and emerging methods

Given the limitations of traditional PMI estimation methods, significant efforts have been made to develop more advanced and reliable techniques. These new approaches leverage technological innovations and scientific advancements to improve accuracy and precision, even in complex forensic scenarios. By integrating molecular biology, biochemistry, and advanced imaging techniques, these methods offer promising alternatives to overcome the challenges faced by conventional methods. The recent advancements in PMI estimation focus on various biological and chemical markers that exhibit predictable changes over time after death. These include: **(A) Molecular and Biochemical Methods:** It explores the degradation patterns of DNA, RNA, and proteins to provide more precise PMI estimates. **(B) Metabolomic Approaches:** Using metabolomics to study the small molecules and metabolites that vary systematically during decomposition. **(C) Microbiome Analysis:** Investigating post-mortem changes in microbial communities, which offer unique time-dependent patterns useful for PMI estimation. **(D)**

Forensic Entomology: Employing advanced techniques to study insect activity and succession on decomposing remains, providing a reliable timeline for PMI estimation. **(E) Imaging Techniques:** Utilizing modern imaging technologies, such as magnetic resonance imaging (MRI) and computed tomography (CT), to observe and quantify internal changes post-mortem. In the following subsections, we will delve deeper into each of these advanced techniques, exploring their methodologies, applications, and the improvements they bring to the field of forensic science.

3.1. Molecular and biochemical methods

Molecular and biochemical methods have significantly advanced PMI estimation by offering highly accurate and precise timelines based on the systematic degradation of biological molecules, such as deoxyribonucleic acid (DNA), ribonucleic acid (RNA), proteins, and metabolites, after death.

3.1.1. DNA degradation

DNA degradation occurs predictably after death due to autolysis and microbial activity, and its rate can be influenced by factors such as temperature, humidity, and pH. Techniques like quantitative polymerase chain reaction (qPCR) and gel electrophoresis are widely used to measure DNA fragmentation, allowing forensic scientists to establish a timeline of DNA decay and estimate the PMI with greater accuracy.

In this regard, few studies have explored the relationship between DNA degradation and PMI across various tissues. For example, research on spleen tissue from autopsies with known PMIs revealed a correlation between the rate of DNA degradation and the PMI (Cina, 1994). Subsequent studies using spleen, liver, and blood samples confirmed these findings, with flow cytometry showing the best correlation with hepatic tissue (N. Di Nunno et al., 2002; N. R. Di Nunno et al., 1998). Comparisons between brain and spleen tissues revealed lower rates of DNA degradation in brain tissue, likely due to lower enzymatic activity (Williams et al., 2015). Other studies have employed the comet assay to study DNA degradation (Shukla, 2017). This technique has demonstrated a clear increase in DNA fragmentation with increasing PMI (Johnson & Ferris,

2002; Tozzo et al., 2020). The findings obtained in heart, liver, and kidney cells demonstrated rapid DNA degradation in the first 6 hours after death (Xin Chen et al., 2005), consistent with other studies (Hao L.G et al., 2007; Luo G.H. et al., 2006). Extended research on mouse brain and dental pulp cells has also revealed a high linear correlation between comet assay parameters and PMI up to 72 hours (Zheng et al., 2012). These results underline the utility of DNA degradation analysis in providing a reliable estimate of PMI, enhancing the accuracy of forensic investigations.

3.1.2. RNA degradation

RNA degradation serves as a sensitive marker for PMI estimation due to its inherent instability and rapid decay post-mortem. Unlike DNA, RNA is more susceptible to degradation (Fordyce et al., 2013), making it a reliable indicator for short-term PMI estimations. Various types of RNA degrade at different rates, with ribosomal RNA (rRNA) being more stable than messenger RNA (mRNA) (Fordyce et al., 2013).

Studies have shown that RNA stability varies significantly by tissue type. For instance, RNA in organs like the pancreas and liver degrades rapidly due to high levels of ribonucleases (Bauer et al., 2003), whereas brain tissue in both humans and rats shows much greater RNA stability (Bauer et al., 2003; Inoue et al., 2002). Further, the degradation of RNA based on the expression of specific genes has been evaluated in the human heart tissues from individuals with varying PMIs (Partemi et al., 2010). The findings demonstrated a negative correlation of NOS3 (Nitric Oxide Synthase 3) expression with PMI (Partemi et al., 2010). Advancements in qPCR have further refined RNA degradation analysis. Research on 18S-rRNA and microRNAs (miRNA) in rat heart tissue over PMIs ranging from 0 to 168 hours showed a strong parabolic relationship between PMI and cycle threshold (Ct) values in qPCR, which are inversely proportional to the amount of target nucleic acid present (W. C. Li et al., 2014). Additionally, mathematical models incorporating qPCR expression of Glyceraldehyde-3-Phosphate-Dehydrogenase (GAPDH) and β-actin (ACTB) in lung and muscle tissues from rats (0 to 6 days post-mortem) and human autopsies (up to 24 hours post-mortem) have shown low error rates for PMI estimation (Lv et al., 2016). Additionally, research on mouse tissues showed a correlation of PMI (up to 8 days) with expression levels of housekeeping genes, miRNA, and circular RNAs (circRNAs) (Tu et al., 2019).

Recent research has expanded on these findings. A microarray screening of 217 mRNA markers in rat cardiac tissue identified cell division cycle 25 homolog B (Cdc25b) as the most reliable marker for early PMI (Tao et al., 2018). Moreover, studies examining mRNA expression in genes involved in apoptosis, such as Fas Ligand (FasL) and phosphatase and tensin homolog (PTEN), showed strong linear correlations with PMI up to 6 hours after death (Zapico et al., 2014), giving rise to the field of thanatotranscriptomics, which focuses on post-mortem gene expression. RNA degradation methods are further complemented by the use of Gene Meter models, which predict PMI based on gene expression changes, achieving high correlation coefficients in studies on zebrafish and mice (Hunter et al., 2017). Additionally, human transcriptomic data from the Genotype-Tissue Expression (GTEx) Database revealed a change in the expression of 266 genes with short- and long-term PMI and tissue-specific RNA degradation patterns (Zhu et al., 2017), with gastrointestinal tract (GIT) tissues showing earlier changes compared to the central nervous system (CNS), during the first hours of death (Ferreira et al., 2018). Despite these advances, the RNA degradation method faces limitations, including variability in RNA stability across tissues and the influence of environmental factors. The rapid degradation of RNA also necessitates precise handling of samples, presenting challenges in real-world forensic scenarios. These limitations underscore the need for complementary approaches to provide more comprehensive PMI estimates.

3.1.3. Protein degradation

Protein degradation offers another important marker for PMI estimation, providing insights based on the systematic breakdown of proteins after death. Unlike RNA, proteins exhibit varied stability across different tissues, with certain proteins degrading at predictable rates. This variability allows forensic scientists to use protein degradation patterns as reliable markers for estimating PMI. Analytical techniques such as mass spectrometry (MS) and Western blotting are frequently employed to measure the breakdown of specific proteins, providing timelines that enhance the accuracy of PMI determination.

Studies on human brain and heart tissues with PMIs ranging from 6 to 58 hours have shown time-dependent increases in autophagy-related proteins, such as LC3-II, p62, Beclin-1, and Atg7 in

heart tissue, while BNIP3 levels decreased as PMI progressed (Javan et al., 2015). Similar degradation patterns were found for LC3, p62, and Atg7, whereas BNIP3 and Beclin-1 levels showed a decline with increasing PMI, in brain tissues (Javan et al., 2015). Additionally, analysis of brain tissue biomarkers up to 72 hours post-mortem revealed a significant decrease in Talin-1, a protein linked to cell adhesion, correlating strongly with PMI (Campell et al., 2016). Proteomics, the large-scale study of proteins, has also been utilized to estimate PMI over longer periods. For instance, liquid chromatography-tandem mass spectrometry (LC-MS/MS) analysis of pig bones with PMIs between 1 and 6 months identified a decrease in plasma and muscle proteins with advancing PMI, alongside increased deamidation of biglycan, a protein crucial for bone growth (Procopio et al., 2018). Seasonal studies on decomposition fluids from domestic pigs using a nano high-performance liquid chromatography (HPLC) system coupled with a Tripple-TOF mass spectrometer (MS) identified common peptides across different seasons, suggesting that profiled peptide analysis could reliably estimate PMI, regardless of environmental conditions (Nolan et al., 2019). Long-term PMI estimation has also been explored through proteomics. An analysis of femur bones from human cadavers with PMIs ranging from 5 to 20 years identified 32 proteins that could distinguish between shorter (5-12 years) and longer (13-20 years) PMIs (Prieto-Bonete et al., 2019a). Further study assessed the impact of intrinsic and extrinsic variables on human proteome analysis in decomposition scenario, discovering that inter-individual and inter-skeletal differences in bone mineral density can influence protein survival, underscoring its promise as a new potential biomarker for PMI estimation (Mickleburgh et al., 2021). Despite these advancements, protein degradation methods or proteomics face certain limitations, including variation in protein stability across tissues and the influence of environmental factors, such as temperature and humidity. These challenges, combined with inter-individual variability, emphasize the need for complementary approaches to ensure accurate PMI estimation.

In conclusion, the exploration of molecular and biochemical methods has led to significant advancements in PMI estimation. DNA degradation, analyzed through qPCR and gel electrophoresis, offers reliable timelines for PMI estimation based on the predictable fragmentation patterns of DNA. Similarly, RNA degradation, assessed using reverse transcription

PCR (RT-PCR), provides valuable insights for short-term PMI estimation due to the rapid decay of RNA molecules. Protein degradation, leveraging the systematic breakdown of proteins post-mortem and analyzed through proteomics techniques like LC-MS/MS and Western blotting, has extended PMI estimation capabilities to both short-term and long-term intervals. However, despite these advancements, each of these methods faces inherent limitations. DNA degradation rates can be influenced by environmental factors, RNA is particularly susceptible to rapid degradation and contamination, and protein degradation is affected by variability in stability across tissues and environmental conditions. These challenges underscore the need for complementary approaches to achieve accurate PMI estimates.

Recently, metabolomics has gained a lot of interest in the field of forensic science. Metabolomics is a comprehensive analysis of small molecules, or metabolites, within cells, tissues, or organisms, offering a detailed snapshot of biochemical alterations that can be correlated with PMI. This approach has the potential for higher accuracy and precision, addressing the gaps left by DNA, RNA, and protein degradation methods. In the following sections, we will explore the application of metabolomics in PMI estimation, highlighting its advantages, and how this emerging field can revolutionize forensic investigations.

3.2. Metabolomics in forensic Science: Revolutionizing post-mortem interval (PMI) estimation

Metabolomics, the comprehensive study of small molecules (metabolites), within biological systems, has emerged as a cutting-edge approach in forensic science (Szeremeta et al., 2021). The metabolome, which represents the complete set of metabolites in an organism, provides a dynamic reflection of the physiological state of cells, tissues, and body fluids (Dunn & Ellis, 2005; Zhao & Lin, 2014). These metabolites, which can be endogenous-produced within the body by gut microbiota processing and/or exogenous, derived from external sources, such as food, drugs, and environmental factors, offer a holistic view of an organism's biochemical status (Agin et al., 2016; Dufour-Rainfray et al., 2020). The study of metabolomics not only allows for the monitoring of biological processes but also provides crucial insights into the functional and metabolic responses to environmental and physiological changes. Therefore, it may aid in the identification

of potential biomarkers for disease diagnosis and risk assessments (Lin et al., 2024; Monteiro et al., 2013; A. Zhang et al., 2015).

In forensic science, metabolomics has shown great potential, particularly in the estimation of PMI (Chighine et al., 2021) and forensic toxicology (Szeremeta et al., 2021). After death, the body's metabolic processes begin to deteriorate, leading to a cascade of biochemical changes (Akçan et al., 2020; Dawidowska et al., 2021). These changes are characterized by the cessation of cellular respiration, altered enzymatic activity, disruption of metabolic pathways, and degradation of cells and tissues (Akçan et al., 2020; Dawidowska et al., 2021). Several studies have highlighted the utility of metabolomics in tracking post-mortem biochemical changes. A study by Ortiz (2019) involved the ^{1}H-Nuclear Magnetic Resonance (NMR) spectroscopy-based metabolomic study of six biological matrices: heart, kidney, liver, spleen, skin, and white adipose tissue from ten adult mice at three time points (immediate, 6 hours and 24 hours after euthanasia). The study detected forty-three metabolites modulated post-mortem. They observed the highest metabolic perturbations, particularly in the kidney, heart, and spleen. In addition, they showed that early metabolic modulations were associated with energy metabolism and DNA synthesis however, microbial metabolism was related to late PMI (Mora-Ortiz et al., 2019). A study by Donaldson and Lamont (2015) investigated the metabolomic profile of post-mortem rat blood using a Gas Chromatography coupled with Mass Spectrometry (GC-MS) approach. The study detected sixty-six metabolites, with twenty-six showing evident PMI-dependent increase (Donaldson & Lamont, 2015). These included eighteen amino acids, glutathione (GSH), 4-Amino-n-butyric acid (GABA), glyoxylate, oxalate, hydroxyproline, creatinine, α-ketoglutarate, and succinate (Donaldson & Lamont, 2015). The observed increase in these metabolites might reflect the breakdown of cellular structures and the subsequent release of intracellular components into the bloodstream as cells degrade. Further research by Pesko et al. (2020) extended these findings through untargeted metabolomic analysis of post-mortem rat and human muscle tissue using Liquid Chromatography – Mass Spectrometry (LC-MS). The study identified several metabolites, which were directly correlated with PMI, including skatole, xanthine, n-acetylneuraminate, 1-methyl nicotinamide, choline phosphate, uracil, threonine, tyrosine, and lysine (Pesko et al., 2020).

These metabolites are linked to various pathways such as protein catabolism, nucleic acid degradation, and energy metabolism, processes that are disrupted following death.

In addition to tissues, metabolomics has been applied to body fluids, such as vitreous humor (VH) and aqueous humor (AH) of the eye, for PMI estimation (Kurup et al., 2023; Locci et al., 2019, 2023). Studies have shown that the concentration of potassium ions ($[K^+]$) in these fluids increases predictably after death (Kurup et al., 2023; Locci et al., 2019, 2023). However, a comparative *ex vivo* study by Locci and colleagues (2021) found that metabolomic profiling of AH offered greater predictive power in estimating PMI within the first 24 hours post-mortem, compared to traditional $[K^+]$ measurements (Locci et al., 2021). Further, a study by Zelentsova et al. (2020) compared the metabolomic profile across human serum, AH, and VH by employing NMR spectroscopy, for estimating PMI. The study demonstrated a better positive correlation of key metabolites with PMI in AH and VH compared to human serum (Zelentsova et al., 2020). These metabolites included hypoxanthine, choline, creatine, betaine, glutamate, and glycine (Zelentsova et al., 2020). This suggests that the anatomically isolated body fluids such as AH and VH better reflect changes in metabolomic profile compared to human serum. Additionally, metabolomic analysis of pericardial fluid has shown promising results in PMI estimation. Chighine et al. (2023) demonstrated that the ^{1}H-NMR metabolomic profile of post-mortem pericardial fluid correlates well with PMI, particularly up to 100 hours post-mortem. The study highlighted the relevance of metabolites such as glycine, ethanolamine, and hypoxanthine in this context (Chighine et al., 2023).

Metabolites, such as hypoxanthine, a key metabolite in the disruption of energy-dependent purine catabolism within oxygen-deprived environments, serve as a marker of cellular energy depletion. Alongside hypoxanthine, the detection of glycerol and choline-products of lipid degradation, and taurine points to ongoing cytoprotective and antioxidative processes (Chouchani et al., 2014; Zelentsova et al., 2020, Locci et al., 2019). As choline levels progressively increase, this likely reflects the cumulative and irreversible hypoxic/ischemic damage to cellular membrane structures. The presence of other metabolites, including creatine, taurine, hypoxanthine, 3-hydroxybutyrate, creatinine, and phenylalanine, further suggests a metabolic shift (Bonicelli et al., 2022). This shift towards tricarboxylic acid (TCA) cycle anaplerosis (whereby

amino acid and ketone bodies are utilized as substrates), helps sustain ATP production during the early to mid-postmortem intervals (Bonicelli et al., 2022). These findings underscore the potential of pericardial fluids as a reliable matrix for PMI estimation, offering a complementary approach to more established methods.

While metabolomic analysis of various tissues and body fluids has shown promise, these matrices are subject to external and internal influences, such as temperature, humidity, geographical location, season, body structure of the deceased, age, and the cause of death. These factors can introduce variability in the metabolomic profile, further complicating PMI estimation. Therefore, a targeted approach focusing on specific tissues with unique anatomical and biochemical properties may offer a more reliable means of estimating PMI.

The pineal gland offers a promising alternative, as its deep intracranial location protects it from environmental fluctuations that could alter its metabolomic profile, and its critical role in the regulation of circadian rhythm through the synthesis and secretion of melatonin may provide time-dependent changes that are useful for estimating PMI. Given these unique properties, this study aims to investigate the metabolomic profile of the pineal gland, leveraging its physiological characteristics to develop a novel model for PMI estimation. In the following section, we will delve deeper into the biology, structure, and function of the pineal gland to better understand its potential for post-mortem metabolomic analysis.

4. The pineal gland: Structure, function, and its role in post-mortem interval (PMI) estimation

4.1. Biology and structure of the pineal gland

The pineal gland is a small, cone-shaped endocrine organ located deep within the brain, specifically in the epithalamus. Measuring about 5 to 8 mm in length, it is positioned between the two cerebral hemispheres and is attached to the roof of the third ventricle. Its deep intracranial location protects it from external environmental fluctuations such as temperature and humidity, which is critical for forensic applications. Histologically, the pineal gland is primarily composed of pinealocytes (~95%), the cells responsible for the rhythmic secretion of N-acetyl-5-

methoxytryptamine, commonly known as melatonin (Peruri et al., 2022). Other cell types include microglia, vascular and leptomeningeal cells (VLMCs), and endothelial cells (Olcese et al., 2019). The pineal gland is highly vascularized, allowing for efficient metabolic exchange, and contributing its distinct metabolomic profile. Over time, calcifications, often referred to as brain sand, accumulate in the gland, particularly in older individuals (Tan et al., 2018). The deep intracranial location and rich blood supply make the pineal gland an ideal tissue for post-mortem analysis, as it remains shielded from rapid environmental degradation, a common issue in other tissues used for forensic purposes.

4.2. Physiological functions: Melatonin secretion, circadian regulation, and metabolic activity

The primary function of the pineal gland is the production and secretion of melatonin, a hormone that regulates the body's circadian rhythms (Tan et al., 2018). The secretion of melatonin is primarily controlled by light exposure and follows a distinct day-night cycle. At night, the hypothalamic suprachiasmatic nucleus (SCN), a central circadian pacemaker, receives signals from the retina and prompts the pineal gland to produce melatonin, which peaks during the night and decreases in daylight (Arendt & Aulinas, 2022).

Melatonin synthesis is driven by the conversion of serotonin into melatonin via two key enzymes: arylalkyl amine N-acetyltransferase (AANAT), the rate-limiting enzyme in the synthesis of melatonin, and hydroxyindole-O-methyltransferase (HIOMT), which catalyzes the final step of the process (Masters et al., 2014). Given the pineal gland's role in circadian regulation, a metabolite involved in melatonin synthesis, serotonin, and AANAT, exhibits predictable patterns based on the time of day (Borjigin et al., 2011; Deguchi, 1979; Gastel et al., 1998). This diurnal rhythm provides an opportunity to investigate not only the time since death but also whether death occurred during the day or night, further enhancing the forensic applicability of the pineal gland. In addition to its role in regulating the sleep-wake cycle, melatonin possesses antioxidant properties, protecting cells from oxidative stress (Tan et al., 2007). It also modulates other physiological processes, including immune response (Moslehi et al., 2022) and energy metabolism (Owino et al., 2019). This robust physiological role suggests that melatonin and its

related metabolic pathways may degrade or shift in predictable ways post-mortem, making the pineal gland an excellent tissue for forensic investigation. Given the pineal gland's high metabolic activity, its metabolites are likely to undergo time-dependent changes following death. The concentrations of certain metabolites may either increase or decrease as cellular respiration ceases and autolysis begins, offering a measurable timeline that could correlate with the PMI (Chighine et al., 2023; Steuer et al., 2024). The pineal gland’s active participation in various metabolic pathways further supports its utility in forensic studies, as the shifts in its metabolomic profile may provide an accurate reflection of the time since death.

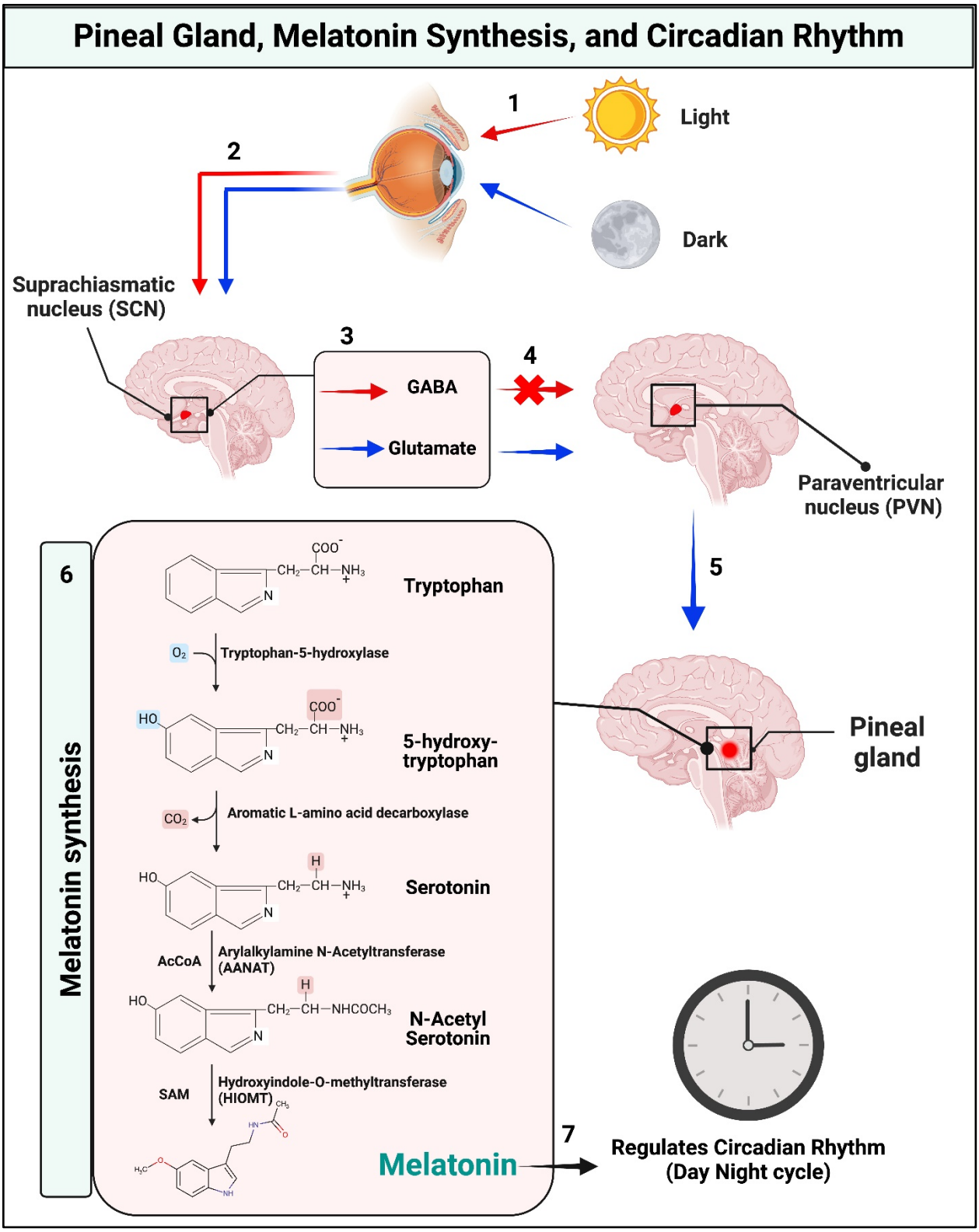

Figure 1: Schematic diagram for the melatonin synthesis by the Pineal gland the main modulator to regulate the circadian rhythm. (1) In the absence of light, **(2)** the suprachiasmatic nucleus (SCN) in the hypothalamus is activated, leading to the **(3)** release of glutamate and

inhibition of γ-aminobutyric acid (GABA) release. **(4)** This glutamate activates the paraventricular nucleus (PVN), which subsequently **(5)** stimulates the pineal gland to synthesize and release melatonin. **(6)** In the melatonin synthesis pathway, tryptophan is first converted to 5-hydroxytryptophan, which is then transformed into serotonin. Serotonin is further converted to N-acetylserotonin by the enzyme arylalkylamine N-acetyltransferase (AANAT), and finally into melatonin by hydroxyindole-O-methyltransferase (HIOMT). **(7)** The resulting melatonin is released into circulation, where it regulates circadian rhythms

2.1. Relevance of the pineal gland to post-mortem interval (PMI) estimation

One of the key challenges in PMI estimation is the variability introduced by external factors like temperature and humidity, which can affect the rate of decomposition (Shedge et al., 2023). However, due to its deep intracranial location and protection from the external environment, the pineal gland is less affected by these factors, making it a more stable matrix for forensic analyses compared to other tissues like blood or skin.

After death, the cessation of cellular processes leads to predictable biochemical changes. Many studies have investigated the circadian changes in the human pineal gland through genomics, transcriptomics, and proteomics approaches (Dumas et al., 2021; Olcese et al., 2019). For instance, research on rat pineal glands has revealed the differential expression of 604 genes between day-time and night-time (Bailey et al., 2009). Of great interest, AANAT was highly expressed during night-time along with other genes (Bailey et al., 2008). Similarly, proteomic analyses of rat pineal glands have demonstrated night-time upregulation of 25 different proteins, including enolase, creatine kinase, and annexin-V, which are involved in several cellular processes, such as glucose metabolism, the Krebs cycle, and energy transduction (Møller et al., 2007a). Importantly, annexin-V, a calcium-dependent membrane binding protein, forms voltage-dependent calcium channels which are essential for the nocturnal increase in AANAT activity (Zawilska & Nowak, 1990). Interestingly, in humans, proteomic studies have identified the upregulation of several glycolytic enzymes, such as 6-phosphofructokinase, glyceraldehyde 3-phosphate dehydrogenase, and hexokinase-1, during the day-time. On the contrary, multiple metabolic proteins, such as enolase-1, lactate dehydrogenase, 6-phosphogluconolactonase, and ATP synthase subunit O were upregulated during night-time (Dumas et al., 2021). These circadian rhythmic changes provide further evidence that the time of death can be inferred based on the

metabolic state of the pineal gland at the time of autopsy. A study by Ackermann and colleagues (2006) found a direct correlation between the time of death, AANAT activity, and melatonin content, with higher levels observed in night-time post-mortem pineal glands (Ackermann et al., 2006). This supports the idea that melatonin and its related metabolites degrade in a time-dependent manner after death, offering a reliable means of PMI estimation.

Overall, the pineal gland's unique combination of anatomical protection, circadian regulation, and active metabolic involvement makes it a compelling tissue for forensic analysis. Its location shields it from environmental factors that can confound traditional PMI estimation methods, and its role in melatonin production provides a time-dependent marker that correlates with both the time of death and the PMI. By leveraging the metabolomic profile of the pineal gland through advanced techniques like ^{1}H-NMR spectroscopy, this study aims to develop a robust model for accurately estimating the PMI, which could offer enhanced precision compared to traditional forensic methods, offering new insights into forensic investigations.

AIMS AND OBJECTIVES

Aim

The primary aim of this research is to conduct a comprehensive metabolomic profiling of post-mortem human pineal glands using ^{1}H-Nuclear Magnetic Resonance (NMR) spectroscopy, to explore metabolic changes associated with post-mortem interval (PMI). This study also seeks to determine how various intrinsic and extrinsic factors, such as time of death (day vs. night), age, gender, weight of the pineal gland, and seasonal variation, may influence the metabolomic profile of the pineal gland. The ultimate goal is to establish a model that may provide an accurate determination of PMI.

Objectives

1. To evaluate the metabolic difference between the two sagittal sections of the pineal gland using ^{1}H-NMR spectroscopy.
2. To assess the impact of interindividual factors (e.g. age, gender, and weight of the pineal gland) and external factors (e.g. season at the time of death) on the pineal gland's metabolic profile.
3. To identify metabolomic differences between deaths occurring during day-time versus nighttime, including an analysis of pathways significantly affected by the time of death.
4. To correlate the metabolomic profile of the pineal gland with post-mortem interval (PMI) for potential PMI estimation, and to identify key metabolic pathways associated with PMI using pathway analysis.

MATERIALS AND METHODS

1. Pineal gland collection

Human pineal glands were collected during consecutive judicial autopsies (n=15) performed at the Forensic and Legal Medicine Institute of the University of Cagliari, Cagliari, Italy. All subjects were selected in accordance with standard forensic protocols and ethical guidelines.

Following routine brain extraction during the autopsy, the brainstem and cerebellum were carefully detached from a mesencephalic section, which provided visibility of the pineal gland. The gland was identified from beneath and excised through a precise section at its base. Immediately following its isolation, the pineal glands were snap-frozen in liquid nitrogen and stored at -80°C until further analysis to preserve their morphology and metabolic integrity.

2. Metabolite Extraction of Pineal glands

Prior to the experiment, pineal glands were thawed on ice and weighed. The weights of the pineal gland samples were consistent across the population range for pineal glands and are reported in **Table 2**, along with the demographic data of the corresponding individuals. Each pineal gland was then bisected into two equal sagittal sections (A and B) using a sterile scalpel. Each section was subsequently weighed to ensure accurate sample quantification for further metabolomic analysis.

As described in **Figure 2 (Section 1)**, the extraction procedure for the metabolomic analysis was performed by liquid-liquid extraction (LLE) method. Briefly, each sagittal section of the pineal gland was homogenized in an ice-cold solution of 600 µl of methanol (HPLC grade, Honeywell, Germany) using a Tissue Lyser equipment (Tissuelyser 2, Qiagen, Hilden, Germany). Then 400 µl of Milli-Q water and 600 µl of chloroform (HPLC grade, Honeywell, Germany) were added to each sample. After homogenization, the mixture was subjected to sonication for 30 minutes then incubated for 20 minutes at -20^{o}C, then centrifuged for 10 minutes at 8600g at 4^{o}C to separate the binary phase. The polar phase (aqueous) contained hydrophilic metabolites, while the non-polar phase (organic) contained lipophilic metabolites. At last, the supernatants (hydrophilic phase) were carefully collected in Eppendorf tubes. 600 µl of the hydrophilic supernatant phases

were dried under vacuum overnight using a Speed Vacuum concentrator (Eppendorf concentrator plus, Eppendorf AG, Hamburg, Germany) (Murgia et al., 2020).

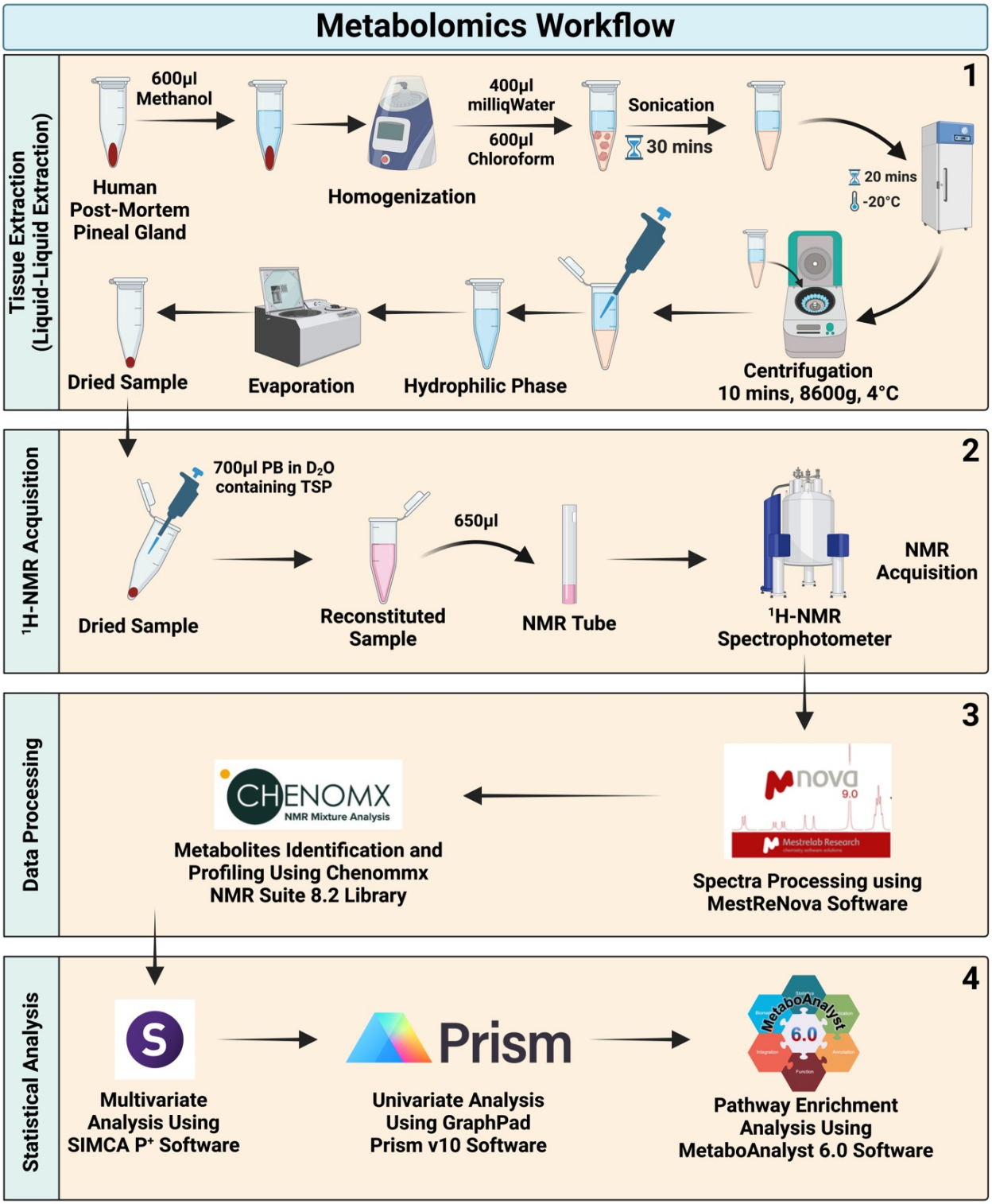

Figure 2: Schematic representation of the metabolomics workflow. (1) Tissue extraction: **(2)** Sample preparation and NMR acquisition, **(3)** Data processing, and **(4)** Statistical analysis.

Abbreviations: TSP, Trimethylsilylpropanoic acid (internal standard for NMR); NMR, Nuclear Magnetic Resonance; SIMCA, Soft Independent Modeling of Class Analogy (software for multivariate statistical analysis); PB, Phosphate buffer; D_2O, Deuterium oxide (heavy water, used as an NMR solvent); MestReNova, Software for NMR spectral processing.

3. Sample preparation for NMR analysis

The dried samples were subsequently reconstituted with 700 µl of a 0.05 M phosphate buffer (PB) solution (pH 7.4) in D_2O (99.9%, Cambridge Isotope Laboratories Inc., Andover, USA) containing the internal standard sodium 3-(trimethyl- silyl)propionate-2,2,3,3,-d4 (TSP, 98 atom % D, Sigma- Aldrich, Milan) at a 0.2 mM final concentration. 650 µl of the resulting solution was transferred into a 5 mm NMR tube for ^{1}H-NMR spectroscopic analysis (Locci et al., 2021) **(Figure 2, Section 2)**.

4. ^{1}H-NMR experiments and data processing

The reconstituted pineal gland samples were analyzed using ^{1}H-NMR spectroscopy to identify and quantify metabolites **(Figure 2, Section 2)**. ^{1}H-NMR experiments were conducted on a Varian UNITY INOVA 500 spectrometer operating at 499.839 MHz for proton measurement, equipped with a 5 mm double-resonance probe (Agilent Technologies, CA, USA). Spectra were acquired at 300K with a spectral width of 6000 Hz, a 90° pulse, an acquisition time of 2 seconds, a relaxation delay of 2 seconds, and 256 scans. A standard *presat* pulse sequence was used to suppress the residual water signal by applying a low-power radiofrequency irradiation for 2 seconds during relaxation delay.

Spectra were processed using MestReNova software (Version 9.0, Mestrelab Research S.L.) **(Figure 2, Section 3)**. Prior to Fourier transformation, free induction decays (FID) were multiplied by an exponential weighting function equivalent to a line broadening of 0.5 Hz and zero-filled to 128K. All spectra were phased, baseline corrected, and referenced to the TSP peak at 0.00 ppm. The spectral region 0.80 – 9.00 ppm was segmented into consecutive bins of 0.01 ppm width. The integrated area within each bin was normalized to a constant sum of 100 for each spectrum to minimize differences in sample concentrations. The spectral region containing the residual

water signal and the regions containing the resonances of exogenous molecules (ethanol) were excluded before from the integration process. Metabolite assignments in the ^{1}H-NMR spectra were performed based on literature data (HMDB database), Chenomx NMR Suite 8.2 Library (Chenomx Inc., Edmonton, Canada), and comparison with spectra of standard compounds recorded under the same experimental conditions. Using the Chenomx NMR Suite Profiler tool, the metabolites of each spectrum were profiled (reported in **Table 3**) and normalized to the weight of the pineal gland sample. The final data sets (both the binned and the profiled one) were submitted to multivariate statistical analysis after applying mean centering and Pareto scaling (Locci et al., 2021).

5. Multivariate and Univariate Data Analysis

To analyze the metabolomic data obtained from ^{1}H-NMR spectroscopy and to explore data patterns, classify sample groups, and correlate metabolite profiles with PMI, a combination of unsupervised and supervised multivariate statistical methods was employed **(Figure 2, Section 4)**. Principal Component Analysis (PCA), an unsupervised dimensionality reduction technique, was used as an exploratory method to visualize the overall structure of the dataset. PCA was applied to identify specific trends, such as metabolomic differences between pineal gland samples, and detect potential outliers within the dataset. To further investigate and classify the samples based on predefined groups, supervised Orthogonal Partial Least Squares Discriminant Analysis (OPLS-DA) was employed. This supervised method maximized separation between groups (e.g., daytime vs. night-time deaths) and identified metabolites responsible for the observed differences. In addition, OPLS regression was used to explore the correlation between the metabolomic profiles of the pineal gland samples and the PMI. To ensure the robustness and generalizability of the multivariate models, 7-fold cross-validation was performed. To test for overfitting, permutation testing (n = 500) was conducted. The following criteria were to assess model significance: (a) Q^2(cum) for the model should be larger than all the results from permuted models, (b) the y-intercept of the Q^2(cum) fit should be negative, and (c) R^2Y(cum) for the model should be larger than all the results from permuted models. All multivariate statistical analyses were performed using SIMCA P+ software (Version 14.0, Umetrics, Malmo, Sweden). Outputs

from the analyses included score plots of the samples, loading plots, and S-plots of the variables (metabolites), which were used to interpret the results and identify key metabolites contributing to group separations or correlations with PMI.

For univariate statistical analysis, identified metabolites were analyzed using GraphPad Prism 10.0 software **(Figure 2, Section 4)**. To compare metabolite concentrations between day-time and night-time groups, the Mann-Whitney t-test was applied. To investigate correlations between PMI and metabolite concentrations, Pearson's correlation test was used.

6. Pathway enrichment analysis using MetaboAnalyst

The pathway enrichment analysis was performed using the MetaboAnalyst 6.0 (https://www.metaboanalyst.ca/MetaboAnalyst/ModuleView.xhtml), a web-based platform to identify metabolic pathways significantly impacted by the metabolomic changes observed in the pineal gland **(Figure 2, Section 4)**. Prior to analysis, metabolomic data was pre-processed using specific parameters: normalization by sum, no data transformation, and Pareto scaling (mean-centered and divided by the square root of the standard deviation of each variable). These steps helped to account for differences in metabolite concentrations while highlighting biologically relevant variations across the dataset. Once the data was normalized and scaled, the metabolite concentrations were uploaded into MetaboAnalyst in a .csv format. Metabolites were mapped to the KEGG (Kyoto Encyclopedia of Genes and Genomes) database for human pathways, ensuring comprehensive coverage of human metabolism. Any unmatched metabolites were manually cross-referenced using databases like HMDB and PubChem to ensure accurate mapping.

The pathway enrichment analysis was then conducted, which involved calculating the enrichment score for the top 25 pathways based on the number of metabolites that were significantly altered relative to the total number of metabolites in that pathway. The results were visualized in an enrichment plot, where the x-axis represented the p-values for each pathway, and the size of the circles (bubbles) reflected the enrichment ratio, with larger bubbles corresponding to pathways with higher enrichment scores.

Additionally, a network analysis was performed to explore potential interactions between these enriched pathways. Nodes in the network plot represented individual metabolic pathways, and edges (lines) connecting the nodes indicated relationships based on shared metabolites or metabolic functions. This provided a broader perspective on how metabolic shifts related to PMI are interconnected at a systemic level. All the results from MetaboAnalyst, including enrichment tables, pathway plots, and network diagrams, were exported for further analysis. Only pathways having p-value < 0.05 were considered for the discussion and biological interpretation.

RESULTS

1. Overview of sample characteristics and metabolomic profiling of pineal glands

The pineal glands were collected from corpses of both genders, with an approximately equal distribution (1:1 ratio), aged between 20 and 76 years (mean age = 57.2 ± 14.8 years). The post-mortem interval (PMI) ranged from 1.5 days (44 hours) to 9 days (219 hours). Of the 15 cases studied, nine deaths occurred during day-time (D), and six during night-time (N). The pineal glands were classified into D and N groups based on the interval between sunrise and sunset, as determined by the specific date and season in Cagliari, Italy (GMT+1). The demographic parameters of the studied individuals and characteristics of pineal gland samples are summarized in **Table 2**.

Individual	Sex	Age (years)	Batch	Death at D/N	Time of death (hr)	Season at time of Death	Month of Death	PMI (hr)	PG total weight (mg)	PG section A (weight %)	PG section B (weight %)
1	F	67	1	D	07:20	Summer	June	57.17	139.8	40.4	59.6
2	M	77	1	D	17:50	Summer	April	167.73	93.8	51.5	48.5
3	F	61	1	N	03:30	Winter	March	64	36.7	53.1	46.9
4	M	57	1	D	18:00	Winter	March	49.5	76.1	29.2	70.8
5	F	61	1	D	15:15	Winter	March	219.3	252.8	57.2	42.8
6	F	57	1	N	03:00	Winter	February	61.15	130	56.9	43.1
7	M	63	1	D	20:20	Summer	June	44.83	56	48.2	51.8
8	M	49	1	D	12:30	Winter	November	74.62	127	47.2	52.8
9	F	43	1	D	18:20	Summer	July	98.17	146	63.7	36.3
10	F	77	1	D	18:10	Summer	July	163.23	121	52.9	47.1
11	M	61	1	D	17:30	Winter	November	190.5	375	32.8	67.2
12	F	55	1	N	00:00	Summer	June	65	15	46.7	53.3
13	M	20	1	N	05:30	Summer	May	61.5	48	45.8	54.2
14	M	70	1	N	03:00	Winter	March	70	110	54.5	45.5
15	F	40	1	N	22:45	Winter	October	85.75	107	51.4	48.6

Table 2: Demographic characteristics of the studied individuals and characteristics of corresponding pineal glands. Abbreviations: F: Female, M: Male, D: Day, N: Night, PG: Pineal Gland.

Metabolomic profiling of collected pineal glands was performed using ^{1}H-NMR spectroscopy, and the data processing and normalization were conducted with MestReNova software **(**as described in Materials and Methods, Section 5**)**. A total of 44 metabolites were identified and profiled using the Chenomx NMR Suite Profiler tool **(Table 3)**. These include amino acids, amines, purine, and

pyrimidine derivatives, as well as intermediates of the tricarboxylic acid (TCA) cycle and other organic acids, which belong to a broad range of metabolic classes.

Compound	PubChem (CID)	Compound	PubChem (CID)
4-Aminobutyrate	119	Leucine	6106
Acetate	176	Lysine	5962
Alanine	5950	Methionine	6137
Asparagine	6267	myo-Inositol	892
Aspartate	5960	N-Acetylaspartate	65065
Betaine	248	N-Methylhydantoin	69217
Choline	305	O-Phosphocholine	1014
Creatine	586	Ornithine	6262
Creatinine	588	Phenylalanine	6140
Ethanolamine	700	Proline	145742
Formate	284	Serine	5951
Fumarate	723	Succinate	1110
Glucose	5793	Taurine	1123
Glutamate	33032	Threonine	6288
Glutamine	5961	Trimethylamine	1146
Glycerol	753	Tryptophan	6305
Glycine	750	Tyrosine	6057
Histidine	6274	Uracil	1174
Hypoxanthine	790	Uridine	6029
Inosine	6021	Valine	6287
Isoleucine	6306	Xanthine	1188
Lactate	107689	sn-Glycero-3-phosphocholine	439285

Table 3: List of metabolites identified from ^{1}H-NMR spectra of the post-mortem human pineal glands. Abbreviations: NMR, Nuclear Magnetic Resonance.

2. Metabolomic comparison of the two sagittal sections of the pineal gland

To evaluate potential metabolic differences between the two sagittal sections of the post-mortem human pineal gland, independent ^{1}H-NMR metabolomic profiling was performed. Principal Component Analysis (PCA) was applied to both binned and profiled datasets to explore

potential metabolic variation, with corresponding loading plots used to identify the metabolites contributing to the observed variance.

The PCA score scatter plot obtained from the binned data showed no evident separation between the two sagittal sections, indicating a high degree of similarity in their metabolic profiles **(Figure 3A)**. However, notable interindividual variation was observed, with the first three principal components (PCs) explaining 73.1% of the total variance **(Figure 3A)**. This high percentage suggests that the majority of the metabolic differences in the dataset are effectively captured by these components of two sagittal sections. The corresponding PCA loading plot shows the distribution of metabolites contributing to the variance observed in the pineal gland samples **(Figure 3B)**.

Further, profiled ^{1}H-NMR data were analyzed to provide a more detailed view of the individual metabolites rather than the segmented spectral bins. The PCA score scatter plot derived from the profiled data demonstrated no discernible separation between the two sagittal sections, with the first three components explaining 71.8% of the total variance **(Figure 3C)**. This suggests that the metabolomic profiles of the two sections are highly similar, with most of the metabolic variability accounted for by these components. The loading plot shows the distribution of individual metabolites within the samples **(Figure 3D)**.

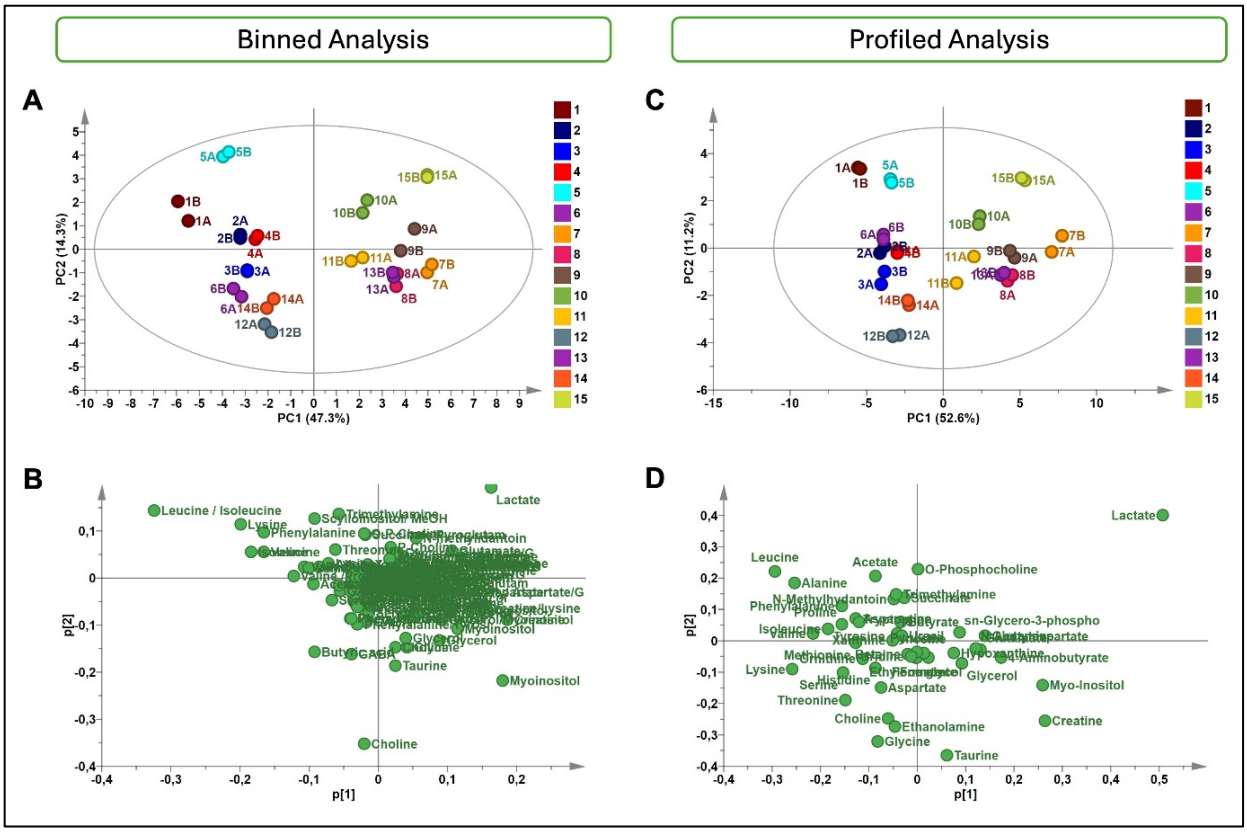

Figure 3: Principal Component Analysis (PCA) found no notable metabolic differences between the two sagittal sections of post-mortem human pineal glands. (A, C) Score scatter plot of (PC1 versus PC2, representing sections A and B from the two sagittal sections of the pineal gland. Scores are color-coded based on individual pineal glands and labelled by two sagittal sections. Score scatter plot obtained from **(A)** Binned data (A = 3, total variance = 73.1%), and **(C)** profiled data (A = 3, total variance = 71.8%). **(B, D)** Loading plot obtained from **(B)** binned data, and **(D)** profiled data, highlighting the metabolites contributing to the sample distribution observed in the score plot.

3. Effects of weight of the pineal gland on its metabolomic profile

To explore whether the weight of the pineal gland influences its metabolic profile, we stratified the pineal glands based on their respective weights and employed PCA. The PCA score scatter plot generated from the binned data revealed no appreciable differences in the distribution of samples based on the weight of the pineal gland **(Figure 4A)**. This suggests that the metabolic profiles of the pineal glands are independent of their weights. Similarly, the PCA score scatter plot derived from the profiled data showed minimal separation between samples of varying

weights **(Figure 4B)**, suggesting that weight is not a critical factor influencing the metabolic composition of the pineal gland.

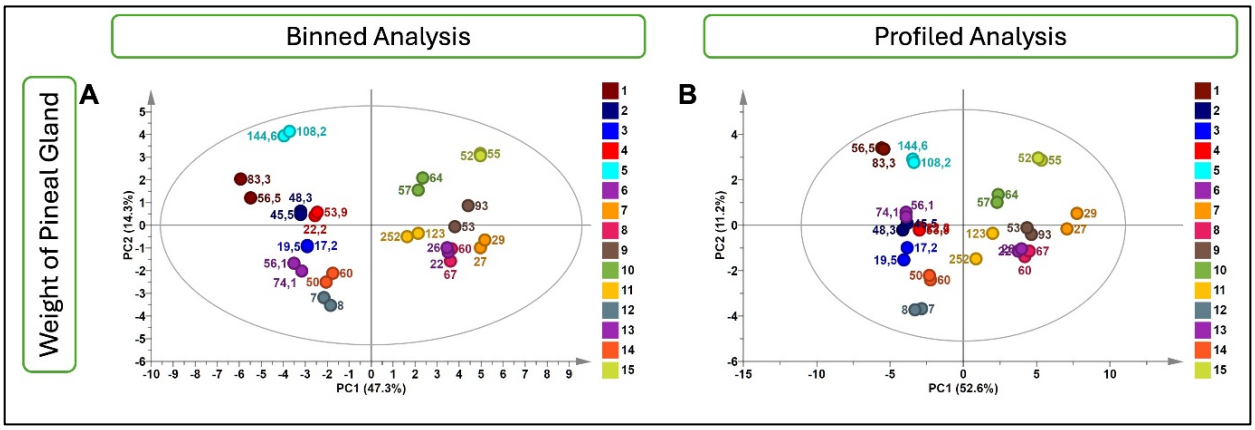

Figure 4: Principal component analysis (PCA) analyses revealed no major metabolic differences in the pineal glands based on the weight of the pineal gland. (A, B) PCA model: Score scatter plot of PC1 versus PC2 for pineal gland samples, representing two sagittal sections from individual pineal glands. Scores are color-coded by the individual pineal gland and labelled by their respective weight. Score scatter plot obtained from **(A)** binned data (A = 3, total variance = 73.1%), and **(B)** profiled data (A = 3, total variance = 71.8%).

4. Effects of gender on the pineal gland's metabolomic profile

To investigate whether gender influences the metabolomic profile of the pineal gland, we stratified the samples by gender. PCA and supervised OPLS-DA were utilized to assess whether the metabolic differences between male and female individuals were substantial.

The PCA score scatter plot generated from the binned data revealed no major separation between male and female pineal gland samples **(Figure 5A)**. Subsequent OPLS-DA yielded R^2 = 0.39 and Q^2 = 0.15 **(Figure 5B)**, indicating relatively low predictive power and model fit, suggesting minimal metabolic differences between male and female samples in the binned dataset.

Similarly, the PCA score scatter plot from the profiled dataset also showed minimal separation between male and female samples, consistent with the binned dataset analysis **(Figure 5C)**. The corresponding OPLS-DA model for the profiled data provided R^2 = 0.36 and Q^2 = 0.13 **(Figure 5D)**, suggesting only marginal predictive power and a moderate model fit. Collectively, the above

findings suggest that gender has only a minor influence on the metabolomic profile of the pineal gland, with no substantial differences observed in either the binned or profiled datasets.

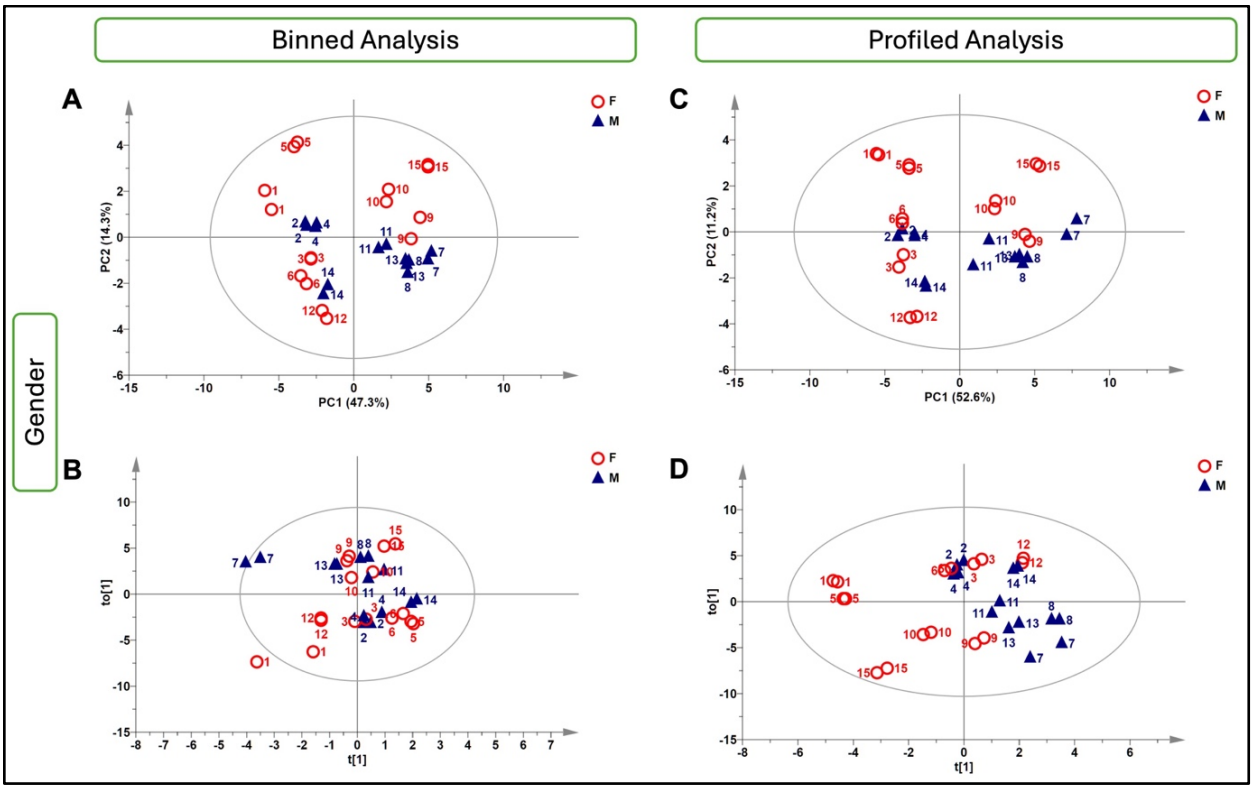

Figure 5: Principal component analysis (PCA) and Orthogonal Partial Least Squares Discriminant Analysis (OPLS-DA) revealed no significant metabolic differences in the pineal glands based on gender. (A, C) PCA model: Score scatter plot of PC1 versus PC2 for pineal gland samples, representing two sagittal sections from individual pineal glands. Scores are color-coded by gender and obtained from **(A)** binned data (A = 3, total variance = 73.1%), and **(C)** profiled data (A = 3, total variance = 71.8%). **(B, D)** OPLS-DA score scatter plot based on gender obtained from **(B)** binned data (A=1+1, R^2Y= 0.39, Q^2Y = 0.15), and **(D)** profiled data (A=1+1, R^2Y= 0.36, Q^2Y = 0.13).

5. Effects of age on the pineal gland's metabolomic profile

To study whether age influences the metabolomic profile of the pineal gland, we classified the samples based on the age of the individuals, and PCA and OPLS regression were used to evaluate the potential correlations between age and metabolic variation.

The PCA score scatter plot derived from the binned data revealed no clear separation between samples based on age **(Figure 6A)**. The distribution of the samples suggests that the metabolic

profiles of the pineal glands are largely independent of age, as no distinct clustering or trends were observed. To explore this further, OPLS regression was applied to the binned dataset, providing R^2 = 0.52 and Q^2 = 0.142 **(Figure 6B)**. These indicate that while the model fit is moderate, the predictive power is weak.

The PCA score scatter plot from the profiled dataset also demonstrated minimal separation between samples of different ages **(Figure 6C)**. The corresponding OPLS regression plot for the profiled dataset provided R^2 = 0.54 and Q^2 = 0.32 **(Figure 6D)**. These values reflect a slight improvement in both fit and predictive power compared to the binned dataset, likely due to the reduced noise and enhanced robustness of the profiled data. Overall, the results suggest that minor age-related variations may exist in specific metabolites, and future studies with larger cohorts are needed to validate these findings and determine the potential influence of age with greater confidence.

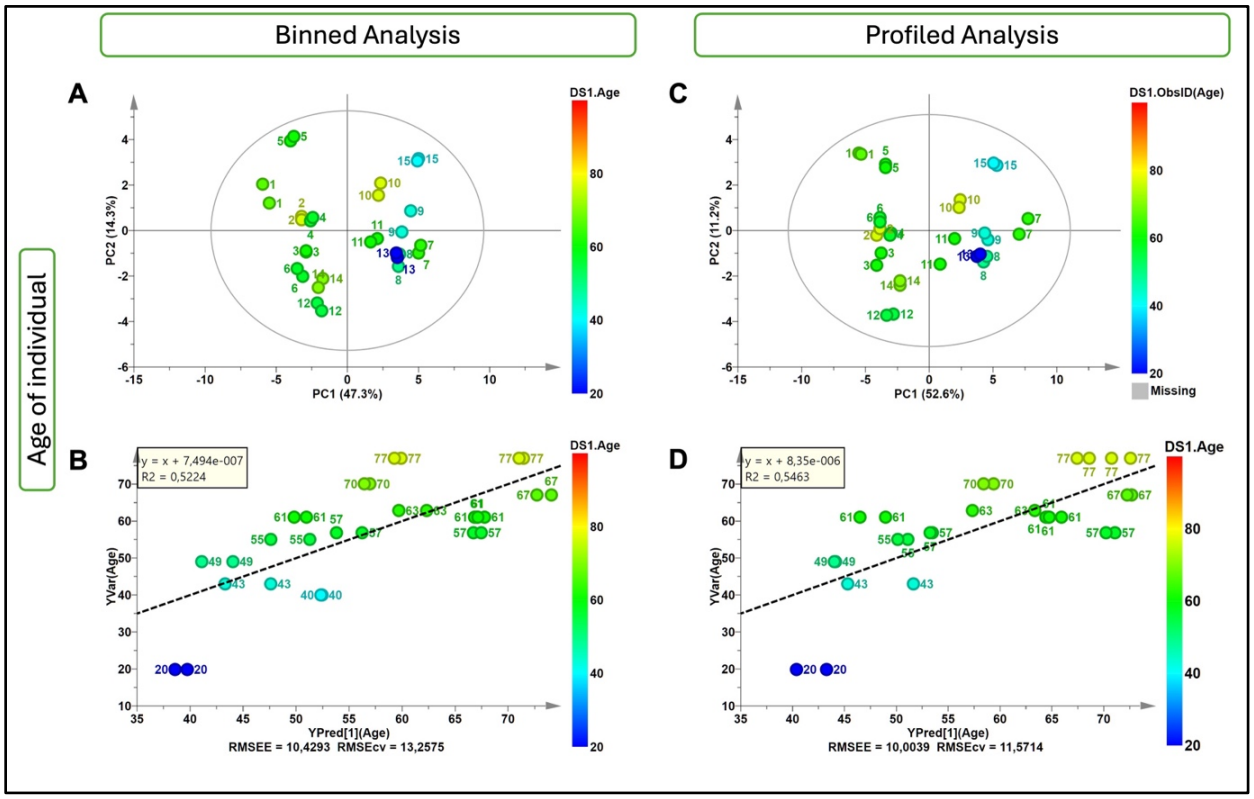

Figure 6: Principal component analysis (PCA) and Orthogonal partial least squares (OPLS) analyses revealed no significant metabolic differences in the pineal glands based on age. (A, C) PCA model: Score scatter plot of PC1 versus PC2 for pineal gland samples, representing two sagittal sections from individual pineal glands. Scores are color-coded by age of individuals of

the respective pineal gland and obtained from **(A)** binned data (A = 3, total variance = 73.1%), and **(C)** profiled data (A = 3, total variance = 71.8%). **(B, D)** OPLS regression curve based on the age of individuals of respective pineal glands (samples are labelled by age of individual of the respective pineal gland) obtained from **(B)** binned data (R^2Y= 0.52, Q^2Y = 0.142), and **(D)** profiled data (R^2Y= 0.54, Q^2Y = 0.32).

6. Effects of season at the time of death on the pineal gland's metabolomic profile

Next, we evaluated the effect of the season at the time of death on the metabolic profile of the pineal gland. For this purpose, we stratified the samples based on the season (summer-April through September vs. winter-October through March) and utilized PCA and supervised OPLS-DA to detect if metabolic differences were affected by season at the time of death.

The PCA score scatter plot obtained from the binned data showed no distinct separation between the samples based on the season (summer vs. winter) **(Figure 7A)**. The OPLS-DA plot for the binned data provided R^2 = 0.49 and Q^2 = 0.19 **(Figure 7B)**, reflecting low predictive power and a moderate model fit.

In addition, the PCA score scatter plot from the profiled data demonstrated no marked differences between samples from summer and winter groups **(Figure 7C)**. The OPLS-DA plot for the profiled data provided R^2 = 0.58 and Q^2 = 0.32 **(Figure 7D)**, further supporting the results that seasonal differences do not exert a significant influence on the metabolomic composition of the pineal gland. However, the Q^2 value for the profiled data is higher than that for the binned data, suggesting that minor season-related variations may exist in the metabolomic profile of pineal glands, and future studies with larger cohorts are needed.

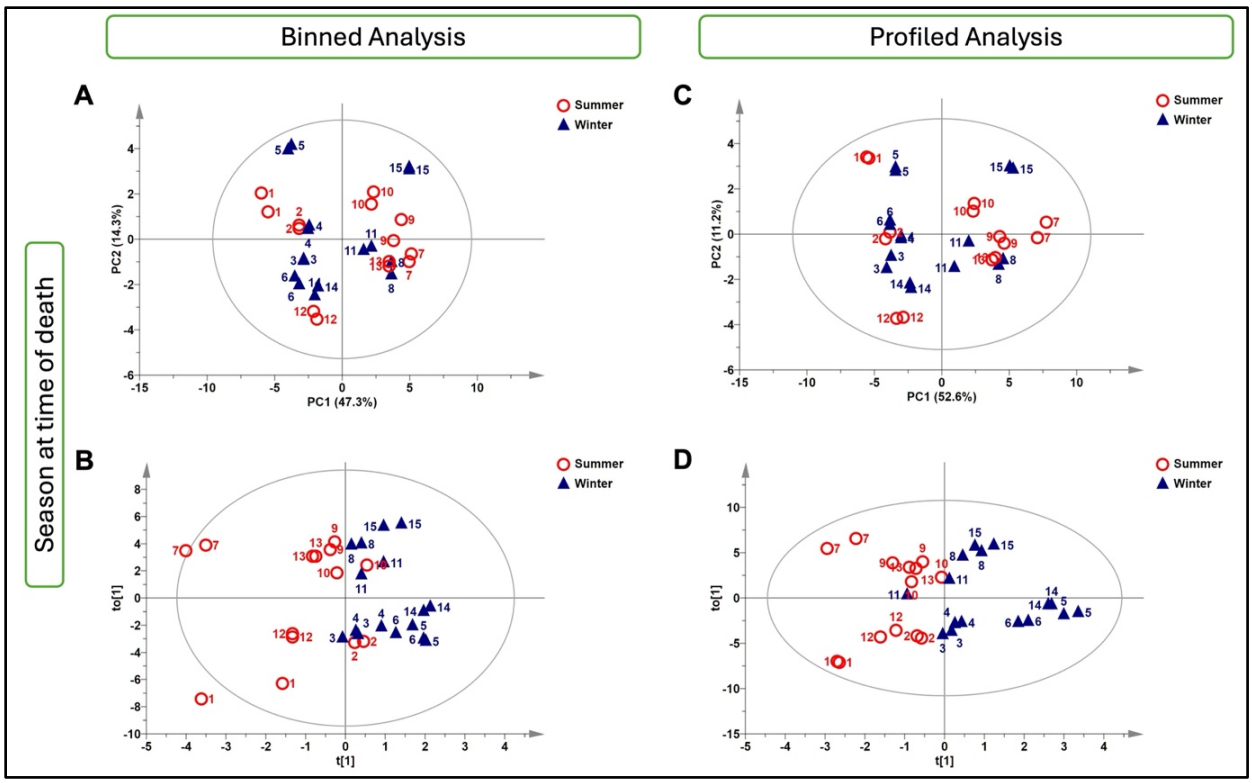

Figure 7: Principal component analysis (PCA) and Orthogonal partial least squares (OPLS) analyses revealed no significant metabolic differences in the pineal glands based on season at the time of death. (A, C) PCA model: Score scatter plot of PC1 versus PC2 for pineal gland samples, representing two sagittal sections from individual pineal glands. Scores are color-coded by season at the time of death (Summer: April to September, Winter: October to March), and obtained from **(A)** binned data (A = 3, total variance = 73.1%), and **(C)** profiled data (A = 3, total variance = 71.8%). **(B, D)** OPLS-DA score scatter plot based on the season at the time of death obtained from **(B)** binned data (A=1+1, R^2Y= 0.49, Q^2Y = 0.19), and **(D)** profiled data (A=1+1, R^2Y= 0.58, Q^2Y = 0.32).

7. Metabolomic differences between day-time and night-time deaths

Next, we investigated the metabolic differences between deaths occurring during day-time and night-time, by categorizing samples based on the time of death. ^{1}H-NMR metabolomic analysis was conducted on both binned and profiled datasets and PCA and OPLS-DA were used to assess separation between the two groups, followed by a predictive loading plot to identify key metabolites distinguishing day-time from night-time deaths.

In the PCA score scatter plot derived from the binned dataset, a clear separation between the day-time and night-time groups is evident **(Figure 8A)**. However, two samples from the N group,

samples 13 and 15, clustered with the day-time group in the multivariate space **(Figure 8A)**. Further forensic review revealed possible explanations for these outliers: sample 13 was involved in a night-time assault (~05:00 AM) and engaged in a struggle, which may have disrupted the individual's circadian rhythm and influenced the metabolomic profile. The individual with sample 15 was hospitalized in an intensive care unit (ICU), who may have had their circadian rhythm affected by the continuous artificial lighting present in the ICU, which mimics daylight, ultimately affecting metabolomic profile. Following the PCA, OPLS-DA was applied to the binned dataset to further assess the separation between day-time and night-time deaths **(Figure 8B)**. The analysis provided a model with $R^2Y = 0.51$ and $Q^2Y = 0.28$, indicating a moderate model fit and weak predictive power. The R^2 value represents the goodness of fit of the model, while the Q^2 value reflects its predictive ability. Despite the overall clear separation between the day-time and night-time groups, samples 13 and 15 continued to cluster with the day-time group, confirming the potential influence of light on these individuals' metabolomic profiles **(Figure 8B)**. The predictive loading plot for the binned dataset identified lactate as a key metabolite elevated during day-time deaths, while choline and taurine were elevated during night-time deaths **(Figure 8C)**.

In the PCA score plot derived from the profiled dataset, a similar clear separation was observed between the day-time and night-time groups **(Figure 8D)**. However, samples 13 and 15 again clustered with the day-time group. The OPLS-DA analysis on the profiled data also showed separation between the day-time and night-time groups, with a model fit of $R^2Y = 0.47$ and $Q^2Y = 0.19$, again indicating weak predictive power **(Figure 8E)**. As with the binned analysis, samples 13 and 15 did not follow the expected pattern for night-time deaths and continued to cluster with the day-time group **(Figure 8E)**. In the predictive loading plot generated from the profiled dataset, the similar trend of metabolic differences between day-time and night-time deaths were observed **(Figure 8F)**. Lactate was significantly higher in day-time deaths, while choline and taurine remained elevated in night-time deaths **(Figure 8F)**. These consistent metabolomic shifts across both the binned and profiled datasets further support the hypothesis that specific metabolites, particularly lactate, choline, and taurine, play critical roles in distinguishing between deaths occurring during the day-time or night-time.

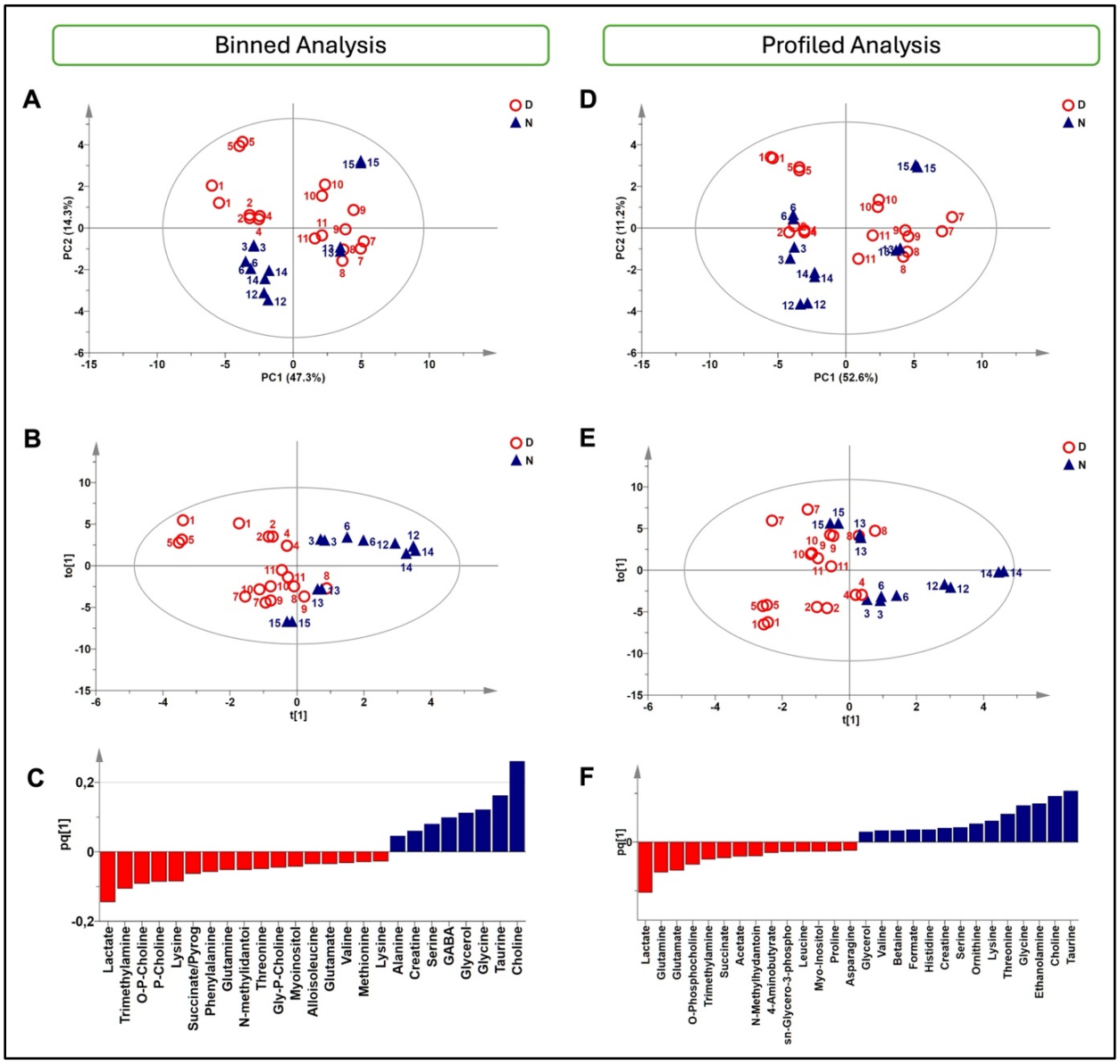

Figure 8: Principal component analysis (PCA) and Orthogonal partial least squares discriminant analysis (OPLS-DA) revealed clear metabolomic distinctions between day-time (D) and night-time (N) deaths. (A, D) PCA model: Score scatter plot of PC1 versus PC2 for pineal gland samples, representing two sagittal sections from individual pineal glands. Scores are color-coded by time of death (D = death occurred during day-time and N = death occurred during night-time) and obtained from **(A)** binned data (A = 3, total variance = 73.1%), and **(D)** profiled data (A = 3, total variance = 71.8%). **(B, E)** OPLS-DA score scatter plot based on time of death obtained from **(B)** binned data (A=1+1, R^2Y= 0.51, Q^2Y = 0.28), and **(E)** profiled data (A=1+1, R^2Y= 0.47, Q^2Y = 0.19). **(C, F)** Predictive loading plot of metabolites obtained by the OPLS-DA model from **(C)** binned data, and **(F)** profiled data.

Next, to further investigate the behavior of samples 13 and 15, we reclassified these two samples as belonging to the day-time group in both the binned and profiled datasets and OPLS-DA modeling was reperformed. This reclassification resulted in an improved model with R^2Y= 0.75, Q^2Y = 0.64 for the binned dataset **(Figure 9A)** and R^2Y= 0.70, Q^2Y = 0.58 for the profiled dataset **(Figure 9B)**. These improved values indicate a better model fit and stronger predictive power, suggesting that the metabolomic profiles of these samples are more reflective of light exposure (light vs. dark) rather than strictly the time of death (day vs. night). The predictive loading plot for both the binned and profiled dataset identified lactate as a key metabolite elevated during day-time deaths, while choline (in both datasets) and lysine (in the profiled dataset) were elevated during night-time deaths **(Figure 9C, D)**.

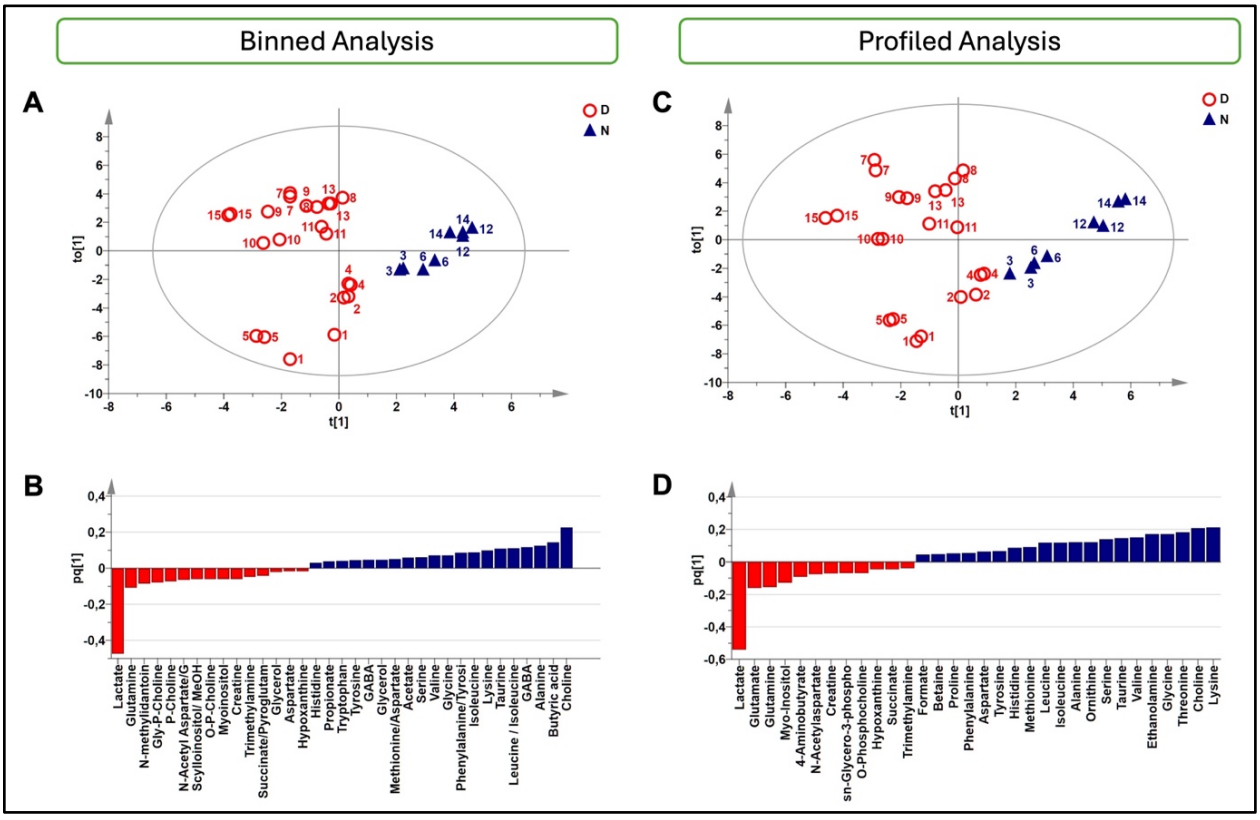

Figure 9: **Orthogonal partial least squares discriminant analysis (OPLS-DA) revealed clear metabolomic distinctions between day-time (D) and night-time (N) deaths, samples 13 and 15 were reclassified as belonging to the D group. (A, C)** OPLS-DA score scatter plot based on time of death obtained from **(A)** binned data (A=1+1, R^2Y= 0.75, Q^2Y = 0.64), and **(C)** profiled data (A=1+1, R^2Y= 0.70, Q^2Y = 0.58). **(B, D)** Predictive loading plot of metabolites obtained by the OPLS-DA model from **(B)** binned data, and **(D)** profiled data.

Next, to ensure the robustness of the OPLS-DA model and to rule out overfitting, a permutation test with 500 permutations was performed. The significance of the model was assessed through 500 applications in which some Q^2 values of permuted Y vectors were equal to the original one and the regression of the Q^2 line had an intercept below zero (−0.38) for both binned and profiled spectra **(Figure 10A, C)**. However, when the permutation test was reperformed with the new OPLS-DA models (where samples 13 and 15 were reclassified as a day-time group), the results showed substantial improvements. The Q^2 values of the permuted Y vectors were lower than the original one and the regression Q^2 line had an intercept below zero (-0.45 for binned data and -0.44 for profiled data) **(Figure 10B, D)**. These findings demonstrate that the reclassified models are not overfitted and exhibit better predictive validity. The observed Q^2 values in the reclassified models indicate enhanced predictive power, confirming that the separation between day-time and night-time deaths is statistically significant and not due to random variation. The improved results from the permutation test further validate the OPLS-DA models and reinforce the conclusions that metabolomic differences between the two groups (day-time and night-time deaths) are robust and reliable in both binned and profiled datasets.

Given that the reclassified models (with samples 13 and 15 assigned to the day-time group) demonstrated better predictive performance and model validity, all subsequent analyses and interpretations were based on these updated models. This approach ensures a more accurate understanding of the metabolomic differences between day-time and night-time deaths.

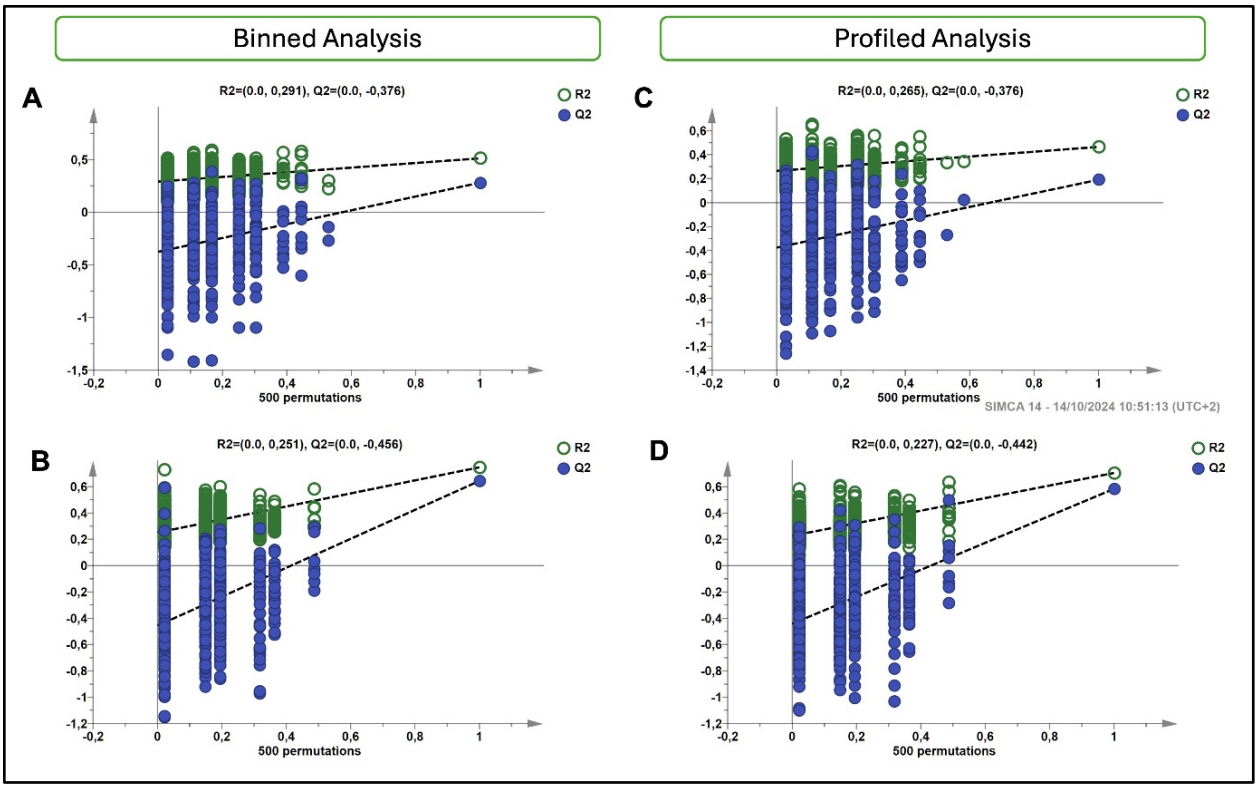

Figure 10: Permutation test results for the OPLS-DA model assessing metabolomic differences between day-time (D) and nighttime (N) deaths, with and without reclassification of samples 13 and 15. (A) Initial permutation test for the binned data (R^2 = 0.0, 0.29 and Q^2 = 0.0, -0.37) and **(C)** profiled data (R^2 = 0.0, 0.26 and Q^2 = 0.0, -0.37), including all samples in their original classification (samples 13 and 15 in the N group). **(B)** Permutation test for the binned data (R^2 = 0.0, 0.25 and Q^2 = 0.0, -0.45) and **(D)** profiled data (R^2 = 0.0, 0.22 and Q^2 = 0.0, -0.44) after reclassifying samples 13 and 15 to the D group. The permutation tests were conducted with 500 permutations to validate the OPLS-DA model's robustness and avoid overfitting. Lower R^2 and Q^2 values in panels B and D reflect the model's refinement following the reclassification of samples 13 and 15. Abbreviation: OPLS-DA, Orthogonal partial least squares discriminant analysis.

8. Identifying key metabolites discriminating between day-time and night-time deaths: Variable importance in projection (VIP) score

To further identify the metabolites contributing most significantly to the differentiation between day-time and night-time deaths, variable importance in projection (VIP) scores were calculated from the OPLS-DA model of profiled spectra. The VIP scores reflect the importance of each metabolite in the model, with metabolites having VIP scores greater than 1 considered significant in distinguishing between the two groups.

The analysis revealed the top 30 metabolites contributing to the separation of the day-time and night-time groups. The heatmap visually represents the relative concentrations of these metabolites, with colored boxes indicating higher concentrations (red) or lower concentrations (blue) in each group **(Figure 11)**. Among the identified metabolites, choline, ethanolamine, xanthine, threonine, lactate, ornithine, glutamine, lysine, valine, glutamate, methionine, glycine, isoleucine, betaine, hypoxanthine, histidine, tyrosine, formate, serine, alanine, and taurine emerged as the most significant contributors (VIP scores > 1)**.**

Among these metabolites' choline, ethanolamine, xanthine, threonine, ornithine, lysine, valine, methionine, glycine, isoleucine, betaine, histidine, tyrosine, formate, serine, alanine, and taurine were elevated in the night-time group, supporting previous findings from the OPLS-DA analysis **(Figure 11)**. Conversely, lactate, glutamine, glutamate, and hypoxanthine were present in higher concentrations in the day-time group **(Figure 11)**. These findings provide further validation of the metabolomic differences between day-time and night-time deaths, with specific metabolites acting as key markers for time-of-death differentiation.

This analysis not only confirms the importance of certain metabolites previously identified through the analyzed datasets but also expands on the range of biochemical pathways involved in the distinction between day-time and night-time deaths. The VIP scores offer a deeper insight into the metabolic shifts that occur depending on the time of death and further underscore the potential forensic value of metabolomic profiling in post-mortem investigations.

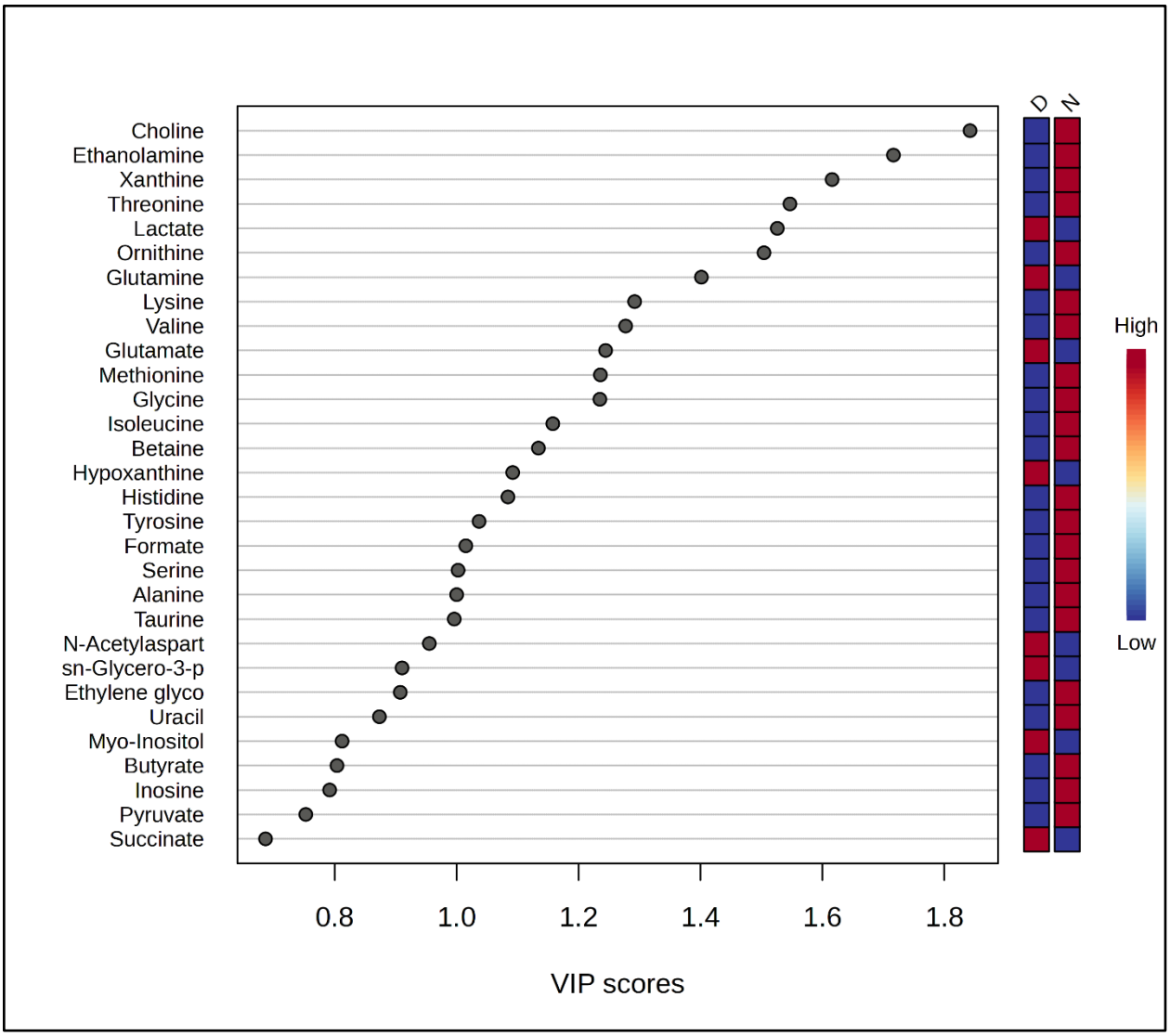

Figure 11: Variable importance projection (VIP) scores from the OPLS-DA model identified key metabolites discriminating between day-time (D) and night-time (N) deaths. The colored heatmap indicates higher (red) or lower (blue) relative concentrations of the corresponding metabolites in each group. Abbreviation: OPLS-DA, Orthogonal partial least squares discriminant analysis.

Following the multivariate analysis, an unpaired t-test (univariate analysis) was employed to statistically validate the differences in metabolite levels between the day-time and night-time groups. This analysis complements the findings from the VIP scores and OPLS-DA, providing specific statistical significance for individual metabolites.

The unpaired t-test identified a few metabolites that were significantly different between the two groups, with a threshold p-value < 0.05 used to determine statistical significance **(Figure 12)**.

Choline, ethanolamine, xanthine, threonine, ornithine, lysine, valine, alanine, glycine, serine, methionine, histidine, isoleucine, inosine, and tyrosine were significantly elevated in the night-time group ($p < 0.05$) **(Figure 12A-P)**. In contrast, metabolites such as lactate, glutamate, glutamine, sn-glycerol-3-phosphocholine, and o-phosphocholine showed significantly higher levels in the day-time group compared to the night-time group ($p < 0.05$) **(Figure 12Q-U)**. These findings are consistent with the multivariate results (VIP scores).

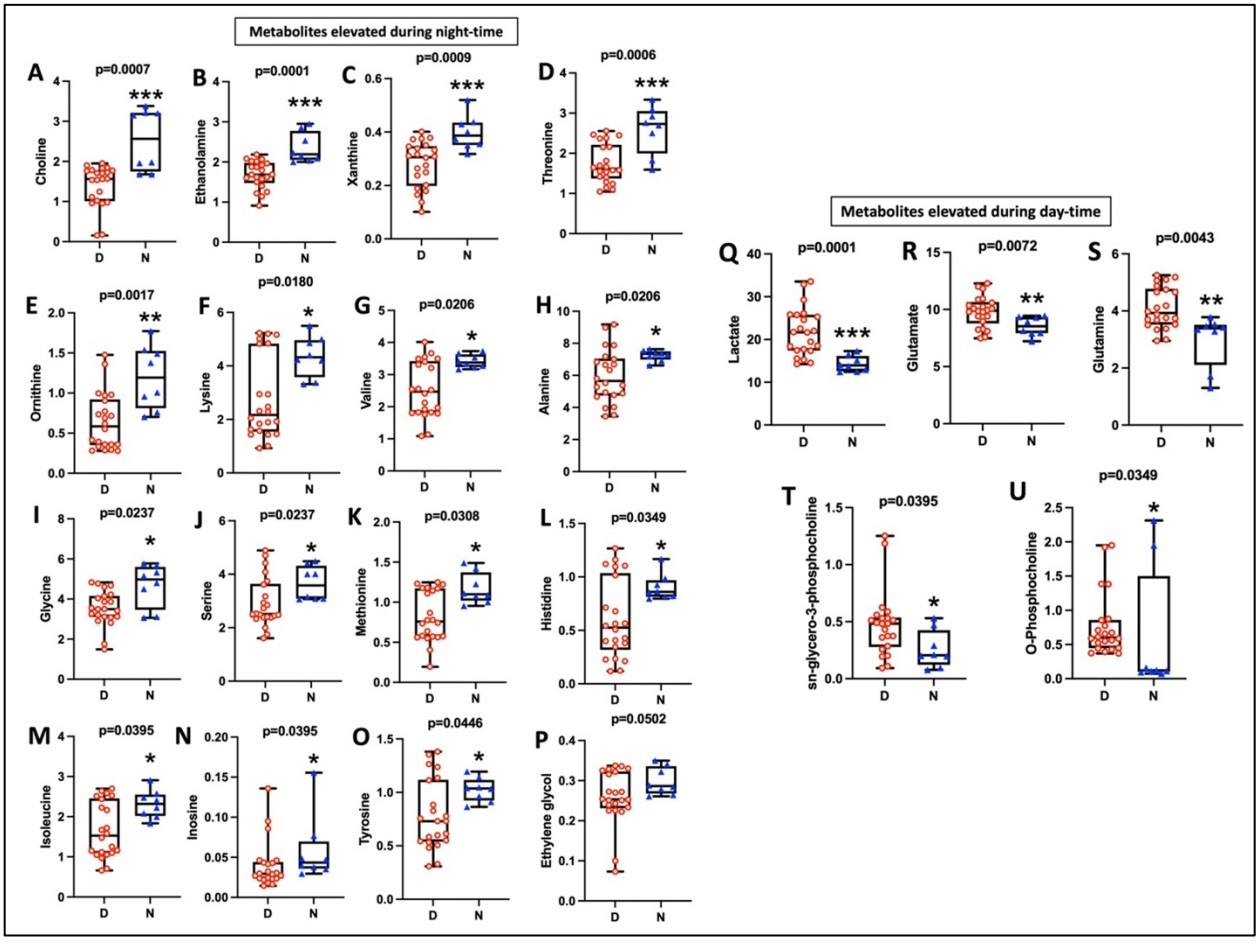

Figure 12: Key metabolites discriminating between day-time (D) and night-time (N) deaths. (A-H) The box plots generated by unpaired t-test of metabolites **(A)** choline, **(B)** ethanolamine, **(C)** xanthine, **(D)** threonine, **(E)** ornithine, **(F)** lysine, **(G)** valine, **(H)** alanine, **(I)** glycine, **(J)** serine, **(K)** methionine, **(L)** histidine, **(M)** isoleucine, **(N)** inosine, **(O)** tyrosine, **(P)** ethylene glycol, **(Q)** lactate, **(R)** glutamate, **(S)** glutamine, **(T)** glycerol-3-phosphocholine, and **(U)** O-phosphocholine between D and N groups. Red dots and blue triangles within boxes indicate the values of individual pineal glands in the D and N groups, respectively. Box plots indicate the top and bottom quartiles; whiskers refer to the top and bottom 90 %. *$p < 0.05$, **$p < 0.01$, and ***$p < 0.001$

9. Enrichment analysis of pineal gland metabolomics: Identification of significantly impacted metabolic pathways in between day-time and night-time deaths

To gain further insights into the biochemical pathways impacted by the metabolomic differences between day-time and night-time deaths, an enrichment analysis was conducted using MetaboAnalyst on the profiled spectra. This analysis identified metabolic pathways significantly perturbed based on the metabolite concentration changes detected in the metabolomic profiles. The enrichment analysis revealed 24 significantly affected metabolic pathways out of the top 41 identified **(Figure 13)**. The x-axis in the pathway overview graph represents p-values, with lower values indicating higher statistical significance, while spot sizes reflect enrichment ratios, with larger spots corresponding to greater pathway enrichment (ranging from 3 to 5) **(Figure 13)**.

The most enriched pathways include glycerophospholipid metabolism, glutathione metabolism, glyoxylate and dicarboxylate metabolism, glycine, serine and threonine metabolism, arginine biosynthesis, porphyrin metabolism, purine metabolism, nitrogen metabolism, pyrimidine metabolism, primary bile acid biosynthesis, lipoic acid metabolism, lysine degradation, biotin metabolism, alanine, aspartate and glutamate metabolism, histidine metabolism, cysteine and methionine metabolism, butanoate metabolism, valine, leucine and isoleucine biosynthesis, pantothenate and CoA biosynthesis, arginine and proline metabolism, selenocompound metabolism, D-Amino acid metabolism, sphingolipid metabolism, and taurine and hypotaurine metabolism **(Figure 13, Table 4)**.

These pathways reflect significant perturbations based on the changes in specific metabolites, as indicated by both the p-values and the enrichment ratios. Notably, metabolites such as taurine, methionine, and choline, previously identified as key contributors through VIP score and univariate analysis, were prominently associated with these enriched pathways. These findings reinforce the importance of these metabolic processes in distinguishing day-time and night-time deaths.

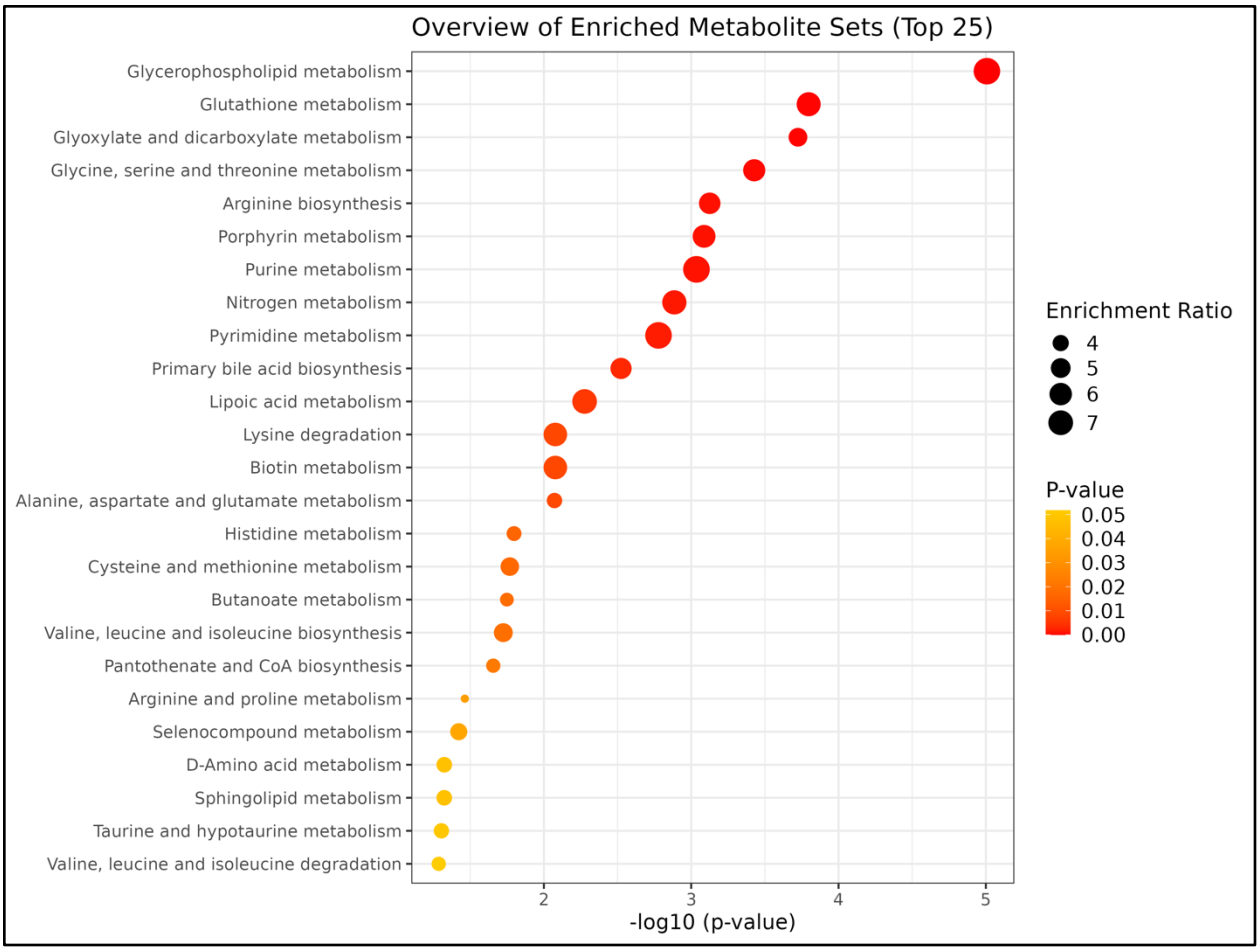

Figure 13: Enrichment analysis revealed significantly impacted metabolic pathways between day-time (D) and night-time (N) deaths. Each dot represents a pathway, with the x-axis indicating p-values (reflecting statistical significance). Larger dot sizes correspond to higher enrichment ratios and dark red color corresponds to lower p-value, indicating a greater impact of that pathway in the data set.

Metabolite set	Total	Hits	Statistic Q	Expected Q	P value	Holm P	FDR
Glycerophospholipid metabolism	36	4	27.362	3.4483	9.8349E-6	4.0323E-4	4.0323E-4
Glutathione metabolism	28	3	23.049	3.4483	1.5951E-4	0.0063805	0.0025766
Glyoxylate and dicarboxylate metabolism	31	7	16.115	3.4483	1.8853E-4	0.0073527	0.0025766
Glycine, serine and threonine metabolism	33	7	20.242	3.4483	3.7351E-4	0.014193	0.0038285
Arginine biosynthesis	14	5	19.395	3.4483	7.4889E-4	0.027709	0.0053966
Porphyrin metabolism	31	2	21.231	3.4483	8.1811E-4	0.029452	0.0053966
Purine metabolism	70	4	27.585	3.4483	9.2137E-4	0.032248	0.0053966

Nitrogen metabolism	6	2	23.369	3.4483	0.001301	0.044265	0.0066723
Pyrimidine metabolism	39	3	27.448	3.4483	0.001667	0.055024	0.0075959
Primary bile acid biosynthesis	46	2	18.97	3.4483	0.002995	0.095845	0.01228
Lipoic acid metabolism	28	2	23.962	3.4483	0.005294	0.16412	0.019732
Lysine degradation	30	1	22.333	3.4483	0.008361	0.25085	0.024826
Biotin metabolism	10	1	22.333	3.4483	0.008361	0.25085	0.024826
Alanine, aspartate and glutamate metabolism	28	10	13.156	3.4483	0.008477	0.25085	0.024826
Histidine metabolism	16	3	12.768	3.4483	0.015951	0.43068	0.042965
Cysteine and methionine metabolism	33	3	15.894	3.4483	0.017034	0.44288	0.042965
Butanoate metabolism	15	4	12.08	3.4483	0.017831	0.44578	0.042965
Valine, leucine and isoleucine biosynthesis	8	4	16.254	3.4483	0.018863	0.45271	0.042965
Pantothenate and CoA biosynthesis	20	3	12.394	3.4483	0.022069	0.50759	0.047623
Arginine and proline metabolism	36	6	10.554	3.4483	0.034417	0.75717	0.070554
Selenocompound metabolism	20	1	14.507	3.4483	0.037842	0.79468	0.073882
D-Amino acid metabolism	15	1	13.309	3.4483	0.047458	0.94917	0.080029
Sphingolipid metabolism	32	1	13.309	3.4483	0.047458	0.94917	0.080029
Taurine and hypotaurine metabolism	8	1	13.073	3.4483	0.049624	0.94917	0.080029
Valine, leucine and isoleucine degradation	39	3	12.392	3.4483	0.051738	0.94917	0.080029
Tyrosine metabolism	42	3	11.431	3.4483	0.051962	0.94917	0.080029
Ubiquinone and other terpenoid-quinone biosynthesis	18	1	12.754	3.4483	0.052702	0.94917	0.080029
Ether lipid metabolism	20	1	12.501	3.4483	0.05528	0.94917	0.080946
Ascorbate and aldarate metabolism	9	1	8.7799	3.4483	0.11185	1.0	0.15286
Inositol phosphate metabolism	30	1	8.7799	3.4483	0.11185	1.0	0.15286
Phenylalanine metabolism	8	2	6.3121	3.4483	0.17197	1.0	0.21722
Phenylalanine, tyrosine and tryptophan biosynthesis	4	2	6.3121	3.4483	0.17197	1.0	0.21722
beta-Alanine metabolism	21	3	5.9046	3.4483	0.17484	1.0	0.21722
Citrate cycle (TCA cycle)	20	3	5.4197	3.4483	0.20016	1.0	0.24137
Propanoate metabolism	21	1	5.373	3.4483	0.21775	1.0	0.25508
Galactose metabolism	27	2	4.9404	3.4483	0.24317	1.0	0.27695
Tryptophan metabolism	41	1	2.5217	3.4483	0.40194	1.0	0.4454
Nicotinate and nicotinamide metabolism	15	1	1.2695	3.4483	0.55331	1.0	0.59699
Glycolysis / Gluconeogenesis	26	2	1.0192	3.4483	0.60672	1.0	0.63471

Pyruvate metabolism	23	3	1.0188	3.4483	0.61922	1.0	0.63471
Glycerolipid metabolism	16	1	0.41725	3.4483	0.73452	1.0	0.73452

Table 4: Results from quantitative enrichment analysis of metabolomic profiles of pineal glands in day-time and night-time death groups.

10. Network analysis of significantly impacted metabolic pathways between day-time and night-time deaths

In addition to identifying the most significantly enriched metabolic pathways, a network analysis was conducted to explore the interconnections between these pathways. This analysis provides a broader perspective on how individual metabolic shifts influence related biochemical processes. The network was constructed using MetaboAnalyst, with nodes representing metabolic pathways and edges indicating relationships based on shared metabolites or metabolic functions.

Network analysis demonstrated that pathways such as arginine biosynthesis and nitrogen metabolism, phenylalanine, tyrosine, and tryptophan biosynthesis, and the cluster of lipoic acid metabolism, citrate cycle, pyruvate metabolism, and glycolysis/gluconeogenesis were interconnected in the network, indicating potential relationships in the metabolic landscape **(Figure 14)**. Interestingly, while the network analysis revealed several key pathways with potential interactions, it is important to note that these pathways were not statistically impacted according to the enrichment analysis **(Figure 13, Table 4)**.

In contrast, pathways that were significantly impacted in the enrichment analysis including bile acid biosynthesis, taurine and hypotaurine metabolism, glycerophospholipid metabolism, and purine and pyrimidine metabolism, did not display clear interactions with other pathways in the network analysis **(Figure 14)**. This lack of network connectivity suggests that these pathways may function more independently in the post-mortem context, without strong metabolic linkages to other pathways.

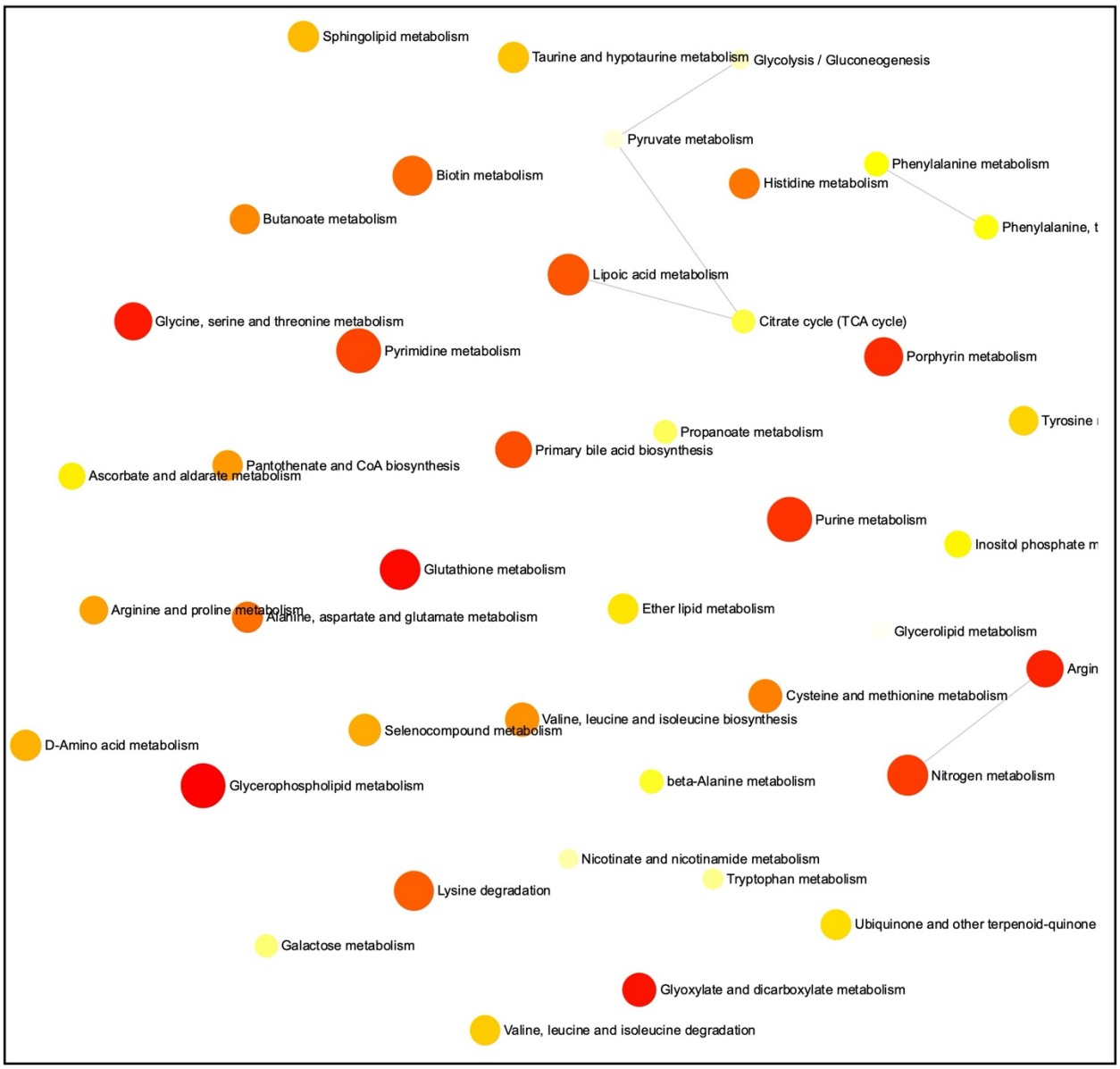

Figure 14: Network analysis highlighted limited interactions among significantly impacted metabolic pathways in Day-time (D) and Night-time (N) Deaths.

11. Key metabolites driving metabolic pathway differences between day-time and night-time deaths

Building upon the results of the enrichment and network analyses, we further examined which metabolites were responsible for the observed changes in the significantly altered metabolic pathways. This approach allowed us to identify the specific metabolites contributing to the differences in metabolomic profiles between day-time (D) and night-time (N) death groups. The

results identified several metabolites that exhibited statistically significant differences between the two groups ($p < 0.05$), with a few metabolites showing non -significant changes.

Notably, metabolites such as phosphocholine (glycerophospholipid metabolism; $p < 0.05$), glutamate (glutathione, glyoxylate and dicarboxylate, porphyrin, arginine, nitrogen, alanine, aspartate and glutamate, butanoate, and histidine metabolism; $p < 0.01$), and glutamine (glyoxylate and dicarboxylate, purine, pyrimidine, arginine, nitrogen, and alanine, aspartate and glutamate metabolism; $p < 0.01$) were found to be significantly elevated during the day-time compared to night-time deaths **(Table 5)**.

On contrary, various metabolites were present in significantly higher concentrations during night-time deaths, such as choline (glycerophospholipid, and glycerine, serine and threonine metabolism; $p = 0.0007$), ethanolamine (glycerophospholipid metabolism; $p = 0.0001$), glycine (glutathione, glyoxylate and dicarboxylate, porphyrin, primary bile acid biosynthesis, lipoic acid, and glycine, serine and threonine metabolism; $p = 0.0237$), ornithine (glutathione and arginine metabolism; $p = 0.0017$), serine (glyoxylate and dicarboxylate, glycine, serine and threonine, cysteine and methionine, D-amino acid, and sphingolipid metabolism; $p = 0.0237$), xanthine ($p = 0.0009$) and inosine ($p = 0.0395$) (purine metabolism), threonine (glycine, serine and threonine metabolism; $p = 0.0006$), alanine (alanine, aspartate and glutamate, and selenocompound metabolism; $p = 0.0206$), lysine (biotin metabolism; $p = 0.0180$), histidine (histidine metabolism; $p = 0.0349$), methionine (cysteine and methionine metabolism; $p = 0.0308$), and valine (pantothenate and CoA biosynthesis; $p = 0.0206$) **(Table 5)**.

Moreover, aspartate, creatine, N-acetylaspartate, 4-aminobutyrate, succinate, butyrate, formate, uridine, uracil, fumarate, taurine, betaine, and asparagine did not exhibit statistically significant changes among two groups **(Table 5)**. These findings emphasize the distinct metabolomic shifts in the pineal gland based on the time of death, highlighting specific metabolic pathways and their associated metabolites as key contributors to circadian-related changes.

Metabolic Pathway	Metabolite	Elevated	*p*-value
Glycerophospholipid metabolism	Phosphocholine	D	**0.0349**
	Glycerophosphocholine	D	n.s.

	Choline	N	**0.0007**
	Ethanolamine	N	**0.0001**
Glutathione metabolism	Glutamate	D	**0.007**
	Glycine	N	**0.023**
	Ornithine	N	**0.001**
Glyoxalate and dicarboxylate metabolism	Glutamate	D	**0.007**
Porphyrin metabolism	Glutamate	D	**0.007**
	Glycine	N	**0.023**
Purine metabolism	Glutamate	D	**0.007**
	Hypoxanthine	D	n.s.
	Xanthine	N	**0.009**
	Inosine	N	**0.039**
Pyrimidine metabolism	Glutamine	D	**0.004**
	Uridine	N	n.s.
	Uracil	N	n.s.
Arginine metabolism	Glutamate	D	**0.007**
	Glutamine	D	**0.004**
	Aspartate	D	n.s.
	Ornithine	N	**0.001**
	Fumarate	N	n.s.
Nitrogen metabolism	Glutamate	D	**0.007**
	Glutamine	D	**0.004**
Primary bile acid biosynthesis	Glycine	N	**0.023**
	Taurine	N	n.s.
Lipoic acid metabolism	Glycine	N	**0.023**
Glycerine, serine, and threonine metabolism	Creatine	D	n.s.
	Serine	N	**0.023**
	Choline	N	**0.0007**
	Glycine	N	**0.023**
	Threonine	N	**0.0006**

	Betaine	N	n.s.
Alanine, aspartate, and glutamate metabolism	Glutamate	D	**0.007**
	Glutamine	D	**0.004**
	N-acetylaspartate	D	n.s.
	Aspartate	D	n.s.
	4-aminobutyrate	D	n.s.
	Succinate	D	n.s.
	Alanine	N	**0.02**
	Asparagine	N	n.s.
Biotin metabolism	Lysine	N	**0.018**
Butanoate metabolism	Glutamate	D	**0.007**
	Butyrate	D	n.s.
	4-aminobutyarate	D	n.s.
	Succinate	D	n.s.
Histidine metabolism	Glutamate	D	**0.007**
	Aspartate	D	n.s.
	Histidine	N	**0.034**
Pantothenate and CoA biosynthesis	Aspartate	D	n.s.
	Valine	N	**0.02**
	Uracil	N	n.s.
Cysteine and methionine metabolism	Serine	N	**0.023**
	Methionine	N	**0.030**
Selenocompound metabolism	Alanine	N	**0.02**
D-amino acid metabolism	Serine	N	**0.023**
Sphingolipid metabolism	Serine	N	**0.023**
Taurine and hypotaurine metabolism	Taurine	N	n.s.

Table 5: Summary of significantly altered metabolic pathways between day-time (D) and night-time (N) deaths, listing key metabolites responsible for observed changes, p-values, and associated pathways. Statistically significant changes in deaths that occur during day-time and night-time ($p < 0.05$) are highlighted in bold, while "n.s." denotes metabolites with non-significant changes. Abbreviations: D, Day-time; N, Night-time.

12. Correlation between the metabolomic profile of the pineal gland and the post-mortem interval (PMI)

Next, to assess the correlation between the metabolomic profile of the pineal gland and the post-mortem interval (PMI), a supervised analytical approach using an OPLS regression model was employed. This analysis was conducted on both binned and profiled datasets derived from ^{1}H-NMR metabolomic profiling, with PMI as the independent variable. In addition, we also aimed to identify key metabolites that demonstrate time-dependent changes post-mortem, by providing a predictive loading plot.

In the OPLS regression curve derived from the binned dataset, a linear correlation of actual PMI with the predictive PMI was observed. The model exhibited strong explanatory power, with a R^2Y value of 0.69, indicating that 69% of the variance in the dataset is explained by the model, and good predictive power of the model, as reflected by the Q^2Y value (0.57), indicating higher predictability. The model's relative error in cross-validation (RMSEcv) was 36.04 hours, over the entire PMI range of 44 to 219 hours **(Figure 15A)**. The predictive loading plot demonstrated that metabolites such as lactate, glutamate, trimethylamine, alanine, lysine, succinate, methionine, phenylalanine, isoleucine, valine, glutamine, tyrosine, aspartate, acetate, histidine, and threonine were increased with increasing PMI **(Figure 15B)**. Conversely, metabolites such as choline, myoinositol, glycerol, GABA (4-aminobutyrate), O-phosphocholine, taurine, N-acetylaspartate, glycine, scylloinositol, and serine were found to decrease with increasing PMI **(Figure 15B)**.

Similarly, the OPLS regression analysis using the profiled dataset also demonstrated a linear correlation between actual PMI and predicted PMI. This profiled model provided an R^2Y value of 0.68, suggesting that approximately 68% of the variance in the dataset is captured by the model. The Q^2Y value (0.51) indicated good predictive accuracy, though the model's relative error in cross-validation (RMSEcv) was slightly higher at 38.59 hours **(Figure 15C)**. The predictive loading plot highlighted similar metabolomic shifts with increasing PMI as that of the binned dataset. Metabolites such as glutamate, alanine, proline, succinate, trimethylamine, acetate, lactate, glycine, histidine, asparagine, leucine, isoleucine, and phenylalanine were positively correlated with PMI **(Figure 15D)**. On the other hand, glycerol, choline, serine, taurine, myoinositol, 4-

aminobutyrate (GABA), O-phosphocholine, and ethanolamine were negatively correlated with PMI **(Figure 15D)**.

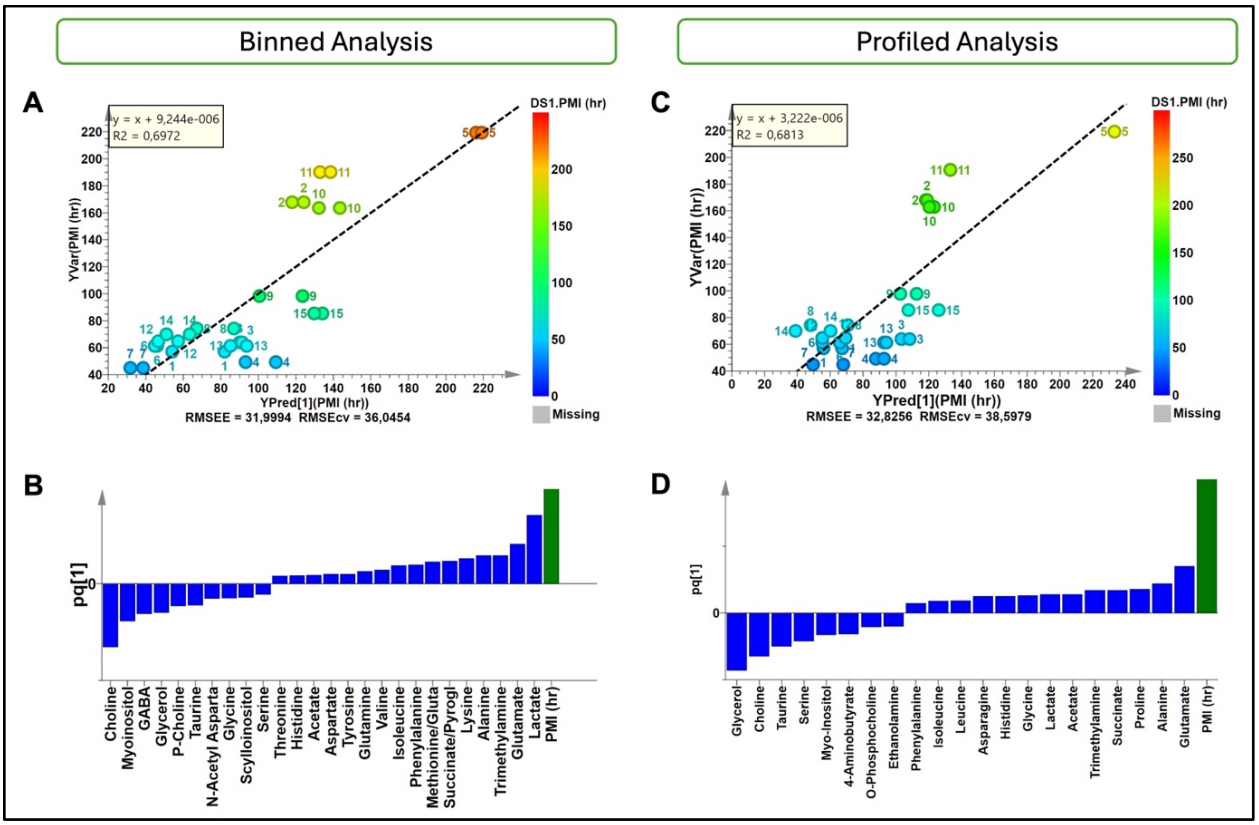

Figure 15: Orthogonal partial least square (OPLS) regression analysis revealed metabolomic correlations with post-mortem interval (PMI). (A, C) OPLS regression curve based on PMI of individual of respective pineal glands obtained from **(A)** binned data ($Q^2Y = 0.57$, $R^2Y = 0.697$), and **(C)** profiled data ($Q^2Y = 0.51$, $R^2Y = 0.681$), **(B, D)** Predictive loading plot of metabolites obtained by the OPLS regression model from **(B)** binned data, and **(D)** profiled dataset.

To cross-validate the OPLS model and avoid overfitting, a permutation test with 500 permutations was performed. The test returned values of $R^2 = (0.0, 0.265)$ and $Q^2 = (0.0, -0.429)$ for binned dataset **(Figure 16A)** and $R^2 = (0.0, 0.214)$ and $Q^2 = (0.0, -0.45)$ for profiled dataset **(Figure 16B)**, suggesting no overfitting and validity of the model.

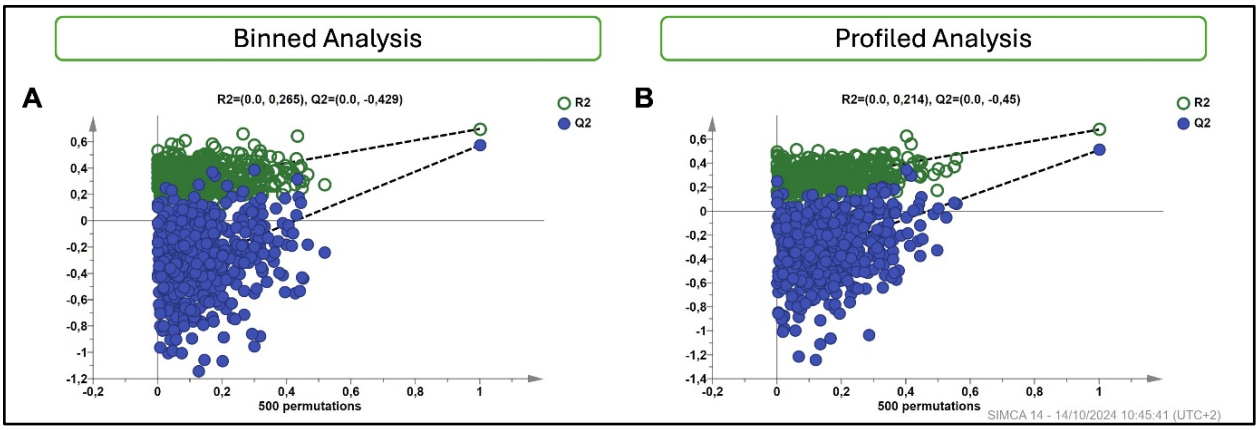

Figure 16: Permutation test for orthogonal partial least square (OPLS) model validation. The permutation test was performed with 500 permutations to assess the robustness of the OPLS model and to avoid overfitting. The R^2 and Q^2 intercept values for **(A)** binned data (R^2 = 0.0, 0.26 and Q^2 = 0.0, -0.42), and **(B)** profiled data (R^2 = 0.0, 0.21 and Q^2 = 0.0, -0.45), indicating that the model is valid.

13. Identifying key metabolites correlated with post-mortem interval (PMI): Variable importance in projection (VIP) scores

To identify metabolites significantly correlated with PMI, Variable Importance in Projection (VIP) scores were calculated from the OPLS model of the profiled spectra. VIP scores reflect each metabolite's relevance within the model, with values above 1 considered to be strongly associated with PMI.

The analysis revealed 11 key metabolites with a strong correlation to PMI **(Figure 17)**. Among these, glycerol, glutamate, choline, taurine, alanine, serine, proline, succinate, trimethylamine, myoinositol, and 4-aminobutyric acid (GABA) emerged as the most significant contributors (VIP > 1)**.** The metabolites glutamate, alanine, proline, succinate, and trimethylamine were increased with an increase in PMI, supporting previous findings from the OPLS analysis **(Figure 17)**. Conversely, glycerol, choline, taurine, serine, myo-inositol, and GABA were decreased with increasing PMI **(Figure 17)**.

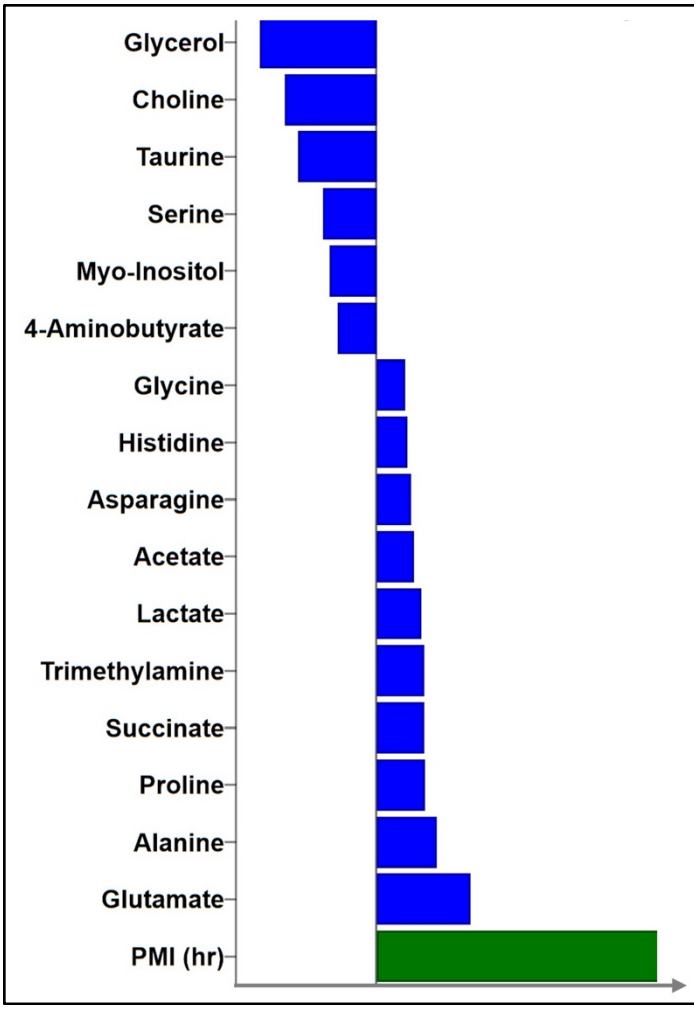

Metabolites	VIP predictive
Glycerol	3.01
Glutamate	2.45
Choline	2.27
Taurine	1.74
Alanine	1.53
Serine	1.47
Proline	1.25
Succinate	1.19
Trimethylamine	1.19
Myo-Inositol	1.15
4-Aminobutyrate	1.10
Acetate	0.98
Lactate	0.97
Glycine	0.91
Histidine	0.88
Asparagine	0.87

Figure 17: **Variable Importance in Projection (VIP) scores from the OPLS regression model identified key metabolites correlated with post-mortem interval (PMI).** Metabolites with VIP scores greater than 1 are considered to have a significant association with PMI. The table on the right lists the VIP scores of each metabolite, highlighting those most strongly correlated with PMI. Abbreviation: OPLS, Orthogonal Partial Least Squares.

Following the multivariate analysis, a Pearson's correlation was conducted to statistically validate the correlation of metabolites with the PMI. This analysis complements the findings from the VIP scores and OPLS regression model, providing specific statistical significance for individual metabolites. Pearson's correlation identified a few metabolites that were significantly correlated with PMI, with a threshold p-value < 0.05 used to determine statistical significance **(Figure 18)**. Choline, inosine, taurine, glycerol, and ethylene glycol were inversely correlated with PMI ($p < 0.05$) **(Figure 18F-J)**. Moreover, succinate, glutamate, tryptophan, trimethylamine, and uracil were found to be significantly increased with PMI ($p < 0.05$) (**Figure 18 A- E)**. These findings are

consistent with the multivariate results, where glycerol, choline, and taurine were found to be decreased with increasing PMI, while succinate and glutamate were positively correlated with PMI **(Figure 17)**.

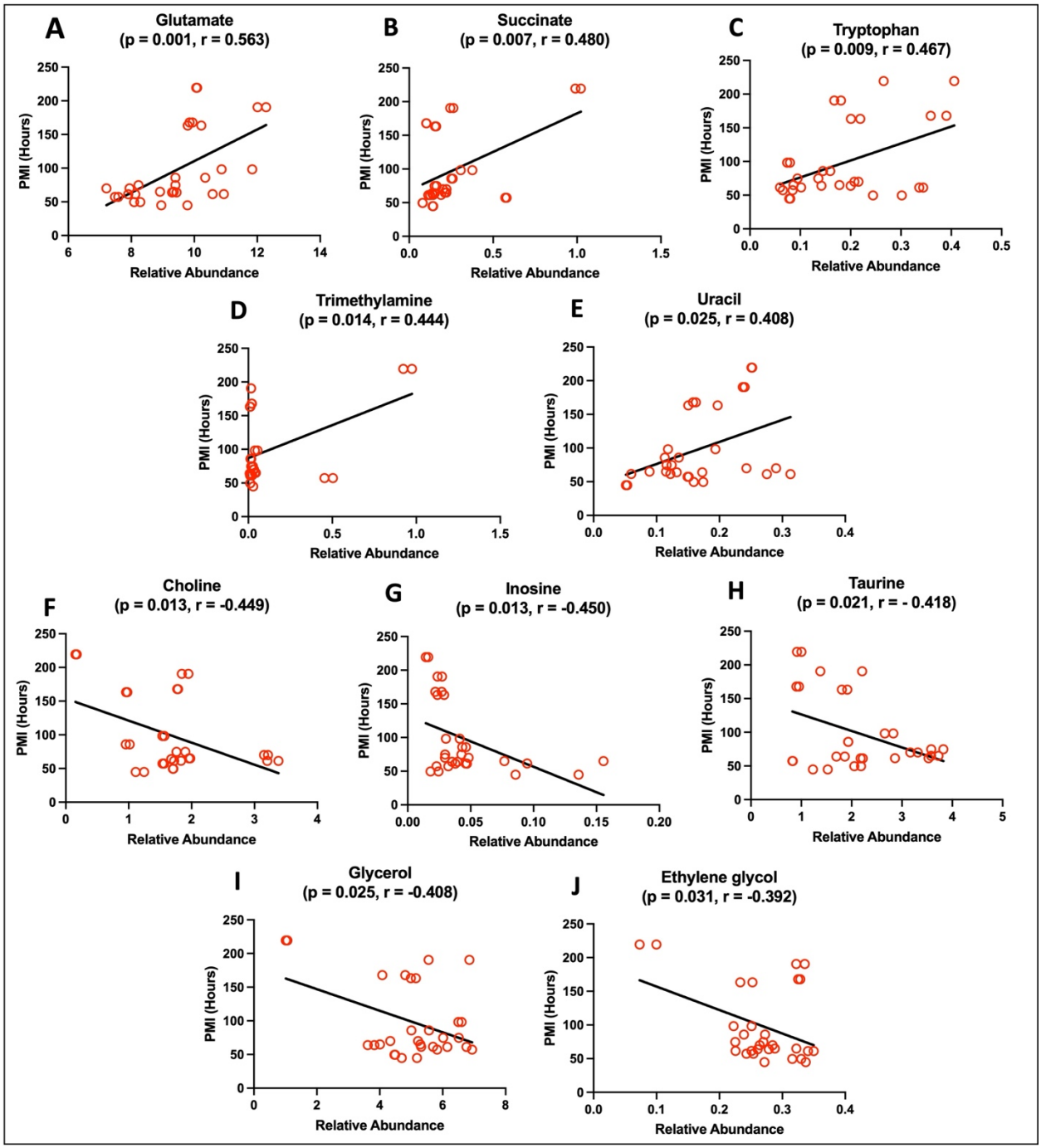

Figure 18: The linear regression plot showing the correlation between post-mortem interval (PMI) and the relative abundance of metabolites. (A-J) Linear regression plots for the concentrations of metabolites. The y-axis represents the PMI (hours), and the x-axis shows the

relative concentration of specific metabolite. A linear regression model was fitted to the data, and Pearson's correlation coefficient (r) was calculated to assess the strength of the relationship. The p-value was determined to evaluate the statistical significance of the correlation. Red dots represent the concentration of the metabolite in individual pineal gland samples.

14. Enrichment analysis of pineal gland metabolomics: Identification of significantly impacted metabolic pathways

To further investigate the biochemical pathways affected by PMI, a pathway enrichment analysis was performed on the ^{1}H-NMR metabolomic data of the pineal glands. The x-axis represents the p-values from the pathway analysis, with lower values indicating higher statistical significance **(Figure 19)**. The spot sizes in the graph represent the enrichment ratios, with larger spots corresponding to greater enrichment (ranging from 2 to 6) **(Figure 19)**.

The enrichment overview graph demonstrated that the top 16 metabolic pathways were significantly enriched in relation to PMI, all with an enrichment score greater than 2, indicating a notable impact of these pathways as PMI increases **(Figure 19, Table 6)**. Among the most affected pathways were butanoate metabolism, histidine metabolism, porphyrin metabolism, glutathione metabolism, nitrogen metabolism, propanoate metabolism, citrate cycle (TCA cycle), tryptophan metabolism, glyoxylate and dicarboxylate metabolism, arginine biosynthesis, alanine, aspartate and glutamate metabolism, taurine and hypotaurine metabolism, glycerolipid metabolism, arginine and proline metabolism, glycerophospholipid metabolism and galactose metabolism **(Figure 19)**. These pathways showed significant perturbations based on the changes in specific metabolites, as indicated by both the p-values and the enrichment ratios.

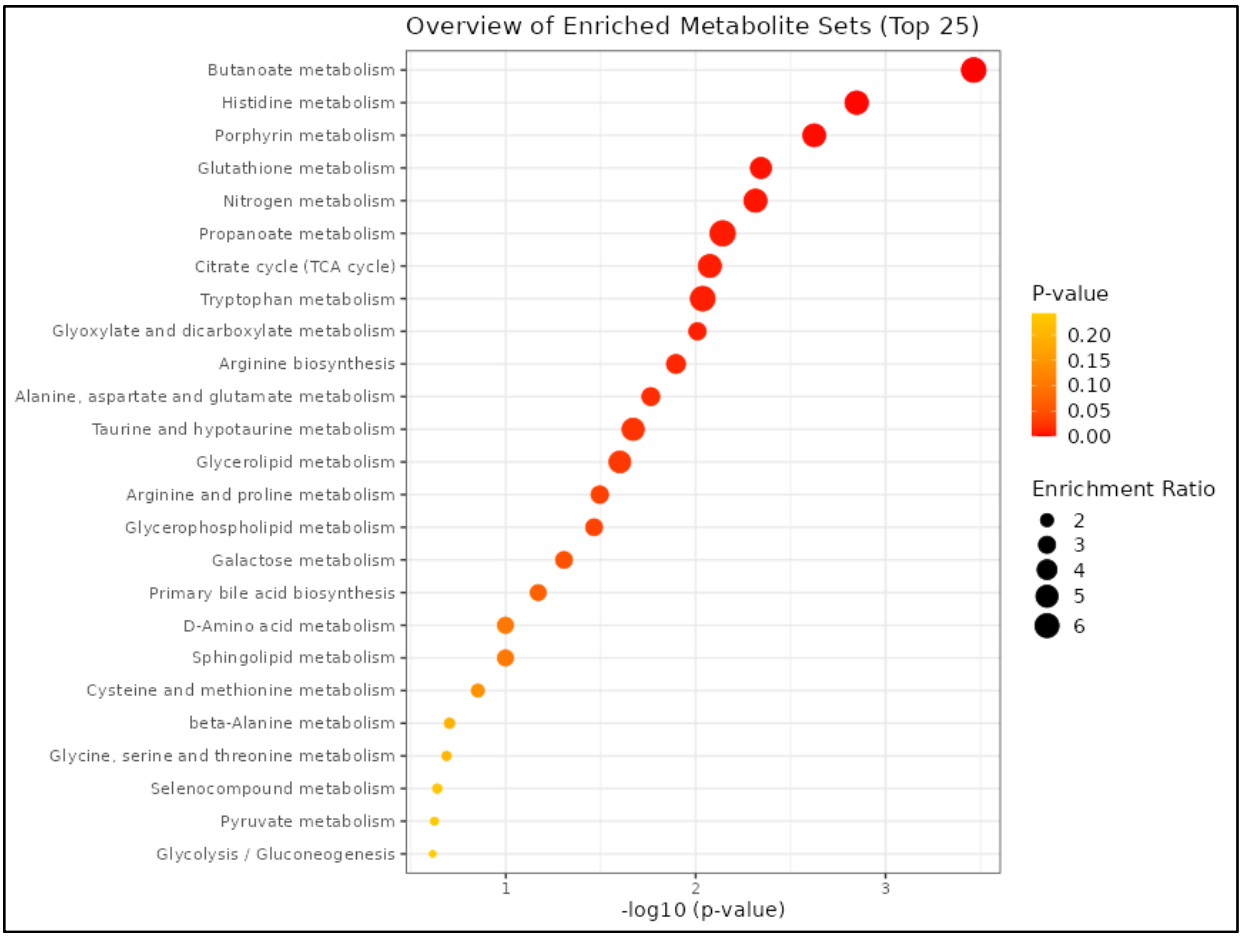

Figure 19. Enrichment analysis of pineal gland metabolomics identified significantly impacted pathways correlated with post-mortem interval (PMI). Each dot represents a pathway, with the x-axis indicating p-values (reflecting statistical significance). Larger dot sizes correspond to higher enrichment ratios and dark red color corresponds to lower p-value, indicating a greater impact of that pathway in the data set.

	Total Cmpd	Hits	Statistic Q	Expected Q	Raw p	Holm p	FDR
Butanoate metabolism	15	4	21.7	3.4483	0.00034314	0.014069	0.014069
Histidine metabolism	16	3	19.424	3.4483	0.0014192	0.056769	0.029094
Porphyrin metabolism	31	2	18.568	3.4483	0.0023746	0.092608	0.032452
Glutathione metabolism	28	3	15.695	3.4483	0.0045318	0.17221	0.039703
Nitrogen metabolism	6	2	18.966	3.4483	0.0048418	0.17915	0.039703
Propanoate metabolism	21	1	23.079	3.4483	0.0072107	0.25959	0.044598
Citrate cycle (TCA cycle)	20	3	18.819	3.4483	0.0084217	0.29476	0.044598

Tryptophan metabolism	41	1	21.859	3.4483	0.0091832	0.31223	0.044598
Glyoxylate and dicarboxylate metabolism	31	7	10.537	3.4483	0.0097898	0.32306	0.044598
Arginine biosynthesis	14	5	12.568	3.4483	0.012702	0.40646	0.052078
Alanine, aspartate and glutamate metabolism	28	10	11.341	3.4483	0.017232	0.5342	0.064229
Taurine and hypotaurine metabolism	8	1	17.515	3.4483	0.021354	0.64063	0.07296
Glycerolipid metabolism	16	1	16.672	3.4483	0.025087	0.72752	0.079121
Arginine and proline metabolism	36	6	10.777	3.4483	0.032013	0.89637	0.093708
Glycerophospholipid metabolism	36	4	10.114	3.4483	0.034283	0.92565	0.093708
Galactose metabolism	27	2	10.109	3.4483	0.049381	1	0.12654
Primary bile acid biosynthesis	46	2	9.1975	3.4483	0.067548	1	0.16291
D-Amino acid metabolism	15	1	9.3431	3.4483	0.10046	1	0.21678
Sphingolipid metabolism	32	1	9.3431	3.4483	0.10046	1	0.21678
Cysteine and methionine metabolism	33	3	6.9045	3.4483	0.14049	1	0.288
beta-Alanine metabolism	21	3	5.4836	3.4483	0.1981	1	0.38241
Glycine, serine and threonine metabolism	33	7	5.0975	3.4483	0.2052	1	0.38241
Selenocompound metabolism	20	1	5.1079	3.4483	0.22979	1	0.39236
Pyruvate metabolism	23	3	4.8794	3.4483	0.23763	1	0.39236
Glycolysis / Gluconeogenesis	26	2	4.8106	3.4483	0.24271	1	0.39236
Ascorbate and aldarate metabolism	9	1	4.5378	3.4483	0.25838	1	0.39236
Inositol phosphate metabolism	30	1	4.5378	3.4483	0.25838	1	0.39236
Ether lipid metabolism	20	1	3.1964	3.4483	0.34451	1	0.50446
Phenylalanine metabolism	8	2	2.844	3.4483	0.3813	1	0.5211

Phenylalanine, tyrosine and tryptophan biosynthesis	4	2	2.844	3.4483	0.3813	1	0.5211
Tyrosine metabolism	42	3	2.2301	3.4483	0.46614	1	0.56626
Valine, leucine and isoleucine degradation	39	3	1.9783	3.4483	0.46839	1	0.56626
Ubiquinone and other terpenoid-quinone biosynthesis	18	1	1.7873	3.4483	0.48124	1	0.56626
Pyrimidine metabolism	39	3	1.8884	3.4483	0.49733	1	0.56626
Lipoic acid metabolism	28	2	1.5333	3.4483	0.52393	1	0.56626
Lysine degradation	30	1	1.4065	3.4483	0.53251	1	0.56626
Biotin metabolism	10	1	1.4065	3.4483	0.53251	1	0.56626
Nicotinate and nicotinamide metabolism	15	1	1.3844	3.4483	0.53576	1	0.56626
Valine, leucine and isoleucine biosynthesis	8	4	1.717	3.4483	0.53864	1	0.56626
Pantothenate and CoA biosynthesis	20	3	2.1416	3.4483	0.55352	1	0.56736
Purine metabolism	70	4	1.3328	3.4483	0.64583	1	0.64583

Table 6. Results from quantitative enrichment analysis of pineal glands from individuals with varied PMI.

15. Key metabolites driving metabolic pathway alterations correlated with Post-Mortem Interval (PMI)

Building on the findings from the enrichment analysis, we further investigated specific metabolites that were significantly correlated with PMI. This allowed us to identify the biochemical changes responsible for the observed pathway perturbations over increasing PMI. The results highlighted several metabolites that exhibited significant correlations with PMI ($p < 0.05$), as well as a few metabolites that showed non-significant trends **(Table 7)**.

Among the metabolites that significantly increased with PMI were glutamate (butanoate metabolism, glutathione metabolism, nitrogen metabolism, and alanine, aspartate, and

glutamate metabolism; p = 0.001), succinate (butanoate, propanoate, TCA cycle, alanine, aspartate, and glutamate metabolism; p = 0.007), tryptophan (tryptophan metabolism; p = 0.009) **(Table 7)**. Conversely, metabolites such as taurine (taurine and hypotaurine metabolism; p = 0.021), glycerol (glycerolipid and galactose metabolism; p = 0.025), and choline (glycerophospholipid metabolism; p = 0.013) showed significant decreases with increasing PMI **(Table 7)**. Other metabolites, such as 4-aminobutyrate, butyrate, histidine, aspartate, glycine, glutamine, fumarate, serine, and acetate exhibited non-significant changes (p > 0.05), suggesting that these metabolites may be less sensitive to PMI-related biochemical shifts **(Table 7)**.

Metabolic Pathway	Metabolite	Correlation with PMI	*p*-value
Butanoate metabolism	Glutamate	Increased	**0.001**
	Succinate	Increased	**0.007**
	4-aminobutyrate	Decreased	n.s.
	Butyrate	Decreased	n.s.
Histidine metabolism	Glutamate	Increased	**0.001**
	Histidine	Increased	n.s.
	Aspartate	Increased	n.s.
Porphyrin metabolism	Glutamate	Increased	**0.001**
	Glycine	Increased	n.s.
Glutathione metabolism	Glutamate	Increased	**0.001**
	Glycine	Increased	n.s.
Nitrogen metabolism	Glutamate	Increased	**0.001**
	Glutamine	Increased	n.s.
Propanoate metabolism	Succinate	Increased	**0.007**
Citrate cycle (TCA cycle)	Succinate	Increased	**0.007**
	Fumarate	Decreased	n.s.
Tryptophan metabolism	Tryptophan	Increased	**0.009**
Glyoxylate and dicarboxylate metabolism	Glutamate	Increased	**0.001**
	Glutamine	Increased	n.s.

	Formate	Decreased	n.s.
	Serine	Decreased	n.s.
Arginine biosynthesis	Glutamate	Increased	**0.001**
	Acetate	Increased	n.s.
	Glycine	Increased	n.s.
	Glutamine	Increased	n.s.
	Aspartate	Increased	n.s.
	Fumarate	Decreased	n.s.
Alanine, aspartate and glutamate metabolism	Glutamate	Increased	**0.001**
	Succinate	Increased	**0.007**
	Asparagine	Increased	n.s.
	Alanine	Increased	n.s.
	Aspartate	Increased	n.s.
	4-aminobutyrate	Decreased	n.s.
	N-acetylaspartate	Decreased	n.s.
	Fumarate	Decreased	n.s.
Taurine and hypotaurine metabolism	Taurine	Decreased	**0.021**
Glycerolipid metabolism	Glycerol	Decreased	**0.025**
Arginine and proline metabolism	Glutamate	Increased	**0.001**
	Proline	Increased	n.s.
	4-aminobutyarate	Decreased	n.s.
Glycerophospholipid metabolism	Choline	Decreased	**0.013**
	Ethanolamine	Decreased	n.s.
	Phosphocholine	Decreased	n.s.
Galactose metabolism	Glycerol	Decreased	**0.025**
	Myoinositol	Decreased	n.s.

Table 7. Metabolic pathways and key metabolites correlated with post-mortem interval (PMI). Statistically significant changes in the correlation of metabolites with PMI ($p < 0.05$) are highlighted in bold, while "n.s." denotes metabolites with non-significant changes.

DISCUSSION

The present work represents the first comprehensive metabolomic analysis of human post-mortem pineal glands, identifying 44 metabolites using ^{1}H-NMR (proton nuclear magnetic resonance) spectroscopy. To date, to our knowledge, no prior studies have explored the metabolomic profiling of human pineal glands or attempted to correlate its metabolic profile with key external factors such as post-mortem interval (PMI) and season at the time of death, or baseline individual characteristics (e.g., age, gender). The findings of this preliminary study demonstrate the potential forensic utility of pineal gland metabolomics for distinguishing deaths occurring during the day-time versus night-time, as well as for estimating PMI, a critical yet unresolved issue in forensic science. By leveraging the pineal gland's metabolic profile, we constructed a regression model for PMI estimation that provides a reliable time frame for the interval since death. Previous human proteomic studies (Dumas et al., 2021) have indicated that the pineal gland retains a certain degree of metabolic activity after death, reflecting its role in circadian rhythm regulation. Given the unique biochemical and anatomical features of the pineal gland, we also explored its potential to classify deaths based on time of day (day-time versus night-time), offering an indirect but valuable forensic tool. In forensic investigations, narrowing down the time of death to a specific window (such as ruling out night-time or day-time death) can be crucial in court proceedings where decisions must meet the standard of “beyond a reasonable doubt”. Additionally, we hypothesized that different anatomical regions of the pineal gland might contribute variably to its overall metabolomic profile. To test this, we analyzed two sagittal sections of each gland, despite differences in their weights. Interestingly, the results showed negligible intraindividual variability, suggesting that the metabolic composition remains consistent across different sections of the pineal gland. This further supports the gland's reliability as a forensic matrix for both PMI estimation and time-of-death classification.

Influence of interindividual and external factors on pineal gland metabolomics

Understanding the influence of interindividual and external factors on the metabolomic profile of the pineal gland is essential for accurate metabolomic-based forensic analysis. In this study, we explored how age, gender, weight of the pineal gland, and season at the time of death affect the pineal gland’s metabolome. Results from principal component analysis (PCA) and orthogonal

partial least square-determinant analysis (OPLS-DA) demonstrated that these factors exert relatively minor influence on the overall metabolic profile. To that, age was not a major determinant of metabolic variation in the pineal gland. The binned and profiled datasets displayed minimal separation between age groups, and OPLS regression models exhibited weak and moderate predictive power, respectively, suggesting that age-related metabolic changes may exist in specific metabolites and warrant further investigation with larger cohorts **(Figure 6)**. Interestingly, while there is limited literature specifically evaluating age-related metabolomic shifts in the pineal gland, one study reported age-associated structural changes, such as the replacement of normal secretory parenchyma with glial tissues, connective tissues, calcifications, and glial cysts (Gheban et al., 2021). However, these structural alterations may not significantly influence the gland's metabolic profile, at least in the post-mortem context (Gheban et al., 2021).

Similarly, gender did not significantly affect the metabolomic profile of the pineal gland, as evidenced by the minimal separation between male and female samples in both PCA and OPLS-DA analyses **(Figure 5)**. While sex-dependent variations in melatonin production and circadian rhythms are well-documented during life (Duffy et al., 2011), these differences were not reflected in post-mortem metabolic profiles in our dataset. Our findings align with previous work from our group, which found no significant gender-based differences in the metabolomic profile of pericardial fluid used for PMI estimation (Chighine et al., 2023). This suggests that certain post-mortem matrices, such as the pineal gland and pericardial fluid, may exhibit metabolic stability across genders, likely driven by the universal biochemical processes of autolysis dominating after death. It is noteworthy, however, that over 30 studies using biofluids such as serum, plasma, and urine have reported gender-specific metabolic changes, with higher levels of creatine in females and creatinine in males (Costanzo et al., 2022).

The weight of the pineal gland also showed limited impact on its metabolic profile, indicating that the metabolic shifts are not influenced by gland size **(Figure 4)**. As the pineal gland is central to melatonin synthesis and the regulation of circadian rhythms, its function is known to be influenced by seasonal variations. For instance, studies have shown increased levels of AANAT,

the rate-limiting enzyme in melatonin synthesis, and elevated melatonin levels in the pineal gland of hamsters during the winter solstice compared to the summer solstice (Xu et al., 2018). Given this, we initially hypothesized that metabolomic profiles of post-mortem pineal glands might be influenced by the season of death (e.g. summer versus winter). However, our results showed no significant seasonal impact. PCA and OPLS-DA **(Figure 7)** analyses indicated low separation between samples collected during summer and winter. This suggests that while melatonin production varies seasonally *in vivo*, post-mortem metabolic processes are primarily driven by autolysis and environmental exposure rather than residual circadian or seasonal signaling.

In summary, our analysis revealed that interindividual factors such as gender and pineal gland weight exert no substantial influence on the metabolomic profile of the post-mortem pineal gland. However, age and season at the time of death showed minor to moderate trends that merit further investigation with large cohorts. These findings highlight the metabolic stability of the pineal gland and its potential as a reliable matrix for PMI estimation. Its deep intracranial location protects it from external environmental influences, and its consistent metabolomic profile across various conditions strengthens its utility in forensic applications. The limited influence of confounding variables suggests that the observed metabolic shifts in the pineal gland are primarily driven by intrinsic, time-dependent post-mortem processes, positioning it as an optimal candidate for further forensic investigations aimed at enhancing the accuracy of PMI estimation.

Metabolic differences between day-time and night-time deaths

Circadian rhythm, an intrinsic biological process following a ~24-hour cycle, regulates numerous physiological functions, including metabolism (Marcheva et al., 2013). The pineal gland, central to melatonin synthesis and secretion, is critical in maintaining these daily rhythms (Bueno et al., 2023). Melatonin production peaks at night and diminishes during the day, influencing various metabolic pathways (Zisapel, 2018). Therefore, we hypothesized that post-mortem metabolomic profiles of the gland would reflect distinct differences based on the time of death (day-time vs. night-time). To investigate these potential metabolic variations, we employed binned and

profiled ^{1}H-NMR datasets and applied unsupervised and supervised multivariate analysis to classify samples between day-time and night-time deaths.

Our findings revealed a clear separation in the metabolomic profile of the pineal gland between day-time and night-time deaths in both binned and profiled datasets, as evidenced by PCA and OPLS-DA plots **(Figure 8)**. This suggests that the metabolic composition of the pineal gland is influenced by the time of death. However, two samples from the night-time group (samples 13 and 15) clustered with the day-time group. Further investigation revealed that these cases had unusual circumstances that might have influenced their metabolomic profiles. For sample 13, circumstances involved a violent struggle during a night-time assault around 05:00 AM, a time when melatonin levels are typically high, but the physical exertion and stress of the situation may have disrupted the individual's metabolic state. Similarly, sample 15 was obtained from an individual hospitalized in an ICU with continuous artificial lighting, which likely disrupted circadian signaling and altered melatonin production, leading to a metabolic profile resembling day-time death. These cases highlight the potential for external factors, such as environmental lighting and physical activity, to modulate the metabolomic signature of the pineal gland, even in a post-mortem context. To further investigate whether these metabolomic changes were influenced by light exposure or the individual's wake/sleep state, we re-classified samples 13 and 15 as day-time cases and recalculated the model **(Figure 9)**. This reclassification resulted in an improved model fit, providing additional support for the hypothesis that light exposure rather than the time of death itself predominantly drives these post-mortem metabolomic changes **(Figure 9)**.

Metabolic distinctions between day-time and night-time deaths: Variable Importance in Projection (VIP) score and enrichment analysis

The metabolic differences between day-time and night-time deaths were further supported by Variable Importance in Projection (VIP) score and enrichment analysis, identifying key metabolites and pathways significantly impacted by the time of death. The VIP scores highlighted key metabolites such as choline, ethanolamine, xanthine, threonine, ornithine, lysine, valine,

methionine, glycine, isoleucine, betaine, histidine, tyrosine, formate, serine, alanine, and taurine, which were significantly elevated during night-time deaths **(Figure 11)**. In contrast, lactate, glutamine, glutamate, and hypoxanthine were more abundant in day-time deaths **(Figure 11).** Univariate statistical analysis further validated these findings **(Figure 12)**.

Choline and ethanolamine, precursors of phosphatidylcholine (PC) and phosphatidylethanolamine (PE), respectively, were elevated during the night-time deaths **(Figure 12A, B)**. These phospholipids are major components of cell membranes and are essential for maintaining structural integrity (Sundler & Akesson, 1975; van der Veen et al., 2017). The nocturnal increase in choline and ethanolamine may reflect heightened cellular turnover and repair processes linked to melatonin synthesis. Furthermore, choline contributes to acetylcholine synthesis, a neurotransmitter modulating the REM (rapid eye movement) sleep (Vazquez & Baghdoyan, 2001). Acetylcholine levels peak during REM sleep, which is prevalent during the later parts of the night (Kametani & Kawamura, 1991; Marrosu et al., 1995; Vazquez & Baghdoyan, 2001). This heightened demand for acetylcholine synthesis may also drive increased choline availability during the night. Ornithine, a metabolite of L-arginine and a key intermediate in the urea cycle was significantly elevated during night-time deaths **(Figure 12E)**. Beyond its role in nitrogen metabolism, ornithine has been linked to circadian rhythm regulation and improved sleep quality. Clinical and pre-clinical studies have shown that L-ornithine supplementation enhances melatonin secretion and improves sleep in a time-dependent manner, when administered at night (Matsuo et al., 2015; Miyake et al., 2014). Thus, elevated levels of ornithine observed in night-time deaths may reflect the pineal gland's night-time metabolic activity, including its contribution to melatonin synthesis and polyamine production in the pineal gland.

Several amino acids such as threonine, lysine, alanine, glycine, serine, and histidine were also elevated during night-time deaths **(Figure 12D, F, H, I, J & L)**. These amino acids can enter the TCA cycle, providing substrates to sustain ATP production to meet the higher energy demands at night for melatonin synthesis (Harrison et al., 2019; Sherry et al., 2015; Yoshimi et al., 2016). Previous study demonstrated higher mitochondrial respiratory chain enzyme activity during

night-time in the rat pineal gland, promoting oxidative phosphorylation and ATP production to support nocturnal activities (Møller et al., 2007). Complementary proteomic studies identified higher levels of glycolytic enzymes in the pineal gland during the day-time, suggesting that glycolysis plays a more prominent role during the day (Dumas et al., 2021). These findings suggest a metabolic shift toward mitochondrial energy production at night and glycolysis during the day, aligning with the gland's circadian rhythm-driven energy demands. Methionine, an essential sulfur-containing amino acid involved in the methylation processes, was significantly elevated during night-time deaths **(Figure 12K)**. Methionine's active form, S-adenosylmethionine (SAM), follows a diurnal rhythm (Guchhait & Monjan, 1981), and contributes to methylation reactions required for melatonin synthesis through dose-dependent O-methylation of hydroxyindoles in the pineal gland (Bondarenko, 2004). The elevated methionine levels observed during the night underscore its critical role in melatonin production and circadian rhythm modulation. Isoleucine, a branched-chain amino acid (BCAA), serves as both an energy substrate and a regulator of protein synthesis, further supporting the gland's nocturnal energy demands and cellular maintenance. **(Figure 12M).** The purine metabolites xanthine and inosine were also elevated in night-time deaths **(Figure 12C, N)**. Xanthine is a key intermediate in purine degradation, and its nocturnal increase may reflect the pineal gland's metabolic adaptations to higher energy demands for melatonin synthesis. Similarly, inosine is a precursor for ATP and GTP synthesis, providing substrates for the increased energy requirements at night. These findings suggest that purine metabolism may be more active during nocturnal periods to support the gland's circadian rhythm-driven functions.

Conversely, increased levels of lactate during day-time deaths **(Figure 12Q)**, align with earlier findings in pineal glands of rats exposed to continuous light, compared to those kept under alternating light and dark conditions (Nir et al., 1970). Lactate, a key product of anaerobic glycolysis, indicates a shift towards glycolytic energy production during the day (X. Li et al., 2022). This shift may occur in response to reduced metabolic demands or the need for rapid energy through anaerobic means (Dumas et al., 2021). Additionally, higher lactate levels during the day could result from reduced oxidative phosphorylation, as seen in continuous light exposure where

disrupted circadian rhythms altered cellular metabolism (Nir et al., 1970). By contrast, night-time metabolism favors oxidative phosphorylation, reducing reliance on glycolysis and leading to lower lactate at night. This is supported by the nocturnal upregulation of mitochondrial enzymes and ATP production to meet melatonin biosynthesis demand (Møller & Høyer, 1979). Thus, the elevated day-time lactate in our study may reflect a metabolic shift away from oxidative processes and toward glycolytic energy production, aligning with the gland's circadian modulation of energy metabolism.

Glutamine, another metabolite elevated during day-time deaths **(Figure 12S)**, plays a critical role in neurotransmitter synthesis and cellular nitrogen balance (Kurmi & Haigis, 2020). Moreover, as a precursor of glutamate (D. Zhang et al., 2024) and GABA (Hertz, 2013), glutamine supports neuronal activity and metabolic demands. Additionally, glutamine contributes to nucleotide biosynthesis (Kurmi & Haigis, 2020) and glutathione production, providing antioxidant defense (Dringen et al., 1999, 2000; Yu et al., 1999). While the pineal gland is relatively protected from oxidative stress during the night due to the antioxidant properties of melatonin (Arendt & Aulinas, 2022), day-time glutamine may contribute to sustaining basal antioxidant defences. Further, higher levels of glutamate, synthesized from glutamine, were observed during day-time deaths **(Figure 12R)**. Glutamate interacts with glutamate receptors on astrocytes in the pineal gland, triggering intracellular calcium signaling and NF-kB activation. This, in turn, promotes the release of pro-inflammatory cytokine, TNF-α, inhibiting melatonin synthesis directly or through its interaction with glutamate in pinealocytes (Villela et al., 2013). These mechanisms suggest that elevated glutamate levels during the day reflect the suppression of melatonin production (Kus et al., 1994), consistent with the diurnal regulation of melatonin synthesis, which peaks at night and diminishes during daylight hours.

We also observed increased levels of sn-glycero-3-phosphocholine (GPC) and O-phosphocholine during day-time deaths **(Figure 12T, U).** These intermediates are precursors to PC biosynthesis (McMaster, 2018), a major lipid component of cell membranes. Thus, the elevation of these intermediates during day-time deaths over night-time suggests that circadian rhythms might

influence lipid metabolism within the pineal gland. Outside the pineal gland context, studies have shown how circadian rhythms influence lipid metabolism. For example, Chua and colleagues demonstrated circadian variation in 35 lipid species in plasma, including triglycerides, diglycerides, and PCs, which were significantly elevated during the early day-time in healthy human males (Chua et al., 2013). These findings suggest a link between circadian rhythms and lipid metabolism in various tissues, though regulatory mechanisms may differ by organ type. While no studies have investigated the circadian regulation of lipid metabolism in the pineal gland, it is plausible that similar processes are at play, particularly given the gland's critical role in circadian rhythm modulation.

Our enrichment analysis revealed significant alterations in metabolic pathways based on the time of death, notably including glycerophospholipid metabolism, glutathione metabolism, glyoxylate and dicarboxylate metabolism, glycine, serine, and threonine metabolism, arginine biosynthesis, porphyrin metabolism, purine metabolism, nitrogen metabolism, pyrimidine metabolism, primary bile acid biosynthesis, lipoic acid metabolism, lysine degradation, biotin metabolism, alanine, aspartate and glutamate metabolism, histidine metabolism, cysteine and methionine metabolism, butanoate metabolism, valine, leucine and isoleucine biosynthesis, pantothenate and CoA biosynthesis, arginine and proline metabolism, selenocompound metabolism, D-Amino acid metabolism, sphingolipid metabolism, and taurine and hypotaurine metabolism **(Figure 13)**. Key metabolites driving these pathways were choline (glycerophospholipid, and glycerine, serine and threonine metabolism), ethanolamine (glycerophospholipid metabolism), glycine (glutathione, glyoxylate and dicarboxylate, porphyrin, primary bile acid biosynthesis, lipoic acid, and glycine, serine and threonine metabolism), ornithine (glutathione and arginine metabolism), serine (glyoxylate and dicarboxylate, glycine, serine and threonine, cysteine and methionine, D-amino acid, and sphingolipid metabolism), xanthine and inosine (purine metabolism), threonine (glycine, serine and threonine metabolism), alanine (alanine, aspartate and glutamate, and selenocompound metabolism), lysine (biotin metabolism), histidine (histidine metabolism), methionine (cysteine and methionine metabolism), and valine (pantothenate and CoA biosynthesis) **(Table 5)**. These findings align closely with results from our univariate analysis,

where the same metabolites were found to be altered. This not only validates our findings but also underscores the importance of these metabolites as markers for metabolic shifts in the pineal gland related to the time of death.

Correlation between the metabolomic profile of the pineal gland and the post-mortem interval (PMI)

Next, we investigated the relationship between the metabolomic profile of the pineal gland and the PMI. The multivariate regression model developed for PMI estimation in this study displayed a relative error of approximately 36 hours across a 9-day post-mortem period **(Figure 16)**, which cannot be explored with biological fluids such as vitreous humor and blood. Typically, these matrices become compromised due to putrefaction, the decomposition of the body by microbial action, as the post-mortem period extends, thus making PMI estimation increasingly difficult (Chighine et al., 2023; Duffy et al., 2011; Locci et al., 2021, 2023). However, our results suggest that the pineal gland metabolome remains resilient to these processes, offering a more robust alternative for PMI estimation even after prolonged periods of decomposition.

Further, studies with other matrices, such as the ocular fluids, pericardial fluid, and brain tissue, have also shown promise for PMI estimation with varying degrees of accuracy. Previous studies from our group employed ovine aqueous humor (AH) to estimate PMI, achieving prediction errors ranging from 59 minutes for PMIs < 500 minutes to 118 minutes for PMIs > 1000 minutes (Locci et. al., 2019). A follow-up study using ovine vitreous humor samples within a PMI window of 6 to 86 hours provided a prediction error of 8.5 hours over the entire range. While promising, these studies were conducted on an animal model under highly controlled conditions (Locci et al., 2023). Additionally, the ovine vitreous humor (VH) samples were derived from isolated sheep heads, which could lead to exogenous bacterial interference with the metabolome, despite the model appearing robust and reliable (Locci et al., 2023). The use of human samples for PMI estimation has been explored as well. Zelentsova et al. (2020) performed quantitative metabolomic profiling of serum, AH, and VH using ^{1}H-NMR spectroscopy (Zelentsova et al., 2020). This study showed that metabolomic changes in ocular fluids (AH and VH) occurred more

gradually than in blood, with a PMI window extending up to 58 hours (Zelentsova et al., 2020). These findings suggest that ocular fluids, like the VH, could serve as a more reliable matrix for PMI estimation compared to blood, which undergoes more rapid biochemical shifts post-mortem. Another study by Boroumand et al. (2023) employed HPLC-MS analysis of peptide fragments in VH to estimate PMI, identifying key biomarkers like thymosin β4 and vimentin fragments that correlated strongly with PMI. However, the model's applicability was limited to earlier post-mortem stages due to negligible concentrations of these markers in the hours immediately following death (Boroumand et al., 2023).

In contrast, the pineal gland's metabolic resilience allows for longer PMIs, as demonstrated in our study, where metabolic signatures remained detectable for up to 9 days. Our findings align with previous work by our group on human pericardial fluid, which showed similar potential for PMI estimation. Chighine et al. (2023) employed ^{1}H-NMR metabolomic analysis to monitor post-mortem changes in pericardial fluid, producing a model with a prediction error of 33-34 hours across a PMI range of 16-170 hours (Chighine et al., 2023). Other studies, by Singh et al. (2006), also support the utility of pericardial fluid for PMI estimation by correlating potassium and other electrolytes with the time since death (Singh et al., 2006). However, despite the success of pericardial fluid, it remains vulnerable to microbial degradation, especially in longer post-mortem periods. Another study by Prieto-Bonete et al. (2019) analyzed long-term PMI estimation using bone proteomics, identifying 32 key proteins that could be used to distinguish between cadavers with PMIs ranging from 5 to 20 years (Prieto-Bonete et al., 2019). While bone proteomics provides insight into long-term post-mortem changes, our findings suggest that the pineal gland could serve a complementary role, particularly in the early to mid-stage post-mortem period (up to 9 days), where current forensic techniques often fail to provide reliable PMI estimates. Overall, our results demonstrate that the pineal gland offers a significant temporal window for accurate PMI estimation, with an extended period of metabolic activity detectable up to 9 days post-mortem. This resilience positions the pineal gland as a promising matrix for forensic casework, especially in cases where traditional methods fail due to putrefaction or environmental degradation. Future studies focusing on larger sample sizes and

the application of high-resolution metabolomic techniques could further enhance the precision of pineal gland-based PMI estimation.

Specific metabolites and biochemical pathways influenced by post-mortem interval (PMI): Insights from VIP score and enrichment analysis

The distinct metabolic differences based on PMI were evaluated by Variable Importance in Projection (VIP) score and enrichment analysis. VIP score identified key metabolites such as glutamate, alanine, proline, succinate, and trimethylamine, which exhibited a positive correlation with PMI **(Figure 17).** Conversely, metabolites, such as glycerol, choline, taurine, serine, myo-inositol, and GABA were negatively correlated with PMI **(Figure 17)**. These results were further validated by univariate linear regression analysis using Pearson's correlation, which confirmed significant positive correlations for glutamate, succinate, tryptophan, trimethylamine, and uracil with PMI, and significant negative correlations for choline, inosine, taurine, glycerol, and ethylene glycol with PMI **(Figure 18)**.

Among the metabolites positively correlated with PMI, glutamate stood out due to its central role in various metabolic pathways, including butanoate, arginine, proline, and glutathione metabolism (Yelamanchi et al., 2016). Its increase with PMI **(Figure 18A)** likely reflects the the breakdown of amino acids and the cessation of cellular respiration, as glutamate is involved in nitrogen transfer and energy production (Cooper & Jeitner, 2016). Similarly, succinate, a key intermediate in the TCA cycle, butanoate, propionate, alanine, aspartate, and glutamate metabolism, exhibited a significant positive correlation with PMI **(Figure 18B)**. The accumulation of succinate is a well-known indicator of anaerobic metabolism (Li et al., 2017). Tryptophan, another metabolite positively correlated with PMI **(Figure 18C),** plays a key role in serotonin and melatonin synthesis (Höglund et al., 2019). This is in accordance with prior studies, where higher levels of tryptophan were significantly correlated with prolonged PMI (Grünblatt et al., 2009, 2010).

In contrast, metabolites such as choline and glycerol, which are essential components of cell membrane lipids, particularly phospholipids and triglycerides, demonstrated significant negative correlations with PMI **(Figure 18F and I)**. These findings deviate from prior studies that reported increased levels of choline and glycerol with PMI in other matrices, such as serum, AH, and VH of rabbits (Zelentsova et al., 2016) and humans (Zelentsova et al., 2020), as well as in rat blood (Fang et al., 2024; Z. Wu et al., 2018). This increase in other matrices is typically attributed to the enzymatic breakdown of lipids from cellular structures, as lipolysis accelerates under post-mortem conditions (Caballero-Moreno et al., 2024). The pineal gland, however, is anatomically distinct in its post-mortem behavior due to its deep positioning within the brain. This isolation may shield it from immediate bacterial invasion and environmental influences, at least during the initial stages post-mortem. A similar trend was observed for taurine **(Figure 18H)**, which also showed a negative correlation with PMI in our dataset. While taurine levels have been reported to increase with PMI in matrices such as human VH (Girela et al., 2008) and femoral blood (Steuer et al., 2024), our findings suggest a decrease in the pineal gland. This discrepancy likely reflects the pineal gland's specific post-mortem metabolic trajectory, influenced by its protected anatomical position and specific biochemical composition. Together, these findings underscore the pineal gland’s potential to offer insights into PMI, distinct from other matrices, making it a valuable forensic tool.

To gain deeper insights into the biochemical pathways influenced by PMI, pathway enrichment analysis was performed on the ^{1}H-NMR metabolomic data. This analysis revealed 16 key metabolic pathways significantly affected by PMI **(Figure 19, Table 6)**. Among the most affected pathways were butanoate metabolism, histidine metabolism, porphyrin metabolism, glutathione metabolism, nitrogen metabolism, propanoate metabolism, citrate cycle (TCA cycle), tryptophan metabolism, glyoxylate and dicarboxylate metabolism, arginine biosynthesis, alanine, aspartate and glutamate metabolism, taurine and hypotaurine metabolism, glycerolipid metabolism, arginine and proline metabolism, glycerophospholipid metabolism, and galactose metabolism. These pathways play critical roles in energy production, amino acid metabolism, and oxidative stress regulation (Brosnan & Brosnan, 2020; G. Wu et al., 2004; L. Zhang et al., 2021). The

perturbation of these pathways highlights the complex biochemical shifts that occur as cellular functions cease. Key metabolites driving these pathways include glutamate (butanoate metabolism, glutathione metabolism, nitrogen metabolism, and alanine, aspartate, and glutamate metabolism), succinate (butanoate, propanoate, TCA cycle, alanine, aspartate, and glutamate metabolism), tryptophan (tryptophan metabolism). Conversely, metabolites such as taurine (taurine and hypotaurine metabolism), glycerol (glycerolipid and galactose metabolism), and choline (glycerophospholipid metabolism) showed significant decreases with increasing PMI **(Table 7)**. These findings suggest that the pineal gland's metabolomic profile not only provides valuable insights into the biochemical changes occurring after death but also serves as a reliable matrix for PMI estimation. The observed correlations between specific metabolites and PMI could potentially aid in the development of more accurate forensic tools for time-of-death estimation, especially in cases where traditional methods are limited due to environmental factors or advanced decomposition.

In conclusion, the present work demonstrates the pineal gland's metabolomic profile as a promising forensic tool, offering insights into circadian-linked metabolic distinctions and its potential applications in PMI estimation. The findings revealed clear metabolic differences in the pineal gland based on whether death occurred during day-time or night-time, likely reflecting the gland's role in regulating circadian rhythms. These results suggest that the pineal gland's metabolomic profile could serve as a unique marker for determining the time window of death, offering an additional forensic tool for scenarios where differentiating between day-time and night-time deaths is relevant. Moreover, the pineal gland's metabolome demonstrated significant potential as a novel matrix for PMI estimation, especially when traditional biological samples are unavailable or compromised. The strong correlation observed between key metabolites and PMI, coupled with the significant enrichment of critical metabolic pathways, highlights the gland's ability to capture time-dependent biochemical changes during decomposition. Metabolic pathways related to energy production, amino acid metabolism, and oxidative stress were particularly affected, reflected in dynamic concentrations of metabolites such as glutamate, succinate, tryptophan, trimethylamine, uracil, choline, inosine, taurine,

glycerol, and ethylene glycol. These insights not only advance our understanding of post-mortem biochemistry but also underscore the forensic relevance of metabolomic profiling in estimating PMI.

This proof-of-concept study further demonstrates the potential of combining metabolomic profiling with advanced multivariate analyses to refine PMI estimation beyond the traditional methods. The pineal gland's unique anatomical and physiological characteristics enable it to provide metabolic information over an extended PMI window, a feature not typically accessible with existing forensic tools. Given the current reliance on the subjective experience of forensic pathologists, the pineal gland's post-mortem metabolome resilience presents an objective and scientifically grounded alternative. Despite lacking the protection of the BBB, the pineal gland shows remarkable metabolic stability post-mortem, likely due to its deep intracranial location, which shields it from environmental exposure and microbial invasion in the early stages of decomposition. This resilience positions the pineal gland as a robust matrix for PMI estimation, capable of capturing biochemical processes related to both time and cause of death.

Nevertheless, this preliminary study has certain limitations that must be acknowledged and addressed in future research. The relatively small sample size (n=15) represents a key limitation that may affect the generalizability of the findings. While robust trends in metabolomic shifts were observed between day-time and night-time deaths and across PMI, validation in larger, more diverse cohorts is essential to confirm these results and improve their forensic applicability. Furthermore, inherent variability in factors such as age, gender, season, cause of death, body mass index, at the time of death, and pre-mortem medications underscores the need for more controlled studies. Validation in the independent cohort will also be critical to assess the reproducibility of the observed metabolic distinctions and enhance the reliability of the findings. Finally, translating these findings into routine forensic workflows poses practical challenges. First, the specialized equipment required for high-resolution metabolomic analysis, such as ^{1}H-NMR spectroscopy, is not yet widely accessible in forensic laboratories, and training would be required to analyze and interpret these datasets. Moreover, the stability and transformation of

metabolites over time, influenced by microbial growth, environmental conditions, and tissue decomposition, further complicate real-time decision-making, especially when PMI estimation is needed weeks or months after death.

Nonetheless, the insights gained from this study demonstrate significant potential for forensic science. The pineal gland's ability to reflect circadian rhythms and PMI-related biochemical shifts offers a novel approach to narrowing down the time-of-death window in cases where conventional methods, such as body temperature, livor mortis, or rigor mortis, are unreliable. This is particularly relevant in advanced decomposition or when environmental factors obscure physical time-of-death indicators. These findings suggest that metabolomic profiling of the pineal gland could complement existing forensic tools, providing an additional layer of evidence for case reconstruction. By addressing the current limitations and building on these promising findings, future research could fully realize the forensic potential of the pineal gland, paving the way for more accurate and objective methods for determining the time of death and PMI.

SUPPLEMENTARY DATA

The data presented in this supplementary section represents a critical extension of the main thesis. While the main thesis focuses on metabolomic analysis of 15 post-mortem pineal glands, this supplementary dataset includes an additional 45 pineal glands, for a total of 60 samples. These additional samples were analyzed to validate and expand upon the insights gained from the initial dataset, to enhance the robustness and generalizability of the findings. However, due to logistical constraints, the 60 samples were processed in three separate batches , leading to observable batch effects in their metabolomic profile. Batch effects are a well-recognized challenge in metabolomic studies, arising when technical variation between batches masks or confounds biological variation. In this dataset, the batch effects introduce variability that limits the interpretability of the results, as evidenced by the Principal Component Analysis (PCA). To address this issue, the raw data have been sent to a certified statistician for advanced batch correction, and the final harmonized dataset will be presented during the thesis defense. While these results are preliminary, they provide valuable insights into the larger dataset's potential and emphasize the importance of addressing technical variation in metabolomics research.
Below, we summarize the sample characteristics, key findings, and the challenges posed by batch effects.

1. Overview of sample characteristics and metabolomic profiling of pineal glands

The pineal glands were collected from decedents of both sexes (M:F Ratio = 1:2.75; 16:F/44:M), aged between 20 and 86 years (mean age = 56.9 ± 16.7 years). The post-mortem interval (PMI) ranged from 1.2 days (28 hours) to 12 days (298 hours), ensuring a broad representation of decomposition stages. Among the 60 cases, 41 deaths occurred during the day-time, and 19 during the night-time. The pineal glands were classified into day-time and night-time groups based on the interval between sunrise and sunset, as determined by the specific date and season in Cagliari, Italy (GMT+1). The demographic parameters of the studied individuals and characteristics of pineal gland samples are summarized in **Table 8**. By capturing a wide range of ages, PMIs, and diurnal contexts, this expanded dataset aimed to uncover metabolic trends that could remain elusive in smaller and less heterogeneous cohorts.

Individual	Sex	Age (years)	Batch	Death at D/N	Time of death (hr)	Season at time of Death	Month of Death	PMI (hr)	PG total weight (mg)
1	F	67	1	D	07:20	Summer	June	57.17	139.8
2	M	77	1	D	17:50	Summer	April	167.73	93.8
3	F	61	1	N	03:30	Winter	March	64	36.7
4	M	57	1	D	18:00	Winter	March	49.5	76.1
5	F	61	1	D	15:15	Winter	March	219.3	252.8
6	F	57	1	N	03:00	Winter	February	61.15	130
7	M	63	1	D	20:20	Summer	June	44.83	56
8	M	49	1	D	12:30	Winter	November	74.62	127
9	F	43	1	D	18:20	Summer	July	98.17	146
10	F	77	1	D	18:10	Summer	July	163.23	121
11	M	61	1	D	17:30	Winter	November	190.5	375
12	F	55	1	N	00:00	Summer	June	65	15
13	M	20	1	N	05:30	Summer	May	61.5	48
14	M	70	1	N	03:00	Winter	March	70	110
15	F	40	1	N	22:45	Winter	October	85.75	107
16	M	35	1	D	20:30	Summer	June	25.05	65
17	F	29	2	D	17:35	Winter	October	44.92	113
18	M	30	2	D	11:00	Winter	November	48.5	44
19	M	48	2	D	11:00	Winter	November	30	56
20	F	41	2	D	07:30	Winter	November	76	175
21	M	40	2	D	11:30	Summer	August	32.48	134
22	M	30	2	D	06:20	Summer	July	80.17	33
23	F	70	2	D	13:40	Summer	April	167.83	77
24	M	35	2	N	/	Summer	May	/	167
25	F	51	2	D	18:00	Summer	May	90.5	28
26	M	76	2	D	08:30	Winter	February	58.47	53
27	M	62	2	D	10:30	Summer	May	33	14
28	M	49	2	N	21:30	Summer	June	94.87	47
29	M	82	2	N	04:42	Summer	May	107.82	26
30	M	69	2	N	01:00	Winter	October	209.63	77
31	M	72	2	N	03:00	Winter	January	66.26	59
32	M	43	2	N	21:00	Winter	December	97.95	84
33	F	74	2	N	21:55	Summer	April	64.58	46
34	F	/	2	D	09:00	Winter	November	149.5	180
35	M	62	2	D	16:30	Winter	March	55.15	101
36	M	38	2	D	10:45	Summer	April	54.65	207
37	M	62	2	N	05:00	Summer	June	81.41	77
38	M	31	3	D	18:00	Winter	October	46	84
39	M	84	3	D	07:15	Summer	May	37.17	72
40	M	49	3	N	00:30	Summer	July	38	15
41	M	53	3	D	10:15	Summer	July	28.26	32
42	M	81	3	D	17.10	Summer	August	99.49	185
43	M	66	3	D	15:00	Summer	June	167	161
44	M	72	3	D	08:15	Winter	November	63.7	43
45	M	56	3	D	18:00	Winter	March	49.5	117
46	M	42	3	N	04:08	Winter	February	181.63	43
47	M	47	3	D	14:30	Summer	July	28.43	57
48	M	77	3	D	08:58	Winter	December	298.77	39
49	M	51	3	N	00:30	Summer	June	43.77	136
50	M	86	3	D	19:00	Summer	July	74.5	23
51	F	66	3	D	14:05	Summer	April	216.2	83
52	M	70	3	D	09:55	Winter	February	151.6	63
53	M	59	3	D	11:05	Summer	June	56.43	15
54	F	78	3	N	23:49	Summer	September	84.7	55
55	M	80	3	D	10:30	Summer	May	52	23
56	M	73	3	N	23:12	Winter	December	87.3	41
57	M	53	3	D	07:25	Summer	June	52.6	58
58	M	/	3	D	07:50	Summer	June	78.67	93
59	M	34	3	D	15:43	Summer	April	50.37	18
60	M	35	3	D	18:00	Summer	August	54.5	32

Table 8: Demographic characteristics of the studied individuals and corresponding pineal gland weights. Abbreviations: F: Female, M: Male, D: Day, N: Night, PG: Pineal Gland.

2. Principal component analysis (PCA) of post-mortem pineal glands

PCA was conducted on the profiled dataset of 60 pineal glands to explore potential metabolic variation, with corresponding loading plots used to identify the metabolites contributing to the observed variance.

The PCA score scatter plot showed high variation, with the first three principal components (PCs) explaining 67.8% of the total variance **(Figure 20A)**. This high percentage suggests that the majority of the metabolic differences in the dataset are effectively captured by these PCs. While such a high level of explained variance is generally encouraging, the PCA results indicated pronounced batch effects. A batch effect was observed when samples were categorized by their respective processing batches (denoted by distinct shapes in the PCA score scatter plot), confirming variability due to the staggered processing of samples in three different batches. Moreover, four samples (16, 33, 40, and 58) were distributed outside the orthogonal space and hence identified as outliers and excluded from further analysis to avoid skewing results. The corresponding PCA loading plot shows the distribution of metabolites that contributed most strongly to the observed distribution of samples **(Figure 20B)**. However, any biological interpretation of these findings remains speculative until batch correction has been implemented, as it is currently unclear whether these metabolite variations reflect genuine biological differences or artificial shifts induced by processing conditions.

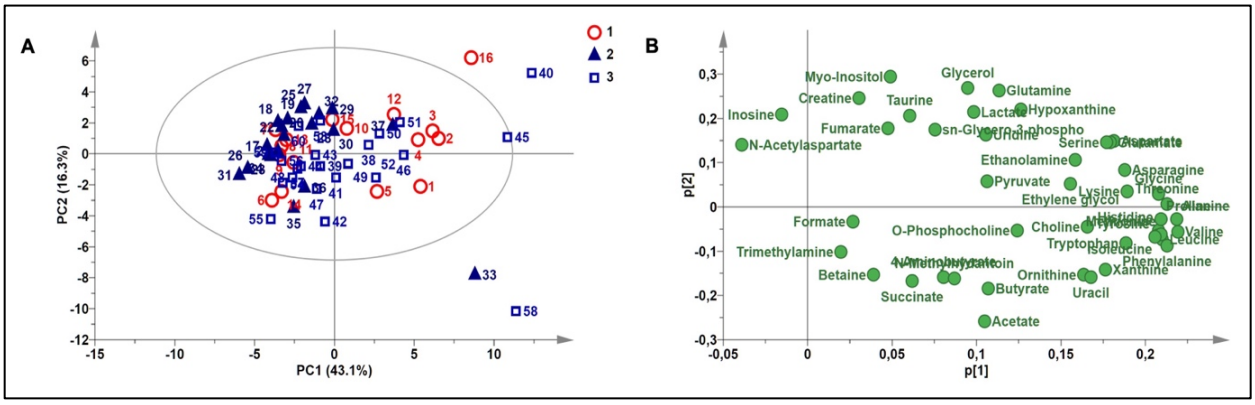

Figure 20: Principal Component Analysis (PCA) of post-mortem human pineal gland samples. **(A)** PCA score scatter plot (PC1 versus PC2) of pineal gland samples (n=60), represented by a distinct shape corresponding to its batch of origin (1, 2, or 3) (A = 3, total variance = 67.8%). **(B)** Corresponding PCA loading plot highlighting the metabolites contributing to the sample distribution observed in the score plot.

3. Seasonal variation and age influence on metabolomic profile of the pineal glands: OPLS-DA and OPLS Regression

Building on earlier findings from the initial set of 15 pineal glands, where certain factors, such as season at the time of death and age of an individual, appeared to exert a modest influence on the metabolomic profile, we attempted to validate and extend these observations using OPLS-DA and OPLS regression on the expanded dataset.

To assess the impact of the season, we stratified the samples based on the season (summer-April through September vs. winter-October through March) and performed supervised OPLS-DA analysis. The resulting model indicated no predictive power and a weak model fit, suggesting that season at the time of death does not significantly impact the metabolomic composition **(Figure 21A).** However, it would be premature to conclude that season exerts no meaningful influence on the pineal gland metabolome. Indeed, trends observed in OPLS-DA score scatter plot and box plots for specific metabolites (n-acetyl aspartate; p=0.018 and pyruvate; p=0.011, **Figure 22)** suggest that seasonal differences may exist but remain obscured, likely due to the presence of batch effects.

Similarly, when evaluating the effect of age on the metabolic profile using OPLS regression, the model exhibited low predictive power and a weak model fit **(Figure 21B)**. These results suggest that, in the current uncorrected dataset, age-related metabolic distinctions are not readily discernible. However, as with the seasonal analyses, ongoing batch corrections may reveal subtler trends that are currently overshadowed due to batch effects.

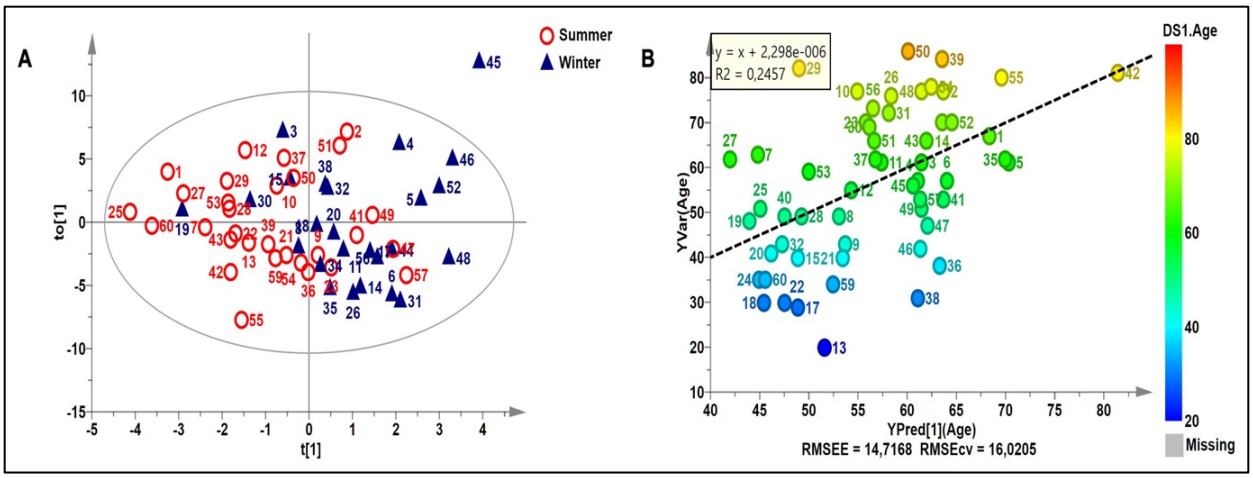

Figure 21: Influence of season and age on the pineal metabolome. (A) OPLS-DA score scatter plot showing the separation of pineal gland samples (n=56) based on season at the time of death (Summer-April through September vs. winter-October through March) (A=1+1, R^2Y= 0.28, Q^2Y = -0.29). **(B)** OPLS regression plot analyzing the correlation between the metabolomic profile and age of the individual (R^2Y= 0.245, Q^2Y = 0.06).

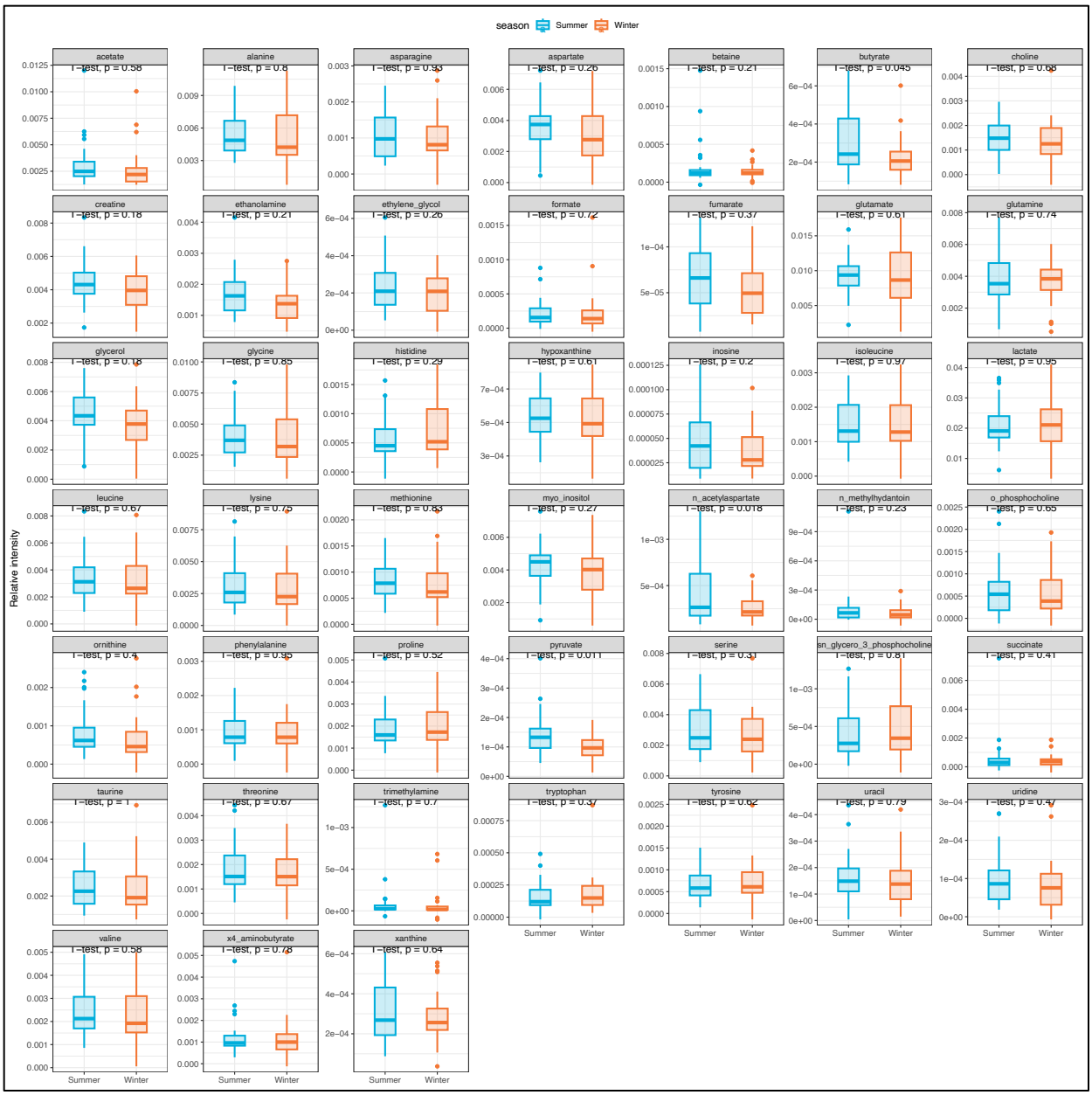

Figure 22: Box plots illustrating the preliminary metabolic differences between deaths that occurred during summer and winter based on univariate (student's t-test) analysis.

4. Metabolic differences between day-time and night-time deaths and their correlation with post-mortem interval (PMI)

We next explored potential metabolic differences related to the time of death by categorizing samples into day-time and night-time groups. Using ^{1}H-NMR metabolomic analysis and OPLS-DA, our preliminary model indicated that the current data do not robustly distinguish pineal gland

metabolome between day-time and night-time groups **(Figure 23A)**. The model's weak performance and lack of predictive power suggest that any subtle metabolic differences may be obscured by the uncorrected batch effects. It is therefore likely that subsequent batch correction will be necessary before drawing definitive conclusions about diurnal variations in the pineal metabolome. Further, a preliminary comparison of individual metabolites suggests that certain metabolites may differ between the two groups. Notably, trimethylamine showed a statistically significant difference (p=0.032) between day-time and night-time deaths **(Figure 24)**. This finding, albeit tentative, points to the possibility that circadian factors could influence specific metabolic pathways within the pineal gland.

Following this, we assessed whether the pineal gland metabolome correlates with PMI using a supervised OPLS regression model. This analysis was conducted on profiled datasets derived from ^{1}H-NMR metabolomic profiling, with PMI as the independent variable. In the OPLS regression curve, a linear correlation of actual PMI with the predictive PMI was observed **(Figure 23B)**. Although the current dataset has not yet undergone batch correction, the model exhibited good explanatory power. However, the predictive power of the model remained limited, reflecting the need for batch correction to improve precision **(Figure 23B)**. The model's relative error (RMSEcv=55.14 hours) further underscores that, while it captures overarching trends, there is a notable margin of error in predicting the exact PMI **(Figure 23B)**. Although the margin of error in predicting PMI remains relatively high, the metabolomic data from the 60 pineal glands still demonstrate a good correlation with PMI. This correlation, despite the current limitations, indicates potential for improvement through batch correction, and further investigation.

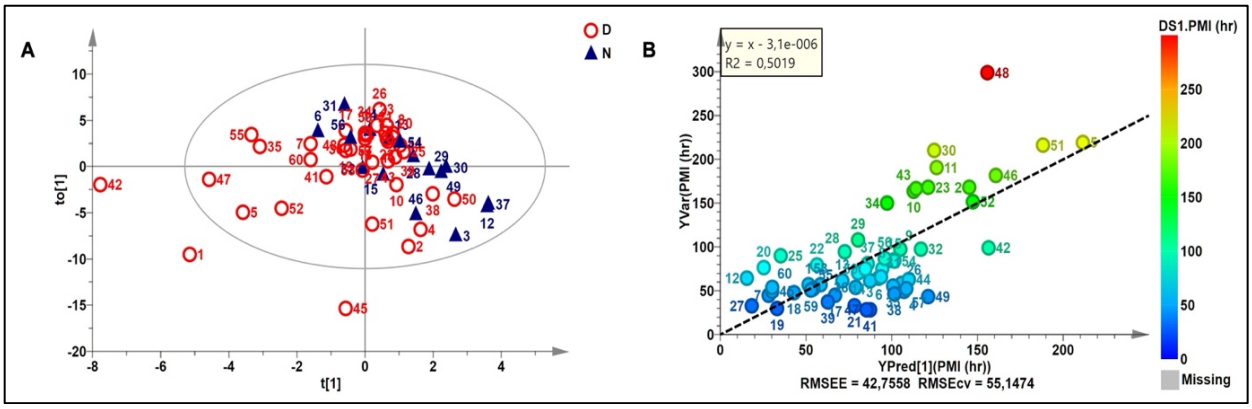

Figure 23: Influence of time of death (day-time vs. night-time) and Post-Mortem Interval (PMI) on the metabolomic profile of post-mortem human pineal glands. (A) OPLS-DA score scatter plot illustrating the separation of pineal gland samples based on time of death (day-time vs. night-time) (A=1+1, R^2Y= 0.14, Q^2Y = -0.07). **(B)** OPLS regression curve showing the correlation between metabolomic profile and PMI (R^2Y= 0.501, Q^2Y = 0.12).

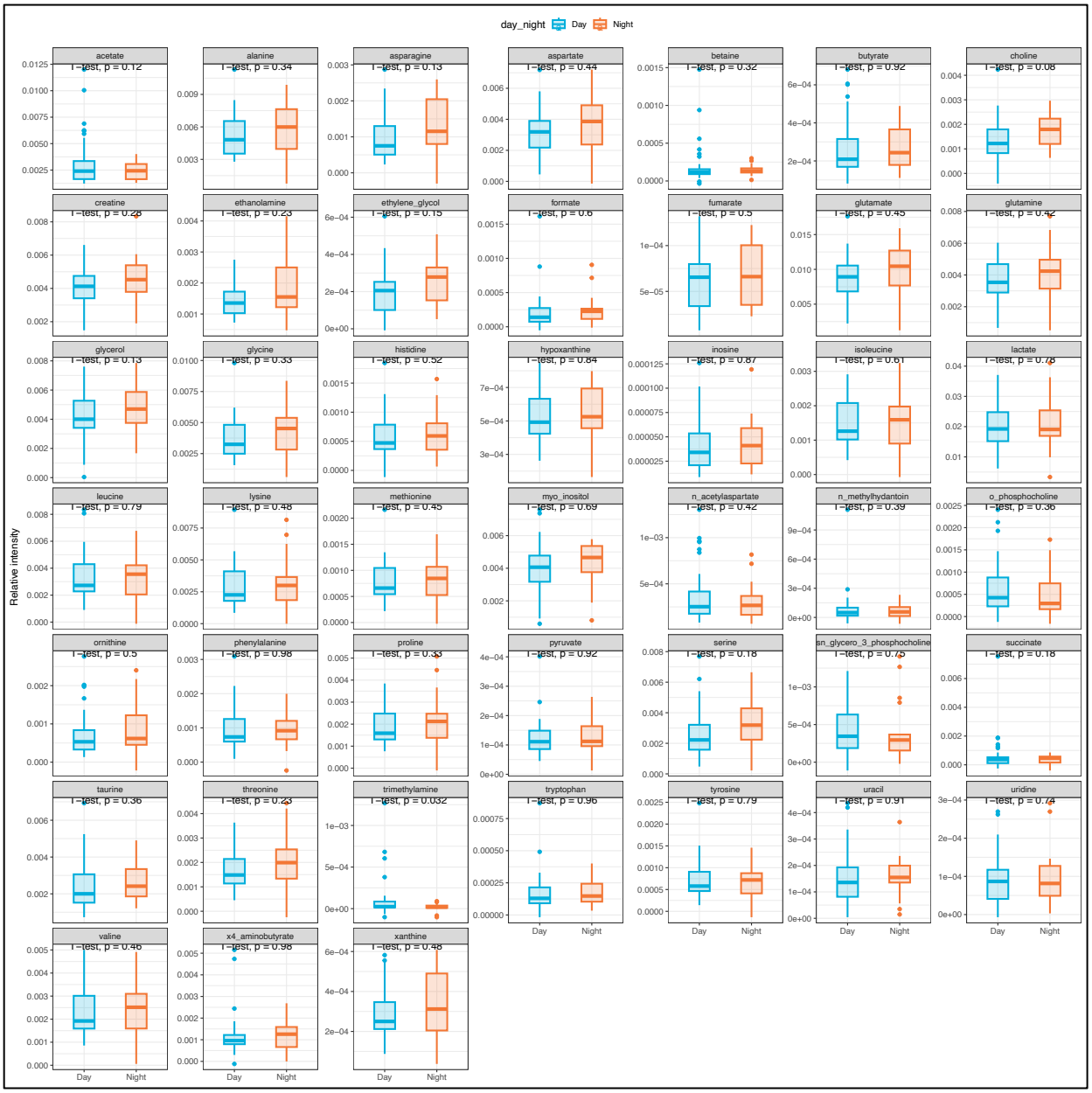

Figure 24: Box plots illustrating metabolic differences between day-time and night-time deaths, based on univariate (student's t-test) analysis.

5. Discussion

The supplementary data presented herein extend the scope of our initial metabolomic analysis of post-mortem human pineal glands, offering a preliminary examination of 60 samples. The aim was to broaden the metabolomic landscape initially characterized by the first 15 samples, thereby enhancing the robustness of our forensic and biological interpretations. Although the increased sample size was intended to refine our understanding of seasonal, temporal (day vs. night), PMI, and demographic (age, sex) influences on the pineal metabolome, the current findings are tempered by pronounced batch effects. These technical variations, introduced by staggered sample processing and potentially differing experimental conditions across batches, have hindered our ability to draw definitive conclusions at this stage. The demographic overview underscores the heterogeneity of the studied cohort, reflecting variations in gender, age, PMI, and estimated time of death relative to daylight hours. Such complexity is inherently valuable, as it creates an opportunity to dissect multifactorial influences on the pineal metabolome. However, before these data can be leveraged to their full potential, the technical confounding factors identified through PCA, namely, the cluster separation by batch, must be resolved.

The PCA and OPLS-based models, which were initially employed to explore the metabolic nuances within and between subgroups (such as age-related effects, seasonal differences, or diurnal influences), revealed weak or non-predictive patterns. For example, neither seasonality (summer vs. winter) nor age demonstrated robust, reproducible impacts on the metabolomic signature, as indicated by poor Q^2 and R^2 values. Similarly, the attempt to discriminate between day-time and night-time deaths yielded minimal predictive power under current conditions. Although some box plots suggested trends, hinting that certain metabolites, may vary with season (choline and pyruvate) or time of death (trimethylamine), these observations remain tentative and must be re-evaluated following data correction. One of the more promising lines of inquiry remains the relationship between the pineal metabolome and PMI. Even in the presence of batch effects, the OPLS regression suggested that metabolomic patterns are not entirely random with respect to PMI, as evidenced by an R^2Y value indicating that about half of the variance was captured. Yet, the predictive capacity remained limited (Q^2Y value was low),

emphasizing the need for a more refined dataset before concluding that the pineal metabolome can be reliably used for PMI estimation.

To address these shortcomings and restore confidence in biological interpretations, a certified statistician is currently applying advanced batch-correction techniques to the raw data. This recalibration is expected to enhance the sensitivity of our models, improve the predictive power of OPLS analyses, and potentially reveal more distinct metabolic profiles related to age, seasonal periods, circadian cycles, and PMI. Importantly, this approach aligns with best practices in metabolomics, where careful data normalization and batch-effect mitigation are essential for ensuring that findings are not confounded by experimental artifacts.

It is important to stress that the inclusion of these 60-sample data as supplementary material does not imply that they are peripheral or of limited value. On the contrary, these data are integral to achieving a more comprehensive, statistically robust understanding of the pineal metabolome's forensic and biological significance. The supplementary designation instead reflects their current, intermediate status: the analyses presented here are preliminary and openly acknowledge the need for further refinement. By situating these findings in the supplementary section, we maintain transparency about the ongoing nature of the work and highlight our commitment to presenting final, batch-corrected, and methodologically rigorous data at the thesis defense.

In conclusion, while the current analysis underscores the challenges posed by batch effects and the complexity of interpreting metabolomic data from diverse human cohorts, it also paves the way for future improvements. The application of advanced batch-correction methods promises to render the dataset more biologically interpretable, facilitating deeper insights into the metabolomic underpinnings of circadian rhythms, age and seasonal influences, PMI estimation, and other forensic determinants. Ultimately, this supplementary dataset, once corrected and validated, may complement and strengthen the findings presented in the main body of the thesis, contributing to a richer, more nuanced understanding of the pineal gland's metabolome.

ACRONYMS & ABBREVIATIONS

AANAT	Arylalkyl amine N-acetyltransferase
AH	Aqueous humor
ATP	Adenosine triphosphate
BCAA	Branched chain amino acid
Cdc25b	Cell division cycle 25 homologue B
circRNA	circular RNA
CoA	Coenzyme A
Ct	Cycle threshold
CT	Computed tomography
D_2O	Deuterium oxide
DNA	Deoxyribonucleic acid
FasL	Fas Ligand
GABA	4-amino-n-butyric acid
GAPDH	Glyceraldehyde-3-Phosphate-Dehydrogenase
GC-MS	Gas chromatography mass spectrometry
GPC	Glycero phosphocholine
GSH	Glutathione
GTEx	Genotype Tissue Expression
GTP	Guanosine triphosphate
HIOMT	Hydroxyindole-O-methyltransferase
HPLC	High performance liquid chromatography
ICU	Intensive care unit
KEGG	Kyoto Encyclopedia of Genes and Genomes
LC-MS	Liquid chromatography mass spectrometry
miRNA	microRNA
MRI	Magnetic resonance imaging
MS	Mass spectrometry
N/A	Not available
NMR	Nuclear Magnetic Resonance

NOS3	Nitric oxide synthase 3
n.s.	Non-significant
OPLS	Orthogonal partial least square
OPLS-DA	Orthogonal partial least square – discriminant analysis
PB	Phosphate buffer
PC	Phosphocholine
PCA	Principal component analysis
PMI	Post-mortem interval
PTEN	Phosphatase and tensin homologue
qPCR	quantitative polymerase chain reaction
REM	Rapid eye movement
RMSEcv	Relative error in cross validation
RNA	Ribonucleic acid
rRNA	ribosomal RNA
RT-PCR	Reverse transcription PCR
SCN	Suprachiasmatic nucleus
TCA	Tri carboxylic acid
TOF	Time of flight
TSP	Sodium 3-(trimethyl- silyl) propionate-2,2,3,3,-d4
VIP	Variable importance in projection
VH	Vitreous humor
VLMC	Vascular and leptomeningeal cell

REFERENCES

Ackermann, K., Bux, R., Rüb, U., Korf, H. W., Kauert, G., & Stehle, J. H. (2006). Characterization of Human Melatonin Synthesis Using Autoptic Pineal Tissue. *Endocrinology*, *147*(7), 3235–3242. https://doi.org/10.1210/EN.2006-0043

Agin, A., Heintz, D., Ruhland, E., Chao de la Barca, J. M., Zumsteg, J., Moal, V., Gauchez, A. S., & Namer, I. J. (2016). Metabolomics – an overview. From basic principles to potential biomarkers (part 1). *Médecine Nucléaire*, *40*(1), 4–10. https://doi.org/10.1016/J.MEDNUC.2015.12.006

Akçan, R., Taştekin, B., Yildirim, M. Ş., Aydogan, H. C., & Sağlam, N. (2020). Omics era in forensic medicine: towards a new age. *Turkish Journal of Medical Sciences*, *50*(5), 1480. https://doi.org/10.3906/SAG-1912-197

Almulhim, A. M., & Menezes, R. G. (2023). Evaluation of Postmortem Changes. *StatPearls*. https://www.ncbi.nlm.nih.gov/books/NBK554464/

Arendt, J., & Aulinas, A. (2022). Physiology of the Pineal Gland and Melatonin. *Endotext*. https://www.ncbi.nlm.nih.gov/books/NBK550972/

Babapulle, C. J., & Jayasundera, N. P. K. (1993). Cellular changes and time since death. *Medicine, Science, and the Law*, *33*(3), 213–222. https://doi.org/10.1177/002580249303300306

Bailey, M. J., Coon, S. L., Carter, D. A., Humphries, A., Kim, J. S., Shi, Q., Gaildrat, P., Morin, F., Ganguly, S., Hogenesch, J. B., Weller, J. L., Rath, M. F., Møller, M., Baler, R., Sugden, D., Rangel, Z. G., Munson, P. J., & Klein, D. C. (2009). Night/Day Changes in Pineal Expression of >600 Genes: CENTRAL ROLE OF ADRENERGIC/cAMP SIGNALING*S. *The Journal of Biological Chemistry*, *284*(12), 7606. https://doi.org/10.1074/JBC.M808394200

Bardale, R. V., Tumram, N. K., Dixit, P. G., & Deshmukh, A. Y. (2012). Evaluation of histologic changes of the skin in postmortem period. *The American Journal of Forensic Medicine and Pathology*, *33*(4), 357–361. https://doi.org/10.1097/PAF.0B013E31822C8F21

Bauer, M., Gramlich, I., Polzin, S., & Patzelt, D. (2003). Quantification of mRNA degradation as possible indicator of postmortem interval - A pilot study. *Legal Medicine*, *5*(4), 220–227. https://doi.org/10.1016/j.legalmed.2003.08.001

Bondarenko, L. A. (2004). Role of methionine in nocturnal melatonin peak in the pineal gland. *Bulletin of Experimental Biology and Medicine*, *137*(5), 431–432. https://doi.org/10.1023/B:BEBM.0000038144.51076.07

Bonicelli, A., Mickleburgh, H. L., Chighine, A., Locci, E., Wescott, D. J., & Procopio, N. (2022). The 'ForensOMICS' approach for postmortem interval estimation from human bone by integrating metabolomics, lipidomics, and proteomics. *ELife*, *11*. https://doi.org/10.7554/ELIFE.83658

Borjigin, J., Samantha Zhang, L., & Calinescu, A. A. (2011). Circadian Regulation of Pineal Gland Rhythmicity. *Molecular and Cellular Endocrinology*, *349*(1), 13. https://doi.org/10.1016/J.MCE.2011.07.009

Boroumand, M., Grassi, V. M., Castagnola, F., De-Giorgio, F., d'Aloja, E., Vetrugno, G., Pascali, V. L., Vincenzoni, F., Iavarone, F., Faa, G., & Castagnola, M. (2023). Estimation of postmortem interval using top-down HPLC–MS analysis of peptide fragments in vitreous humour: A pilot study. *International Journal of Mass Spectrometry*, *483*, 116952. https://doi.org/10.1016/J.IJMS.2022.116952

Brosnan, M. E., & Brosnan, J. T. (2020). Histidine Metabolism and Function. *The Journal of Nutrition*, *150*(Suppl 1), 2570S-2575S. https://doi.org/10.1093/JN/NXAA079

Bueno, C., Amaral, F. G. do, & Spruyt, K. (2023). Editorial: Melatonin and biological rhythms: from bench to bedside. *Frontiers in Neuroscience*, *17*, 1208878. https://doi.org/10.3389/FNINS.2023.1208878/BIBTEX

Byard, R. W. (2020). Estimation of the time since death in the early postmortem period (24–48 hours). *Estimation of the Time since Death: Current Research and Future Trends*, 11–27. https://doi.org/10.1016/B978-0-12-815731-2.00002-9

Caballero-Moreno, L., Luna, A., & Legaz, I. (2024). Lipidomes in Cadaveric Decomposition and Determination of the Postmortem Interval: A Systematic Review. *International Journal of Molecular Sciences*, *25*(2), 984. https://doi.org/10.3390/IJMS25020984

Campell, Z. K., Kwon, I., Finley, S. J., Lee, Y., & Javan, G. T. (2016). Talin: A potential protein biomarker in postmortem investigations. *Journal of Forensic and Legal Medicine*, *44*, 188–191. https://doi.org/10.1016/J.JFLM.2016.10.020

Chighine, A., Locci, E., Nioi, M., & D'Aloja, E. (2021). Looking for Post-Mortem Metabolomic Standardization: Waiting for Godot - The Importance of Post-Mortem Interval in Forensic Metabolomics. *Chemical Research in Toxicology*, *34*(9), 1946–1947. https://doi.org/10.1021/ACS.CHEMRESTOX.1C00211

Chighine, A., Stocchero, M., Ferino, G., De-Giorgio, F., Conte, C., Nioi, M., d'Aloja, E., & Locci, E. (2023). Metabolomics investigation of post-mortem human pericardial fluid. *International Journal of Legal Medicine*, *137*(6), 1875. https://doi.org/10.1007/S00414-023-03050-W

Chouchani, E. T., Pell, V. R., Gaude, E., Aksentijević, D., Sundier, S. Y., Robb, E. L., Logan, A., Nadtochiy, S. M., Ord, E. N. J., Smith, A. C., Eyassu, F., Shirley, R., Hu, C. H., Dare, A. J., James, A. M., Rogatti, S., Hartley, R. C., Eaton, S., Costa, A. S. H., … Murphy, M. P. (2014). Ischaemic accumulation of succinate controls reperfusion injury through mitochondrial ROS. *Nature*, *515*(7527), 431–435. https://doi.org/10.1038/NATURE13909

Chua, E. C. P., Shui, G., Lee, I. T. G., Lau, P., Tan, L. C., Yeo, S. C., Lam, B. D., Bulchand, S., Summers, S. A., Puvanendran, K., Rozen, S. G., Wenk, M. R., & Gooley, J. J. (2013). Extensive diversity in circadian regulation of plasma lipids and evidence for different circadian metabolic phenotypes in humans. *Proceedings of the National Academy of Sciences of the United States of America*, *110*(35), 14468–14473. https://doi.org/10.1073/PNAS.1222647110/-/DCSUPPLEMENTAL

Cina, S. J. (1994). Flow cytometric evaluation of DNA degradation: a predictor of postmortem interval? *The American Journal of Forensic Medicine and Pathology*, *15*(4), 300–302. https://doi.org/10.1097/00000433-199412000-00004

Clark, M. A., Worrell, M. B., & Pless, J. E. (1997). *Forensic Taphonomy: The Postmortem Fate of Human Remains: Vol. Chapter 9*.

Cockle, D. L., & Bell, L. S. (2017). The environmental variables that impact human decomposition in terrestrially exposed contexts within Canada. *Science & Justice : Journal of the Forensic Science Society*, *57*(2), 107–117. https://doi.org/10.1016/J.SCIJUS.2016.11.001

Cooper, A. J. L., & Jeitner, T. M. (2016). Central Role of Glutamate Metabolism in the Maintenance of Nitrogen Homeostasis in Normal and Hyperammonemic Brain. *Biomolecules*, *6*(2). https://doi.org/10.3390/BIOM6020016

Costanzo, M., Caterino, M., Sotgiu, G., Ruoppolo, M., Franconi, F., & Campesi, I. (2022). Sex differences in the human metabolome. *Biology of Sex Differences*, *13*(1), 1–18. https://doi.org/10.1186/S13293-022-00440-4/TABLES/7

Dawidowska, J., Krzyżanowska, M., Markuszewski, M. J., & Kaliszan, M. (2021). The Application of Metabolomics in Forensic Science with Focus on Forensic Toxicology and Time-of-Death Estimation. *Metabolites*, *11*(12). https://doi.org/10.3390/METABO11120801

De Saram, G. S. W., Webster, G., & Kathirgamatamby, N. (1956). Post-Mortem Temperature and the Time of Death. *Journal of Criminal Law and Criminology*, *46*(4). https://scholarlycommons.law.northwestern.edu/jclc

Deguchi, T. (1979). Circadian Rhythm of Serotonin N-Acetyltransferase Activity in Organ Culture of Chicken Pineal Gland. *Science*, *203*(4386), 1245–1247. https://doi.org/10.1126/SCIENCE.424750

Di Nunno, N., Costantinides, F., Cina, S. J., Rizzardi, C., Di Nunno, C., & Melato, M. (2002). What is the best sample for determining the early postmortem period by on-the-spot flow cytometry analysis? *The American Journal of Forensic Medicine and Pathology*, *23*(2), 173–180. https://doi.org/10.1097/00000433-200206000-00013

Di Nunno, N. R., Costantinides, F., Bernasconi, P., Bottin, C., & Melato, M. (1998). Is flow cytometric evaluation of DNA degradation a reliable method to investigate the early postmortem period? *The American Journal of Forensic Medicine and Pathology*, *19*(1), 50–53. https://doi.org/10.1097/00000433-199803000-00008

Donaldson, A. E., & Lamont, I. L. (2015). Metabolomics of post-mortem blood: identifying potential markers of post-mortem interval. *Metabolomics*, *11*(1), 237–245. https://doi.org/10.1007/S11306-014-0691-5/FIGURES/2

Dringen, R., Gutterer, J. M., & Hirrlinger, J. (2000). Glutathione metabolism in brain. *European Journal of Biochemistry*, *267*(16), 4912–4916. https://doi.org/10.1046/J.1432-1327.2000.01597.X

Dringen, R., Pfeiffer, B., & Hamprecht, B. (1999). Synthesis of the Antioxidant Glutathione in Neurons: Supply by Astrocytes of CysGly as Precursor for Neuronal Glutathione. *Journal of Neuroscience*, *19*(2), 562–569. https://doi.org/10.1523/JNEUROSCI.19-02-00562.1999

Duffy, J. F., Cain, S. W., Chang, A. M., Phillips, A. J. K., Muñch, M. Y., Gronfier, C., Wyatt, J. K., Dijk, D. J., Wright, K. P., & Czeisler, C. A. (2011). Sex difference in the near-24-hour intrinsic period of the human circadian timing system. *Proceedings of the National Academy of Sciences of the United States of America*, *108*(SUPPL. 3), 15602–15608. https://doi.org/10.1073/PNAS.1010666108/ASSET/BC485C3D-2F8D-4CE5-8B20-7D53181134B1/ASSETS/GRAPHIC/PNAS.1010666108FIG04.JPEG

Dufour-Rainfray, D., Lambérioux, M., Boulard, P., Guidotti, M., Delaye, J. B., Ribeiro, M. J., Gauchez, A. S., Balageas, A. C., Emond, P., & Agin, A. (2020). Metabolomics – an overview. From basic principles to potential biomarkers (part 2). *Médecine Nucléaire*, *44*(3), 158–163. https://doi.org/10.1016/J.MEDNUC.2020.02.004

Dumas, G., Goubran-Botros, H., Matondo, M., Pagan, C., Boulègue, C., Chaze, T., Chamot-Rooke, J., Maronde, E., & Bourgeron, T. (2021). Mass-spectrometry analysis of the human pineal proteome during night and day and in autism. *Journal of Pineal Research*, *70*(3). https://doi.org/10.1111/JPI.12713

Dunn, W. B., & Ellis, D. I. (2005). Metabolomics: Current analytical platforms and methodologies. *TrAC Trends in Analytical Chemistry*, *24*(4), 285–294. https://doi.org/10.1016/J.TRAC.2004.11.021

Eden, R. E., & Thomas, B. (2023). Algor Mortis. *RevSALUS - Revista Científica Da Rede Académica Das Ciências Da Saúde Da Lusofonia*, *4*(Sup). https://doi.org/10.51126/revsalus.v4isup.304

Fang, S., Dai, X., Shi, X., Xiao, L., Ye, Y., & Liao, L. (2024). A pilot study investigating early postmortem interval of rats based on ambient temperature and postmortem interval-related metabolites in blood. *Forensic Science, Medicine, and Pathology*, *20*(2), 560–568. https://doi.org/10.1007/S12024-023-00643-0/TABLES/3

Ferreira, P. G., Muñoz-Aguirre, M., Reverter, F., Sá Godinho, C. P., Sousa, A., Amadoz, A., Sodaei, R., Hidalgo, M. R., Pervouchine, D., Carbonell-Caballero, J., Nurtdinov, R., Breschi, A., Amador, R., Oliveira, P., Çubuk, C., Curado, J., Aguet, F., Oliveira, C., Dopazo, J., … Guigó, R. (2018). The effects of death and post-mortem cold ischemia on human tissue transcriptomes. *Nature Communications*, *9*(1). https://doi.org/10.1038/S41467-017-02772-X

Fiedler, S., & Graw, M. (2003). Decomposition of buried corpses, with special reference to the formation of adipocere. *Naturwissenschaften*, *90*(7), 291–300. https://doi.org/10.1007/S00114-003-0437-0/FIGURES/2

Fordyce, S. L., Kampmann, M. L., van Doorn, N. L., & Gilbert, M. T. P. (2013). Long-term RNA persistence in postmortem contexts. *Investigative Genetics*, *4*(1), 7. https://doi.org/10.1186/2041-2223-4-7

Gastel, J. A., Roseboom, P. H., Rinaldi, P. A., Weller, J. L., & Klein, D. C. (1998). Melatonin production: proteasomal proteolysis in serotonin N-acetyltransferase regulation. *Science (New York, N.Y.)*, *279*(5355), 1358–1360. https://doi.org/10.1126/SCIENCE.279.5355.1358

Gheban, B. A., Colosi, H. A., Gheban-Rosca, I. A., Pop, B., Domșa, A. M. T., Georgiu, C., Gheban, D., Crișan, D., & Crișan, M. (2021). Age-Related Changes of the Pineal Gland in Humans: A Digital Anatomo-Histological Morphometric Study on Autopsy Cases with Comparison to Predigital-Era Studies. *Medicina 2021, Vol. 57, Page 383*, *57*(4), 383. https://doi.org/10.3390/MEDICINA57040383

Girela, E., Villanueva, E., Irigoyen, P., Girela, V., Hernández-Cueto, C., & Peinado, J. M. (2008). Free Amino Acid Concentrations in Vitreous Humor and Cerebrospinal Fluid in Relation to the Cause of Death and Postmortem Interval. *Journal of Forensic Sciences*, *53*(3), 730–733. https://doi.org/10.1111/J.1556-4029.2008.00726.X

Goff, M. L. (2009). Early post-mortem changes and stages of decomposition in exposed cadavers. *Experimental and Applied Acarology*, *49*(1–2), 21–36. https://doi.org/10.1007/S10493-009-9284-9/FIGURES/13

Grünblatt, E., Monoranu, C. M., Apfelbacher, M., Keller, D., Michel, T. M., Alafuzoff, I., Ferrer, I., Al-Saraj, S., Keyvani, K., Schmitt, A., Falkai, P., Schittenhelm, J., McLean, C., Halliday, G. M., Harper, C., Deckert, J., Roggendorf, W., & Riederer, P. (2009). Tryptophan is a marker of human postmortem brain tissue quality. *Journal of Neurochemistry*, *110*(5), 1400–1408. https://doi.org/10.1111/J.1471-4159.2009.06233.X

Grünblatt, E., Proft, F., Apfelbacher, M., Deckert, J., Roggendorf, W., Riederer, P., & Monoranu, C. M. (2010). Brain tryptophan rather than pH-value is altered as consequence of artificial

postmortem interval and storage conditions. *Neurochemistry International*, *57*(7), 819–822. https://doi.org/10.1016/J.NEUINT.2010.08.020

Guchhait, R. B., & Monjan, A. A. (1981). Circadian rhythm in pineal methionine S-adenosyltransferase. *Journal of Neurochemistry*, *36*(6), 2092–2093. https://doi.org/10.1111/J.1471-4159.1981.TB10840.X

Haas, C., Neubauer, J., Salzmann, A. P., Hanson, E., & Ballantyne, J. (2021). Forensic transcriptome analysis using massively parallel sequencing. *Forensic Science International: Genetics*, *52*. https://doi.org/10.1016/J.FSIGEN.2021.102486

Hao L.G, Deng S.X., & Zhao X.C. (2007). Recent advancement in relationship between DNA degradation and postmortem interval. *Fa Yi Xue Za Zhi*.

Harrison, A., Hardison, R. L., Wallace, R. M., Fitch, J., Heimlich, D. R., Bryan, M. O., Dubois, L., John-Williams, L. S., Sebra, R. P., White, P., Moseley, M. A., Thompson, J. W., Justice, S. S., & Mason, K. M. (2019). Reprioritization of biofilm metabolism is associated with nutrient adaptation and long-term survival of Haemophilus influenzae. *Npj Biofilms and Microbiomes 2019 5:1*, *5*(1), 1–14. https://doi.org/10.1038/s41522-019-0105-6

Hertz, L. (2013). The glutamate-glutamine (GABA) cycle: Importance of late postnatal development and potential reciprocal interactions between biosynthesis and degradation. *Frontiers in Endocrinology*, *4*(MAY), 51460. https://doi.org/10.3389/FENDO.2013.00059/BIBTEX

Höglund, E., Øverli, Ø., & Winberg, S. (2019). Tryptophan metabolic pathways and brain serotonergic activity: A comparative review. *Frontiers in Endocrinology*, *10*(APR), 435368. https://doi.org/10.3389/FENDO.2019.00158/BIBTEX

Houlton, T. M. R., & Wilkinson, C. (2018). Facial preservation following extreme mummification: Shrunken heads. *Forensic Science International*, *286*, 31–41. https://doi.org/10.1016/J.FORSCIINT.2018.02.028

Hunter, M. C., Pozhitkov, A. E., & Noble, P. A. (2017). Accurate predictions of postmortem interval using linear regression analyses of gene meter expression data. *Forensic Science International*, *275*, 90–101. https://doi.org/10.1016/J.FORSCIINT.2017.02.027

Inoue, H., Kimura, A., & Tuji, T. (2002). Degradation profile of mRNA in a dead rat body: Basic semi-quantification study. *Forensic Science International*, *130*(2–3), 127–132. https://doi.org/10.1016/S0379-0738(02)00352-3

Jaafar, S., & Nokes, L. D. M. (1994). Examination of the eye as a means to determine the early postmortem period: a review of the literature. *Forensic Science International*, *64*(2–3), 185–189. https://doi.org/10.1016/0379-0738(94)90230-5

Javan, G. T., Kwon, I., Finley, S. J., & Lee, Y. (2015). Progression of thanatophagy in cadaver brain and heart tissues. *Biochemistry and Biophysics Reports*, *5*, 152–159. https://doi.org/10.1016/J.BBREP.2015.11.013

Johnson, L. A., & Ferris, J. A. J. (2002). Analysis of postmortem DNA degradation by single-cell gel electrophoresis. *Forensic Science International*, *126*(1), 43–47. https://doi.org/10.1016/S0379-0738(02)00027-0

Kametani, H., & Kawamura, H. (1991). Circadian rhythm of cortical acetylcholine release as measured by in vivo microdialysis in freely moving rats. *Neuroscience Letters*, *132*(2), 263–266. https://doi.org/10.1016/0304-3940(91)90316-L

Kori, S. (2018). Time since Death from Rigor Mortis: Forensic Prospective. *Journal of Forensic Sciences & Criminal Investigation*, *9*(5), 1–10. https://doi.org/10.19080/JFSCI.2018.09.555771

Kurmi, K., & Haigis, M. C. (2020). Nitrogen Metabolism in Cancer and Immunity. *Trends in Cell Biology*, *30*(5), 408–424. https://doi.org/10.1016/J.TCB.2020.02.005

Kurup, S. S., Bharathi, M., Narayan, G., R, V., R, R., & Suvvari, T. K. (2023). Estimation of Time Since Death From Potassium Levels in Vitreous Humor in Cases of Unnatural Death: A Facility-Based Cross-Sectional Study. *Cureus*, *15*(5). https://doi.org/10.7759/CUREUS.39572

Kus, L., Handa, R. J., & McNulty, J. A. (1994). Glutamate inhibition of the adrenergic-stimulated production of melatonin in rat pineal gland in vitro. *Journal of Neurochemistry*, *62*(6), 2241–2245. https://doi.org/10.1046/J.1471-4159.1994.62062241.X

Leccia, C., Alunni, V., & Quatrehomme, G. (2018). Modern (forensic) mummies: A study of twenty cases. *Forensic Science International*, *288*, 330.e1-330.e9. https://doi.org/10.1016/J.FORSCIINT.2018.04.029

Li, Q., Huang, B., Wu, H., Li, Z., & Ye, Q. (2017). Efficient anaerobic production of succinate from glycerol in engineered Escherichia coli by using dual carbon sources and limiting oxygen supply in preceding aerobic culture. *Bioresource Technology*, *231*, 75–84. https://doi.org/10.1016/J.BIORTECH.2017.01.051

Li, W. C., Ma, K. J., Lv, Y. H., Zhang, P., Pan, H., Zhang, H., Wang, H. J., Ma, D., & Chen, L. (2014). Postmortem interval determination using 18S-rRNA and microRNA. *Science & Justice*, *54*(4), 307–310. https://doi.org/10.1016/J.SCIJUS.2014.03.001

Li, X., Yang, Y., Zhang, B., Lin, X., Fu, X., An, Y., Zou, Y., Wang, J. X., Wang, Z., & Yu, T. (2022). Lactate metabolism in human health and disease. *Signal Transduction and Targeted Therapy 2022 7:1*, *7*(1), 1–22. https://doi.org/10.1038/s41392-022-01151-3

Lin, C., Tian, Q., Guo, S., Xie, D., Cai, Y., Wang, Z., Chu, H., Qiu, S., Tang, S., & Zhang, A. (2024). Metabolomics for Clinical Biomarker Discovery and Therapeutic Target Identification. *Molecules 2024, Vol. 29, Page 2198*, *29*(10), 2198. https://doi.org/10.3390/MOLECULES29102198

Locci, E., Stocchero, M., Gottardo, R., Chighine, A., De-Giorgio, F., Ferino, G., Nioi, M., Demontis, R., Tagliaro, F., & d'Aloja, E. (2023). PMI estimation through metabolomics and potassium analysis on animal vitreous humour. *International Journal of Legal Medicine*, *137*(3), 887–895. https://doi.org/10.1007/S00414-023-02975-6/TABLES/1

Locci, E., Stocchero, M., Gottardo, R., De-Giorgio, F., Demontis, R., Nioi, M., Chighine, A., Tagliaro, F., & d'Aloja, E. (2021). Comparative use of aqueous humour 1H NMR metabolomics and potassium concentration for PMI estimation in an animal model. *International Journal of Legal Medicine*, *135*(3), 845–852. https://doi.org/10.1007/S00414-020-02468-W/FIGURES/2

Locci, E., Stocchero, M., Noto, A., Chighine, A., Natali, L., Napoli, P. E., Caria, R., De-Giorgio, F., Nioi, M., & d'Aloja, E. (2019). A 1 H NMR metabolomic approach for the estimation of the time since death using aqueous humour: an animal model. *Metabolomics*, *15*(5), 1–13. https://doi.org/10.1007/S11306-019-1533-2/FIGURES/5

Luo G.H., Chen Y.C, Cheng J.D., Wang J.F., & Gao C.L. (2006). Relationship between DNA degradation and postmortem interval of corrupt corpse. *Fa Yi Xue Za Zhi*.

Lv, Y. H., Ma, J. L., Pan, H., Zhang, H., Li, W. C., Xue, A. M., Wang, H. J., Ma, K. J., & Chen, L. (2016). RNA degradation as described by a mathematical model for postmortem interval determination. *Journal of Forensic and Legal Medicine*, *44*, 43–52. https://doi.org/10.1016/J.JFLM.2016.08.015

Madea, B. (2016). Methods for determining time of death. *Forensic Science, Medicine, and Pathology*, *12*(4), 451–485. https://doi.org/10.1007/S12024-016-9776-Y

Marcheva, B., Ramsey, K. M., Peek, C. B., Affinati, A., Maury, E., & Bass, J. (2013). Circadian Clocks and Metabolism. *Handbook of Experimental Pharmacology*, *217*(217), 127. https://doi.org/10.1007/978-3-642-25950-0_6

Marks, M. K., & Tersigni, M. A. (2005). DECOMPOSITION, PATTERNS AND RATES. *Encyclopedia of Forensic and Legal Medicine*, 148–152. https://doi.org/10.1016/B0-12-369399-3/00415-8

Marrosu, F., Portas, C., Mascia, M. S., Casu, M. A., Fà, M., Giagheddu, M., Imperato, A., & Gessa, G. L. (1995). Microdialysis measurement of cortical and hippocampal acetylcholine release during sleep-wake cycle in freely moving cats. *Brain Research*, *671*(2), 329–332. https://doi.org/10.1016/0006-8993(94)01399-3

Masters, A., Pandi-Perumal, S. R., Seixas, A., Girardin, J.-L., & McFarlane, S. I. (2014). Melatonin, the Hormone of Darkness: From Sleep Promotion to Ebola Treatment. *Brain Disorders & Therapy*, *4*(1). https://doi.org/10.4172/2168-975X.1000151

Matsuo, H., Iwamoto, A., Otsuka, T., Hishida, Y., Akiduki, S., Aoki, M., Furuse, M., & Yasuo, S. (2015). Effects of time of L-ornithine administration on the diurnal rhythms of plasma growth hormone, melatonin, and corticosterone levels in mice. *Chronobiology International*, *32*(2), 225–234. https://doi.org/10.3109/07420528.2014.965312

McMaster, C. R. (2018). From yeast to humans – roles of the Kennedy pathway for phosphatidylcholine synthesis. *FEBS Letters*, *592*(8), 1256–1272. https://doi.org/10.1002/1873-3468.12919

Meurs, J. (2023). Immediate Postmortem Changes. *Encyclopedia of Forensic Sciences: Volume 1-4, Third Edition*, *3*, 218–223. https://doi.org/10.1016/B978-0-12-823677-2.00022-2

Mickleburgh, H. L., Schwalbe, E. C., Bonicelli, A., Mizukami, H., Sellitto, F., Starace, S., Wescott, D. J., Carter, D. O., & Procopio, N. (2021). Human Bone Proteomes before and after Decomposition: Investigating the Effects of Biological Variation and Taphonomic Alteration on Bone Protein Profiles and the Implications for Forensic Proteomics. *Journal of Proteome Research*, *20*(5), 2533–2546. https://doi.org/10.1021/ACS.JPROTEOME.0C00992/SUPPL_FILE/PR0C00992_SI_001.PDF

Miyake, M., Kirisako, T., Kokubo, T., Miura, Y., Morishita, K., Okamura, H., & Tsuda, A. (2014). Randomised controlled trial of the effects of L-ornithine on stress markers and sleep quality in healthy workers. *Nutrition Journal*, *13*(1). https://doi.org/10.1186/1475-2891-13-53

Møller, M., & Høyer, P. E. (1979). Histochemical demonstration of a circadian rhythm of succinate dehydrogenase in rat pineal gland. Influence of coenzyme Q10 addition. *Histochemistry*, *59*(4), 259–269. https://doi.org/10.1007/BF00689608/METRICS

Møller, M., Sparre, T., Bache, N., Roepstorff, P., & Vorum, H. (2007). Proteomic analysis of day–night variations in protein levels in the rat pineal gland. *PROTEOMICS*, *7*(12), 2009–2018. https://doi.org/10.1002/PMIC.200600963

Monteiro, M. S., Carvalho, M., Bastos, M. L., & Guedes de Pinho, P. (2013). Metabolomics analysis for biomarker discovery: advances and challenges. *Current Medicinal Chemistry*, *20*(2), 257–271. https://doi.org/10.2174/092986713804806621

Mora-Ortiz, M., Trichard, M., Oregioni, A., & Claus, S. P. (2019). Thanatometabolomics: introducing NMR-based metabolomics to identify metabolic biomarkers of the time of death. *Metabolomics*, *15*(3), 37. https://doi.org/10.1007/S11306-019-1498-1

Moslehi, M., Moazamiyanfar, R., Dakkali, M. S., Rezaei, S., Rastegar-Pouyani, N., Jafarzadeh, E., Mouludi, K., Khodamoradi, E., Taeb, S., & Najafi, M. (2022). Modulation of the immune system by melatonin; implications for cancer therapy. *International Immunopharmacology*, *108*, 108890. https://doi.org/10.1016/J.INTIMP.2022.108890

Murgia, F., Atzori, L., Carboni, E., Santoru, M. L., Hendren, A., Pisanu, A., Caboni, P., Boi, L., Fusco, G., & Carta, A. R. (2020). Metabolomics Fingerprint Induced by the Intranigral Inoculation of Exogenous Human Alpha-Synuclein Oligomers in a Rat Model of Parkinson's Disease. *International Journal of Molecular Sciences*, *21*(18), 1–18. https://doi.org/10.3390/IJMS21186745

Nir, I., Hirschmann, N., & Sulman, F. G. (1970). The Effect of Light and Darkness on Lactic Acid Content of the Pineal Gland. *Https://Doi.Org/10.3181/00379727-133-34495*, *133*(2), 452–455. https://doi.org/10.3181/00379727-133-34495

Nolan, A. N. D., Mead, R. J., Maker, G., Bringans, S., & Speers, S. J. (2019). The impact of environmental factors on the production of peptides in mammalian decomposition fluid in relation to the estimation of post-mortem interval: A summer/winter comparison in Western Australia. *Forensic Science International*, *303*. https://doi.org/10.1016/J.FORSCIINT.2019.109957

Olcese, J. M., Cretoiu, D., Klein, D. C., Coon, S. L., Fu, C., Hartley, S. W., Holtzclaw, L., Mays, J. C., Kelly, M. C., Kelley, M. W., Mullikin, J. C., Rath, M. F., & Savastano, L. E. (2019). Single Cell Sequencing of the Pineal Gland: The Next Chapter. *Frontiers in Endocrinology | Www.Frontiersin.Org*, *10*, 590. https://doi.org/10.3389/fendo.2019.00590

Owino, S., Buonfiglio, D. D. C., Tchio, C., & Tosini, G. (2019). Melatonin signaling a key regulator of glucose homeostasis and energy metabolism. *Frontiers in Endocrinology*, *10*(JULY), 460748. https://doi.org/10.3389/FENDO.2019.00488/BIBTEX

Paczkowski, S., & Schütz, S. (2011). Post-mortem volatiles of vertebrate tissue. *Applied Microbiology and Biotechnology 2011 91:4*, *91*(4), 917–935. https://doi.org/10.1007/S00253-011-3417-X

Partemi, S., Berne, P. M., Batlle, M., Berruezo, A., Mont, L., Riuró, H., Ortiz, J. T., Roig, E., Pascali, V. L., Brugada, R., Brugada, J., & Oliva, A. (2010). Analysis of mRNA from human heart tissue and putative applications in forensic molecular pathology. *Forensic Science International*, *203*(1–3), 99–105. https://doi.org/10.1016/J.FORSCIINT.2010.07.005

Pasca, P., & Ulasan, K. : (2014). Decomposition Process and Post Mortem Changes: Review. *Sains Malaysiana*, *43*(12), 1873–1882.

Peruri, A., Morgan, A., D'souza, A., Mellon, B., Hung, C. W., Kayal, G., Shin, H., Nguyen, K., Zahed, M., Yount, M., Ellis, R., Wynne, T., Fritz, V., Simmons, Z., & Roballo, K. C. S. (2022). *Pineal Gland from the Cell Culture to Animal Models: A Review*. https://doi.org/10.3390/life12071057

Pesko, B. K., Weidt, S., McLaughlin, M., Wescott, D. J., Torrance, H., Burgess, K., & Burchmore, R. (2020). Postmortomics: The Potential of Untargeted Metabolomics to Highlight Markers for Time Since Death. *OMICS : A Journal of Integrative Biology*, *24*(11), 649. https://doi.org/10.1089/OMI.2020.0084

Prahlow, J. A., & Byard, R. W. (2012). Postmortem Changes and Time of Death. *Atlas of Forensic Pathology*, 145–198. https://doi.org/10.1007/978-1-61779-058-4_8

Prieto-Bonete, G., Pérez-Cárceles, M. D., Maurandi-López, A., Pérez-Martínez, C., & Luna, A. (2019a). Association between protein profile and postmortem interval in human bone remains. *Journal of Proteomics*, *192*, 54–63. https://doi.org/10.1016/J.JPROT.2018.08.008

Prieto-Bonete, G., Pérez-Cárceles, M. D., Maurandi-López, A., Pérez-Martínez, C., & Luna, A. (2019b). Association between protein profile and postmortem interval in human bone remains. *Journal of Proteomics*, *192*, 54–63. https://doi.org/10.1016/J.JPROT.2018.08.008

Procopio, N., Williams, A., Chamberlain, A. T., & Buckley, M. (2018). Forensic proteomics for the evaluation of the post-mortem decay in bones. *Journal of Proteomics*, *177*, 21–30. https://doi.org/10.1016/J.JPROT.2018.01.016

Shedge, R., Krishan, K., Warrier, V., & Kanchan, T. (2023). Postmortem Changes. *StatPearls*. https://www.ncbi.nlm.nih.gov/books/NBK539741/

Sherry, E. B., Lee, P., & Choi, I. Y. (2015). In Vivo NMR Studies of the Brain with Hereditary or Acquired Metabolic Disorders. *Neurochemical Research*, *40*(12), 2647–2685. https://doi.org/10.1007/S11064-015-1772-1

Shirley, N. R., Wilson, R. J., & Jantz, L. M. (2011). Cadaver use at the University of Tennessee's Anthropological Research Facility. *Clinical Anatomy*, *24*(3), 372–380. https://doi.org/10.1002/CA.21154

Shukla, R. K. (2017). Forensic Application of Comet Assay: An Emerging Technique. *Forensic Sciences Research*, *2*(4), 180–184. https://doi.org/10.1080/20961790.2017.1379893

Singh, D., Prashad, R., Sharma, S. K., & Pandey, A. N. (2006). Estimation of postmortem interval from human pericardial fluid electrolytes concentrations in Chandigarh zone of India: Log transformed linear regression model. *Legal Medicine*, *8*(5), 279–287. https://doi.org/10.1016/J.LEGALMED.2006.06.004

Steuer, A. E., Wartmann, Y., Schellenberg, R., Mantinieks, D., Glowacki, L. L., Gerostamoulos, D., Kraemer, T., & Brockbals, L. (2024). Postmortem metabolomics: influence of time since death on the level of endogenous compounds in human femoral blood. Necessary to be considered in metabolome study planning? *Metabolomics*, *20*(3), 51. https://doi.org/10.1007/S11306-024-02117-Y

Sundler, R., & Akesson, B. (1975). Biosynthesis of phosphatidylethanolamines and phosphatidylcholines from ethanolamine and choline in rat liver. *Biochemical Journal*, *146*(2), 309–315. https://doi.org/10.1042/BJ1460309

Sund-Levander, M., Forsberg, C., & Wahren, L. K. (2002). Normal oral, rectal, tympanic and axillary body temperature in adult men and women: a systematic literature review. *Scandinavian Journal of Caring Sciences*, *16*(2), 122–128. https://doi.org/10.1046/J.1471-6712.2002.00069.X

Szeremeta, M., Pietrowska, K., Niemcunowicz-Janica, A., Kretowski, A., & Ciborowski, M. (2021). Applications of Metabolomics in Forensic Toxicology and Forensic Medicine. *International Journal of Molecular Sciences*, *22*(6), 3010. https://doi.org/10.3390/IJMS22063010

Tan, D. X., Manchester, L. C., Terron, M. P., Flores, L. J., & Reiter, R. J. (2007). One molecule, many derivatives: a never-ending interaction of melatonin with reactive oxygen and nitrogen species? *Journal of Pineal Research*, *42*(1), 28–42. https://doi.org/10.1111/J.1600-079X.2006.00407.X

Tan, D. X., Xu, B., Zhou, X., & Reiter, R. J. (2018). Pineal Calcification, Melatonin Production, Aging, Associated Health Consequences and Rejuvenation of the Pineal Gland. *Molecules (Basel, Switzerland)*, *23*(2). https://doi.org/10.3390/MOLECULES23020301

Tao, L., Ma, J., Han, L., Xu, H., Zeng, Y., Yehui, L., Li, W., Ma, K., Xiao, B., & Chen, L. (2018). Early postmortem interval estimation based on Cdc25b mRNA in rat cardiac tissue. *Legal Medicine (Tokyo, Japan)*, *35*, 18–24. https://doi.org/10.1016/J.LEGALMED.2018.09.004

Teo Chee Hau, Noor Hazfalinda Hamzah, Hing Hiang Lian, & Sri Pawita Albakri Amir Hamzah. (2014). Decomposition Process and Post Mortem Changes: Review. *Sains Malaysiana*, *43*(12), 1873–1882.

Tozzo, P., Scrivano, S., Sanavio, M., & Caenazzo, L. (2020). The role of DNA degradation in the estimation of post-mortem interval: A systematic review of the current literature. *International Journal of Molecular Sciences*, *21*(10). https://doi.org/10.3390/ijms21103540

Tsokos, M. (2005). POSTMORTEM CHANGES | Overview. *Encyclopedia of Forensic and Legal Medicine*, 456–476. https://doi.org/10.1016/B0-12-369399-3/00091-4

Tsokos M, & Byard RW. (2016). Post mortem changes - overview. In: Encyclopedia of Forensic and Legal Medicine. In *Post mortem changes - overview. In: Encyclopedia of Forensic and Legal Medicine* (2nd ed., Vol. 4, pp. 10–31).

Tu, C., Du, T., Ye, X., Shao, C., Xie, J., & Shen, Y. (2019). Using miRNAs and circRNAs to estimate PMI in advanced stage. *Legal Medicine (Tokyo, Japan)*, *38*, 51–57. https://doi.org/10.1016/J.LEGALMED.2019.04.002

Ubelaker, D. H., & Zarenko, K. M. (2011). Adipocere: what is known after over two centuries of research. *Forensic Science International*, *208*(1–3), 167–172. https://doi.org/10.1016/J.FORSCIINT.2010.11.024

Van Den Oever, R. (1976). A review of the literature as to the present possibilities and limitations in estimating the time of death. *Medicine, Science, and the Law*, *16*(4), 269–276. https://doi.org/10.1177/002580247601600411

van der Veen, J. N., Kennelly, J. P., Wan, S., Vance, J. E., Vance, D. E., & Jacobs, R. L. (2017). The critical role of phosphatidylcholine and phosphatidylethanolamine metabolism in health and disease. *Biochimica et Biophysica Acta. Biomembranes*, *1859*(9 Pt B), 1558–1572. https://doi.org/10.1016/J.BBAMEM.2017.04.006

Vazquez, J., & Baghdoyan, H. A. (2001). Basal forebrain acetylcholine release during REM sleep is significantly greater than during waking. *American Journal of Physiology. Regulatory, Integrative and Comparative Physiology*, *280*(2). https://doi.org/10.1152/AJPREGU.2001.280.2.R598

Villela, D., Atherino, V. F., Lima, L. D. S., Moutinho, A. A., Amaral, F. G. Do, Peres, R., Martins De Lima, T., Torrão, A. D. S., Cipolla-Neto, J., Scavone, C., & Afeche, S. C. (2013). Modulation of pineal melatonin synthesis by glutamate involves paracrine interactions between pinealocytes and astrocytes through NF-κB activation. *BioMed Research International*, *2013*. https://doi.org/10.1155/2013/618432

Williams, T., Soni, S., White, J., Can, G., & Javan, G. T. (2015). Evaluation of DNA degradation using flow cytometry: promising tool for postmortem interval determination. *The American Journal of Forensic Medicine and Pathology*, *36*(2), 104–110. https://doi.org/10.1097/PAF.0000000000000146

Wróblewski, B., & Ellis, M. (1970). Eye changes after death. *The British Journal of Surgery*, *57*(1), 69–71. https://doi.org/10.1002/BJS.1800570117

Wu, G., Fang, Y. Z., Yang, S., Lupton, J. R., & Turner, N. D. (2004). Glutathione Metabolism and Its Implications for Health. *The Journal of Nutrition*, *134*(3), 489–492. https://doi.org/10.1093/JN/134.3.489

Wu, Z., Lu, X., Chen, F., Dai, X., Ye, Y., Yan, Y., & Liao, L. (2018). Estimation of early postmortem interval in rats by GC–MS-based metabolomics. *Legal Medicine*, *31*, 42–48. https://doi.org/10.1016/J.LEGALMED.2017.12.014

Xin Chen, Yi-wen Shen, & Yun-ju Gu. (2005). The research of relationship between DNA degradation and postmortem interval. *Fa Yi Xue Za Zhi* , *21*(2), 115–117.

Yelamanchi, S. D., Jayaram, S., Thomas, J. K., Gundimeda, S., Khan, A. A., Singhal, A., Keshava Prasad, T. S., Pandey, A., Somani, B. L., & Gowda, H. (2016). A pathway map of glutamate metabolism. *Journal of Cell Communication and Signaling*, *10*(1), 69. https://doi.org/10.1007/S12079-015-0315-5

Yoshimi, N., Futamura, T., Kakumoto, K., Salehi, A. M., Sellgren, C. M., Holmén-Larsson, J., Jakobsson, J., Pålsson, E., Landén, M., & Hashimoto, K. (2016). Blood metabolomics analysis identifies abnormalities in the citric acid cycle, urea cycle, and amino acid metabolism in bipolar disorder. *BBA Clinical*, *5*, 151–158. https://doi.org/10.1016/J.BBACLI.2016.03.008

Yu, J. C., Jiang, Z. M., & Li, D. M. (1999). Glutamine: a precursor of glutathione and its effect on liver. *World Journal of Gastroenterology*, *5*(2), 143. https://doi.org/10.3748/WJG.V5.I2.143

Zapico, S. C., Menéndez, S. T., & Núñez, P. (2014). Cell death proteins as markers of early postmortem interval. *Cellular and Molecular Life Sciences*, *71*(15), 2957–2962. https://doi.org/10.1007/S00018-013-1531-X/FIGURES/3

Zawilska, J. B., & Nowak, J. Z. (1990). Calcium influx through voltage-sensitive calcium channels regulates in vivo serotonin N-acetyltransferase (NAT) activity in hen retina and pineal gland. *Neuroscience Letters*, *118*(1), 17–20. https://doi.org/10.1016/0304-3940(90)90238-5

Zelentsova, E. A., Yanshole, L. V., Melnikov, A. D., Kudryavtsev, I. S., Novoselov, V. P., & Tsentalovich, Y. P. (2020). Post-mortem changes in metabolomic profiles of human serum, aqueous humor and vitreous humor. *Metabolomics*, *16*(7), 1–10. https://doi.org/10.1007/S11306-020-01700-3/TABLES/2

Zelentsova, E. A., Yanshole, L. V., Snytnikova, O. A., Yanshole, V. V., Tsentalovich, Y. P., & Sagdeev, R. Z. (2016). Post-mortem changes in the metabolomic compositions of rabbit blood, aqueous and vitreous humors. *Metabolomics*, *12*(11), 1–11. https://doi.org/10.1007/S11306-016-1118-2/FIGURES/5

Zhang, A., Sun, H., Yan, G., Wang, P., & Wang, X. (2015). Metabolomics for Biomarker Discovery: Moving to the Clinic. *BioMed Research International*, *2015*(1), 354671. https://doi.org/10.1155/2015/354671

Zhang, D., Hua, Z., & Li, Z. (2024). The role of glutamate and glutamine metabolism and related transporters in nerve cells. *CNS Neuroscience & Therapeutics*, *30*(2), e14617. https://doi.org/10.1111/CNS.14617

Zhang, L., Liu, C., Jiang, Q., & Yin, Y. (2021). Butyrate in Energy Metabolism: There Is Still More to Learn. *Trends in Endocrinology and Metabolism*, *32*(3), 159–169. https://doi.org/10.1016/J.TEM.2020.12.003/ASSET/BEBE931A-313B-442E-96C6-6190F4EF5259/MAIN.ASSETS/GR1.SML

Zhao, Y. Y., & Lin, R. C. (2014). UPLC–MSE application in disease biomarker discovery: The discoveries in proteomics to metabolomics. *Chemico-Biological Interactions*, *215*(1), 7–16. https://doi.org/10.1016/J.CBI.2014.02.014

Zheng, J., Li, X., Shan, D., Zhang, H., & Guan, D. (2012). DNA degradation within mouse brain and dental pulp cells 72 hours postmortem. *Neural Regeneration Research*, *7*(4), 290–294. https://doi.org/10.3969/J.ISSN.1673-5374.2012.04.009

Zhou, C., & Byard, R. W. (2011). Factors and processes causing accelerated decomposition in human cadavers – An overview. *Journal of Forensic and Legal Medicine*, *18*(1), 6–9. https://doi.org/10.1016/J.JFLM.2010.10.003

Zhu, Y., Wang, L., Yin, Y., & Yang, E. (2017). Systematic analysis of gene expression patterns associated with postmortem interval in human tissues. *Scientific Reports*, *7*(1). https://doi.org/10.1038/S41598-017-05882-0

Zisapel, N. (2018). New perspectives on the role of melatonin in human sleep, circadian rhythms and their regulation. *British Journal of Pharmacology*, *175*(16), 3190. https://doi.org/10.1111/BPH.14116